Tree-Structured Like Representations for Continuous and Graph Indexed Markov Random Fields

Submitted in partial fulfillment of the requirements for

the degree of

Doctor of Philosophy

in

Electrical and Computer Engineering

Divyanshu Vats

B.S., Mathematics, The University of Texas at Austin
B.S., Electrical Engineering, The University of Texas at Austin
M.S., Electrical and Computer Engineering, Carnegie Mellon University

Carnegie Mellon University

Pittsburgh, PA

May, 2011

Abstract

Markov random fields (MRFs) are ubiquitous models for conveniently capturing complex statistical dependencies given a collection of random variables. For example, when modeling the temperature distribution of a continuously indexed region, it is common to assume that the temperature at one point depends on some differential neighborhood. MRFs can capture such dependencies using a set of conditional independence relationships and thereby lead to compact representations of random signals. Other examples of using MRFs is when modeling a finite collection of gene expressions or when modeling pixel intensities in images.

Although MRFs lead to compact representations for high-dimensional spatially varying random signals, the resulting representations are often noncausal and thus standard recursive algorithms popular for processing causal signals (temporal signals) can no longer be applied. The central theme of this thesis is to find alternate representations in arbitrary MRFs in the form of a tree so that standard recursive algorithms, like the Kalman filter and the belief propagation algorithm, for trees can be applied to MRFs. We study two kinds of MRFs in this thesis: (i) MRFs indexed over high-dimensional continuous indices, and (ii) MRFs indexed over graphs.

For MRFs indexed over high-dimensional continuous indices, we show that, a natural tree-structured like representation, in this case a chain, exists on a collection of hypersurfaces embedded in the continuous index set. For Gaussian MRFs, this leads to telescoping representations in the form of a linear stochastic differential equation that initiates at the boundary of the MRF and recurses inwards in a telescoping manner. Using the telescop-

ing representation, we derive algorithms for recursively processing random signals indexed over continuous domains.

For MRFs indexed over graphs (commonly referred to as graphical models,) where the edges in the graph capture various conditional independence relationships among random variables, we show that a tree-structured like representation can be derived by appropriately clustering nodes in the graph so that the graph over the clusters is a tree. We call the resulting graph a block-tree. Like the telescoping representation for MRFs indexed over continuous indices, the block-tree representation leads to algorithms for recursive processing of graphical models. Using the block-tree representation, we propose a framework for generalizing common algorithms over graphical models. As an example, we show how block-trees can be used to perform generalized belief propagation over graphical models to obtain more accurate inference algorithms.

Acknowledgment

I would like to thank my advisor, Prof. José M. F. Moura, for his guidance, support, and encouragement during these past five years at Carnegie Mellon University. Prof. Moura has been a continuous source of knowledge and passion that I can only hope to emulate someday. Not only has he given me constant feedback on various research paper drafts and presentations, which I know will help me in my future research and academic pursuits, but he has also guided and given me the freedom to pursue various research problems of my own interest.

I would like to thank my thesis committee members Prof. Vijayakumar Bhagavatula, Prof. Rohit Negi, Prof. Markus Püschel, Prof. Bernard Levy, and Dr. Ta-Hsin Li for all their valuable feedback on my thesis research that helped me channelize my thoughts and shape my research ideas. I thank Prof. Levy for agreeing to be on my committee on such notice and also for his papers on reciprocal processes and Markov random fields. I thank Prof. Negi for allowing me to be his teaching assistant on two occasions and guiding me through the tricky task of creating homework and exam problems.

I would like to thank Prof. Brian Evans and Prof. Joydeep Ghosh from UT Austin and Prof. Richard Baraniuk from Rice University for supporting my graduate school applications. I thank Prof. Evans for introducing me to research and for advising me as an undergraduate student. I thank Prof. Baraniuk for giving me the opportunity to work at Rice University as an undergraduate student and introducing me to various research problems. I thank Vishal Monga for guiding me as an undergraduate student and again as a graduate student when I spent a summer working at Xerox Research.

I would like to thank my office mates Kyle Anderson, Aurora Schmidt, Marek Telgarsky, Soummya Kar, and Dusan Jakovetic for all the insightful discussions on both research and non-research related topics. In addition to my office mates, I would like to thank my fellow ECE students Aliaksei Sandryhaila, Frédéric de Mesmay, Joel Harley, Nicholas ODonoughue, James Weimer, Joao Mota, Augusto Santos, Joya Deri, and June Zhang for their helpful feedback on departmental presentations and the discussions on various research topics. I would like to thank Carol Patterson for all the logistical help. I thank the ECE Graduate Organization (EGO) for organizing various social events throughout the year.

I would like to thank my friends from Austin and Pittsburgh for making life enjoyable outside the office. I thank my in-laws and sister-in-law for all their encouragement and support. I thank my parents for encouraging me to pursue my passions and always supporting me in my endeavors. I thank them for teaching me the value of education and I hope to someday be the educator and researcher that they are. I thank my sister for all her encouragement and support. Finally, this thesis would not have been possible without the love and support of my wife. I thank her for being patient with me as I worked towards this thesis. I thank her for helping me get through some tough times. I thank her for listening to my research ideas and pointing me to relevant references. Most importantly, I thank her for teaching me to have a dream.

The work in this thesis was supported in part by DARPA under award HR0011-05-1-0028.

Contents

Abstract ii

Acknowledgment iv

1 Introduction 1

1.1 Motivation . . . 1

1.2 Markov Random Fields Over Continous Indices . . . 2

1.2.1 Literature Review . . . 2

1.2.2 Summary of Contributions . . . 4

1.3 Markov Random Fields Over Graphs . . . 5

1.3.1 Literature Review . . . 5

1.3.2 Summary of Contributions . . . 6

1.4 Thesis Summary and Organization . . . 7

1.5 Bibliographical Notes . . . 8

2 Telescoping Representations for Continuous Indexed Markov Random Fields 9

2.1 Introduction . . . 9

2.1.1 Summary of Contributions . . . 10

2.1.2 Related Work . . . 11

2.1.3 Chapter Organization . . . 12

2.2 Gauss-Markov Random Fields . . . 13

2.3 Telescoping Representation: GMRFs on a Unit Disc . . . 17

2.3.1 Main Theorem . . . 18

2.3.2 Homogeneous and Isotropic GMRFs . . . 22

2.4 Telescoping Representation: GMRFs on arbitrary domains 25
2.4.1 Telescoping Surfaces Using Homotopy 25
2.4.2 Generating Similar Telescoping Surfaces 28
2.4.3 Telescoping Representations 29
2.5 GMRFs Pinned to Two Boundaries 30
2.6 Recursive Estimation of GMRFs 33
2.7 Summary 36

3 Block-Tree Structures in Markov Random Fields Over Graphs 37
3.1 Introduction 37
3.2 Background and Problem Statement 39
3.2.1 Graphs and Graphical Models 39
3.2.2 Inference Algorithms 42
3.2.3 Belief Propagation 44
3.2.4 Junction-Tree 45
3.2.5 Problem Statement 51
3.3 Tree Structures in Graphs Using Block-Trees 52
3.3.1 Constructing Block-Trees 52
3.3.2 A Linear Time Block-Tree Construction Algorithm 56
3.3.3 Block-Trees Vs. Junction-Trees 57
3.4 Inference of Graphical Models Using Block-Trees 58
3.4.1 Belief Propagation on Block-Trees 58
3.4.2 Optimal Block-Trees 60
3.4.3 Greedy Algorithms For Finding Optimal Block-Trees 61
3.5 Inference Over Graphical Models: Block-Tree Vs. Junction-Tree 63
3.5.1 Example: Single Cycle Graphical Models 63
3.5.2 Example: Erdős-Rényi Graph 64
3.5.3 Discussion 65
3.6 Summary 66

4 Generalizing Algorithms on Graphical Models Using Block-Graphs **69**

4.1 Introduction 69

4.2 Generalized Algorithms Using Block-Graphs 71

4.2.1 General Theory 72

4.2.2 Approximate Inference Using Block-Graphs 73

4.3 Constructing Block-Graphs 74

4.4 Numerical Simulations 76

4.5 Related Work 79

4.6 Summary 81

5 Conclusion and Future Work **83**

5.1 List of Contributions 83

5.2 Chapter Summaries 84

5.2.1 Chapter 2: Tree-Structures in MRFs over Continuous Indices 84

5.2.2 Chapter 3: Block-Tree Structures in MRFs over Graphs 85

5.2.3 Chapter 4: Generalizing Algorithms on Graphical Models 85

5.3 Suggestions for Future Work 86

5.3.1 Estimation of Random Fields Over Continuous Indices 86

5.3.2 Other Applications of Using Block-Graphs 86

5.3.3 Learning Graphical Models Using Block-Graphs 87

A Appendix to Chapter 2 **89**

A.1 Computing $b_j(s,r)$ in Theorem 2.2.1 89

A.2 Proof of Theorem 2.3.1: Telescoping Representation 92

A.3 Proof of Theorem 2.6.1: Recursive Filter 96

A.4 Proof of Theorem 2.6.2: Recursive Smoother 102

Bibliography **118**

List of Figures

1.1 Conditional independence relationships for Markov processes (left), reciprocal processes (middle), and Markov random fields (right). For a Markov process, the past $\perp$ future | present. For reciprocal processes and Markov random fields, interior $\perp$ exterior | boundary. 3

1.2 Examples of hypersurfaces on which we derive recursive representations. In (a),(b), and (c) we have have hypersurfaces for a field defined on a dics. In (d), we have surfaces defined on an arbitrary region. 4

1.3 Examples of various graphical models and a graphical model defined on a block-tree. 5

2.1 Different kinds of telescoping recursions for an MRF defined on a disc. . . 10

2.2 (a) An example of complementary sets on a random field defined on S with boundary ∂S. (b) Corresponding notion of complementary sets for a random process. 14

2.3 A random field defined on a unit disc. The boundary of the field, i.e., the field values defined on the circle with radius 1 is denoted by $x(\partial S)$. The field values at a distance of $1-\lambda$ from the center of the field are given by $x(\partial S^{\lambda})$. Each point is characterized in polar coordinates as $x_{\lambda}(\theta)$, where $1-\lambda$ is the distance to the center and θ denotes the angle. 18

2.4 Telescoping surfaces defined using different homotopies. 26

2.5 Telescoping surfaces defined using different homotopies on arbitrary regions. . . 29

2.6 An example of a random field pinned to two boundaries. 30

2.7 Starting with the original domain with two boundaries (shown in red), we first fold along the diameter (shown as a dotted line). This leads to a semi-circle. In the semi-circle, we observe that the boundaries are shown in thicker lines. This corresponds to the overlapping of boundaries when folding. Next, we fold along the radius shown as a dotted line. After this, we continually fold the domain in the radial direction. We then fold from the middle of the line so that both boundary values now overlap and the random field that was pinned to two boundaries can now be interpreted as pinned to one boundary. 32

3.1 Types of Graph Structures 38

3.2 Different examples of graphical models 42

3.3 Belief propagation on trees: (a) messages, shown via dashed lines, are first passed from the leaves to the root, (b) and then passed from the root to the leaves. 45

3.4 (a) An undirected graph, (b) Not a valid junction-tree since $\{1, 2\}$ separates $\{1, 3\}$ and $\{3, 4\}$,but $3 \notin \{1, 2\}$. In other words, the running intersection property says that for two clusters with a common node, all the clusters on the path between the two clusters must have that common node. (c) A valid junction-tree for the graph in (a). 46

3.5 (a) Tree-structured graph (b) The graph over cliques (c) A junction-tree for (a). 48

3.6 (a) Original single cycle graph. (b) Triangulated graph of (a). (c) Weighted graph over cliques. (d) Final junction-tree. 48

3.7 (a) A grid graph (b) Triangulated graph of (a). (c) Weighted graph over cliques. (d) Junction-tree 49

3.8 (a) Partial grid graph. (b) Triangulated graph from (a). (c) Weighted graph over cliques. The weightless edges all have weight one. (d) One possible junction-tree from (c). (e) Another possible junction-tree from (c). 50

3.9 (a) Initial estimates of the clusters. (b) Final estimates of the clusters. (c) Final block-tree. 54

3.10 (a) Original estimates of the clusters in the grid graph when running the forward pass of Algorithm 2 (b) The final clusters after running the backwards pass of Algorithm 2 (c) Final block-tree. 55
3.11 (a) Original estimates of the clusters in the partial grid when running the forward pass of Algorithm 2 (b) The final clusters after running the backwards pass of Algorithm 2 (c) Final block-tree. 55
3.12 (a) Junction-tree for the block-tree in Fig. 3.10(c) (b) Junction-tree for the block-tree in Fig. 3.11(c) 57
3.13 The relationship between the set of all block-trees and the set of all junction-trees for a given graph G. 58
3.14 (a) Original estimates of the clusters in the partial grid using $V_1 = \{7, 4\}$ as the root cluster (b) Splitting of clusters (c) Final block-tree. 61
3.15 Plot showing the performance of three different greedy heuristics for finding optimal block-trees. 62
3.16 Complexity of inference 64
3.17 Algorithm to choose between a block-tree and a junction-tree for inference over graphical models. 66

4.1 A framework for generalizing algorithms on graphical models. 72
4.2 Example illustrating how to generalize algorithms on graphical models. . . 73
4.3 Explaining Step 6 in the block-graph construction algorithm. Given the block-graph in (a), if we merge nodes 2 and 3, we get the block-graph in (b). If we merge nodes 3 and 4, we get the block-graph in (c). Notice that the block-graph in (c) has just one loop. 76
4.4 Comparison of convergence and accuracy of using LBP on graphs vs. using LBP on block-graphs for a 7×7 grid graph. Results are over 500 runs. The iterations and accuracy results are when all the algorithms converge. 78

4.5 Comparison of convergence and accuracy of using LBP on graphs vs. using LBP on block-graphs for a 8×8 grid graph. Results are over 200 runs. The iterations and accuracy results are when all the algorithms converge. 78

4.6 Comparison of convergence and accuracy of using LBP on graphs vs. using LBP on block-graphs for a 30×30 grid graph. Results are over 100 runs. Since finding the true node potentials is computatinally intractable, we use a higher order block-graph to estimate the ground truth. 80

5.1 An example of the tree-structures we derive in this thesis. For MRFs over continuous indices, we derive tree representations over hypersurfaces. For MRFs over graphs, we derive tree representations over a disjoint collection of clusters over nodes. 84

Chapter 1

Introduction

1.1 Motivation

Recent advances in technology, including data storage and sensing, have led to massive data collection in nearly all fields of study. A central challenge in analyzing these large data sets is to find parsimonious stochastic models to describe the data and further derive efficient algorithms that use these stochastic models to make decisions on future observations. Such algorithms can have a major impact on a variety of different problems in various domains. For example, in weather monitoring, it is of interest to detect catastrophic events like fire, hurricane, and floods given noisy measurements from sensor networks [14]. In analyzing satellite images or hyperspectral images, it is of interest to detect the presence or absence of certain objects and also to denoise images cluttered with noise [30], [85]. In computational biology, given stochastic models for gene expressions, it is of interest to design algorithms for detecting the presence or absence of a particular diseases [27], [65]. Another example in this domain is to predict protein structures given a particular protein sequence [113], [118]. In communication systems, it is of interest to derive efficient and accurate algorithms for decoding a noisy message [28].

A common feature of the problems listed above is that we are given a global probability distribution over a collection of random variables, using which we want to make local estimates about the state of each random variable. Even when the global probability dis-

tribution encodes local dependencies among random variables, for example, intensities of pixels only depending on its neighboring pixel values or genes correlated with similar type of genes, the problem of manipulating such probability distributions for local decisions is computationally challenging.

The central theme in this thesis is to find structures in global probability distributions that can enable efficient algorithms for processing data. Motivated by algorithms that are efficient on tree-structured like distributions, like Kalman filters [39], [40], recursive smoothers [37], and belief propagation [69], we focus on finding *tree-structured like representations* for a collection of random variables modeled as a Markov random field (MRFs). In particular, we consider two kinds of MRFs: (i) MRFs indexed over continuous indices, and (ii) MRFs indexed over graphs. For both of these kinds of MRFs, we show that tree-structures can be found, which enable the extension of current known algorithms to more complex probability distributions.

1.2 Markov Random Fields Over Continous Indices

1.2.1 Literature Review

When modeling random processes, a collection of random variables indexed over some continuous interval of the real line, the Markov property leads to recursive representations. Such representations lend themselves to efficient algorithms, an example of which is the celebrated Kalman filter. Informally, the Markov property for random processes says that given knowledge of the past and present, the future values only depend on the present values. This conditional relationship between past, present, and future is also termed a *causal* relationship. Markov random processes have been studied extensively and have been used successfully as mathematical models for time-varying random signals.

In 1931, Schrödinger [81] considered the problem of studying the dynamics of a random process conditioned on both past and future values. A general study of such processes was conducted in 1932 by Bernstein [9], where he introduced the notion of a reciprocal process. Informally, a random process defined on an interval $[0, T]$ is reciprocal if given any interval

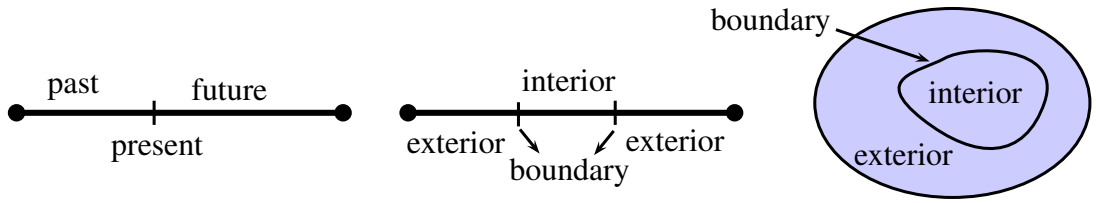

Figure 1.1: Conditional independence relationships for Markov processes (left), reciprocal processes (middle), and Markov random fields (right). For a Markov process, the past $\perp$ future | present. For reciprocal processes and Markov random fields, interior $\perp$ exterior | boundary.

$[a, b] \subset [0, T]$, the process defined on the *interior* $[a, b]$ is conditionally independent of the process defined on the *exterior* $[0, T] \backslash [a, b]$ given the process at both a and b. Comparing the definition of a reciprocal process to that of a Markov process, we see that the exterior can be mapped to the past, the interior can be mapped to the future, and the boundary of the interior can be mapped to the present. One can immediately infer that reciprocal processes are not Markov, however, as shown in [32], Markov processes are reciprocal. Thus, reciprocal processes extend the class of Markov processes by encoding more conditional independence relationships among random variables. Properties and characterizations of reciprocal processes are well studied in the literature (see [43]–[46], [51]) and there have been many works that derive efficient recursive algorithms on reciprocal processes, see [1], [2], [7], [88] for some examples.

In 1956, Lévy introduced Markov random fields (MRFs) that generalized the notion of reciprocal processes to random fields, a collection of random variables indexed over a high-dimensional continuous index set. To define an MRF, we can interpret the interior of the field as any closed region within the given index set, the exterior as the complement of the interior, and the boundary as the set of points separating the interior and the exterior. As in the case of reciprocal processes, the Markov property for random fields says that the field defined on the interior is independent of the field defined on the exterior given the field defined on the boundary. Fig. 1.1 shows a comparison of the conditional independence relationships defined for Markov processes, reciprocal processes, and Markov random fields.

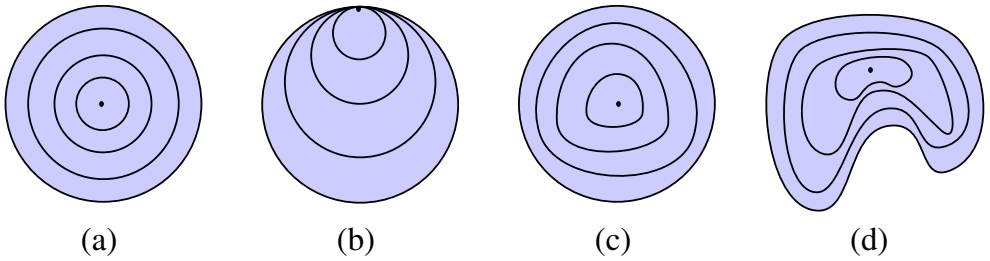

Figure 1.2: Examples of hypersurfaces on which we derive recursive representations. In (a),(b), and (c) we have have hypersurfaces for a field defined on a dics. In (d), we have surfaces defined on an arbitrary region.

Following the introduction of MRFs by Lévy, several authors have studied various properties and characterizations of MRFs, see [38], [58], [73] for some examples. Further, MRFs have been used to study the black body radiation problem [59], to study underwater ambient noise in the ocean [13], and to study temperature distributions in the atmosphere [36]. However, unlike Markov and reciprocal processes, there exists no general theory for deriving recursive algorithms on MRFs. Attempts to enable efficient processing of random fields have been considered in the past; however, all past work either assumes some kind of temporal behavior in the spatial signal [67], [105], [106], [108] or assumes a particular structure on the MRF [84].

1.2.2 Summary of Contributions

In Chapter 2, we introduce a framework for deriving algorithms for recursive processing of Markov random fields (MRFs). We define the notion of a *state* for MRFs that collect the values of the field on any smooth hypersurface separating the continuous domain into two non-intersecting regions. We use this notion of state and an appropriate collection of states spanning the MRF domain to derive a telescoping representation for MRFs such that the representations initiate at the boundary of the MRF and recurse on the hypersurfaces in a telescoping manner. Thus, the hypersurfaces form a tree-structured like representation for the MRF. For Gaussian MRFs, we show that the telescoping representations can be captured using a linear stochastic differential equation driven by Brownian motion. Using the telescoping representation, we derive recursive estimators that extend the Kalman-

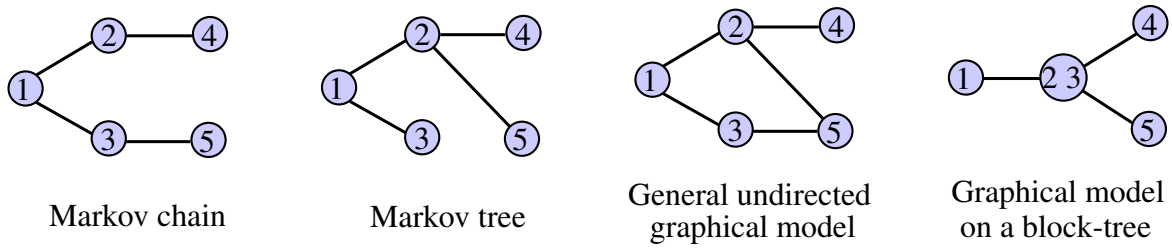

Figure 1.3: Examples of various graphical models and a graphical model defined on a block-tree.

Bucy filter and other standard recursive smoothers to random fields.

Using the notion of homotopy, we show that an MRF can admit multiple different telescoping representations. For example, in Fig. 1.2, we show various collections of hypersurfaces for an MRF defined on a disc and an MRF defined on an arbitrary continuous region. For each collection of hypersurfaces, we can define a telescoping representation. Moreover, our telescoping representations extend to arbitrary domains with smooth boundaries indexed over $\mathbb{R}^d$, for $d \geq 2$, and even to domains that are pinned to two boundaries, an example of which is the temperature distribution of a thick cylinder with boundary conditions on the inside and outside walls.

1.3 Markov Random Fields Over Graphs

1.3.1 Literature Review

Markov random fields over graphs, also known as graphical models, have been studied extensively in the literature [48]. The nodes in a graph correspond to random variables (or random vectors) and the edges in the graph capture various conditional independence relationships among the random variables. One of the most common graphical models is the discrete-time Markov process, also known as a Markov chain, which is represented by a chain-structured graph. A generalization of the Markov chain is a Markov tree, defined on a tree-structured graph. See the first three graphs in Fig 1.3 for some examples.

It is well known that various algorithms over graphical models are efficient for tree-structured graphs. For example, given the joint probability distribution of a random

vector modeled as a graphical model, it is of interest in various applications to find the marginal distribution of each random variable. This problem is often referred to as inference. As an example, given a set of noisy observations $\mathbf{y} = \{y_s\}$ of a random vector $\mathbf{x} = \{x_s\}$, we want to estimate or infer each x_s given the observations $\mathbf{y}$. To do this, we need to marginalize the distribution $p(\mathbf{x}|\mathbf{y})$. Inference in tree-structured graphical models can be achieved *exactly* using the belief propagation (BP) algorithm of Pearl [69], which works by exchanging messages between nodes connected via edges.

For graphical models with loops or cycles, see Fig. 1.3 for an example, performing exact inference requires the construction of a junction-tree [77]. A junction-tree is a tree-structured graph formed by clustering nodes in the original graph in such a way that the clusters have *overlapping* nodes. A message passing algorithm over the junction-tree can be derived so that we get exact inference algorithms for graphical models with cycles [49], [82]. However, there are two main drawbacks in using junction trees for inference. Firstly, constructing junction-trees has a worst case complexity that is quadratic in the number of nodes in the graph. Thus, using junction-trees for inference may not be desirable for applications involving time-varying graphical models. Secondly, when the junction-trees have large clusters, the complexity of inference will be large. This makes the junction-tree approach to inference computationally intractable. This has motivated many works that derive efficient approximate inference algorithms. We refer to [96] for a review of such algorithms.

1.3.2 Summary of Contributions

We propose an alternative framework for finding tree-structures in graphs. Instead of forming a tree on a set of overlapping clusters, we propose to use a set of disjoint clusters. This leads us to the definition of a block-tree, which is a tree-structured graph over clusters that are disjoint. An example of a block-tree is shown in Fig. 1.3. We show that block-trees can be constructed efficiently with complexity linear in the number of edges in the graph. This naturally makes constructing block-trees faster than constructing junction-trees. Another advantage of block-trees is that the belief propagation algorithm for trees

easily generalizes to block-trees, leading to algorithms for inference over graphical models with cycles.

Although block-trees are useful for finding tree-structures in graphical models, as in the case of junction-trees, using block-trees for inference can be computationally intractable for situations when the size of clusters is too large. In Chapter 4, we use block-trees to propose a framework for generalizing various algorithms over graphical models. By splitting large clusters in a block-tree in a structured manner, we form a graph (not a tree) over the clusters. Our framework for generalizing algorithms over graphical models uses the block-graph for computation rather than the original graph. We use this framework to derive efficient approximate inference algorithms.

1.4 Thesis Summary and Organization

The central theme in this thesis is to find tree-structured like representations for a collection of random variables modeled as a Markov random field (MRF). Examples of random signals modeled as MRFs include the steady state temperature distribution in a material, images, gene expressions, among others.

In Chapter 2, we study MRFs over continuous indices. For such MRFs, we show that a tree like representation can be derived over a collection of hypersurfaces within the continuous index set. See Fig. 1.2 for examples of such hypersurfaces. Using this representation, we derive extensions of the Kalman filter and the Rauch-Tung-Striebel smoother to Gaussian MRFs indexed over continuous indices.

In Chapter 3, we study MRFs over graphs. We show that by appropriately clustering nodes in the original graph, we get a tree-structured like representation for such MRFs. We call the tree-structured graph over the clusters a block-tree. See Fig. 1.2 for an example of a block-tree. We outline a linear time complexity algorithm for constructing block-trees. For the problem of inference (computing marginal distributions), we show the merits of using block-trees over junction-trees, another framework for finding tree-structures in graphs using a set of overlapping clusters.

In Chapter 4, we propose a framework for generalizing various algorithms over graphical models. The key idea is to map the original graph into a block-graph, defined as graph over disjoint clusters of nodes. We propose an efficient algorithm for constructing block-graphs by modifying our algorithm for constructing block-trees. As a particular example, we demonstrate the use of block-graphs in improving the accuracy of loopy belief propagation for inference in graphical models.

Chapter 5 concludes this thesis and discusses suggestions for future research.

1.5 Bibliographical Notes

Parts of the material presented in this thesis have been published as conference and journal papers.

- The material in Chapter 2 has been published in the IEEE Transactions on Information Theory [92] in March 2011 and presented in part at the 2010 IEEE Conference on Decision and Control [89]. The results were motivated by earlier work done on studying reciprocal processes in [87] and [88].

- Preliminary results from Chapter 3 were presented at the 2010 IEEE International Conference Acoustics, Speech, and Signal Processing [90].

Chapter 2

Telescoping Representations for Continuous Indexed Markov Random Fields

2.1 Introduction

In this Chapter, we derive recursive representations for spatially distributed signals, such as temperature in materials, concentration of components in process control, intensity of images, density of a gas in a room, stress level of different locations in a structure, or pollutant concentration in a lake [72], [80], [86]. These signals are often modeled using *random fields*, which are random signals indexed over $\mathbb{R}^d$ or $\mathbb{Z}^d$, for $d \geq 2$. Our focus in this Chapter will be on random signals indexed over $\mathbb{R}^d$ and subsequent Chapters in this thesis will consider random signals indexed over discrete indices.

For random *processes*, that are indexed over $\mathbb{R}$, recursive algorithms are recovered by assuming causality. In particular, for Markov random processes, the future states depend only on the present state given both the past and present states. When modeling spatial distributions by random fields, it is more appropriate to assume noncausality as opposed to causality. This leads to noncausal Markov random fields (MRFs): the field inside a domain is independent of the field outside the domain given the field on (or

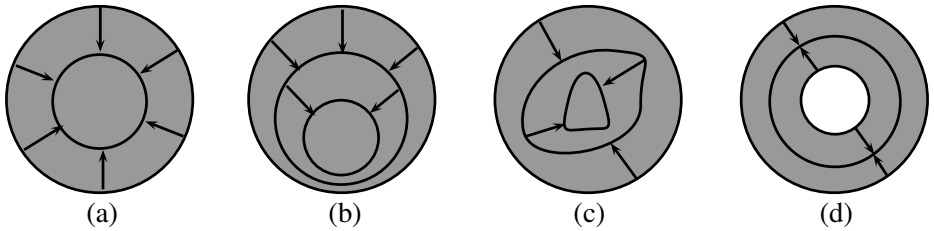

Figure 2.1: Different kinds of telescoping recursions for an MRF defined on a disc.

near) the domain boundary [54]. The need for recursive algorithms for noncausal MRFs arises to reduce the increased computational complexity due to the noncausality and the multidimensionality of the index set. The assumption of noncausality presents problems in developing recursive algorithms, such as the Kalman-Bucy filter for noncausal MRFs.

2.1.1 Summary of Contributions

Telescoping Recursive Representations

We present *telescoping recursive representations* for noncausal Gaussian Markov random fields (GMRFs) defined on a closed continuous index set in $\mathbb{R}^d$, $d \geq 2$. The telescoping recursions initiate at the boundary of the field and recurse inwards. For example, in Fig. 2.1(a), for an MRF defined on a unit disc, we derive telescoping representations that recurse radially inwards to the center of the field. For the same field, we derive an equivalent representation where the telescoping surfaces are not necessarily symmetric about the center of the disc, see Fig. 2.1(b). The telescoping surfaces, under appropriate conditions, can be arbitrary as shown in Fig. 2.1(c). Finally, for GMRFs pinned to two boundaries, the telescoping representation initiates from both the boundaries and recurses towards a hypersurface within the field as shown in Fig. 2.1(d).

We parametrize the field using two parameters: $\lambda \in [0, 1]$ and $\theta \in \Theta \subset \mathbb{R}^{d-1}$. The parameter λ indicates the position of the telescoping surface and the set Θ parameterizes the boundary of the index set. For example, for the unit disc with recursions as in Fig. 2.1(a), the telescoping surfaces are circles, and we can use polar coordinates to parameterize the field: radius λ and angle $\theta \in \Theta = [-\pi, \pi]$. The telescoping surfaces are

represented using a *homotopy* from the boundary of the field to a point within the index set (which is not on the boundary). The net effort for $d = 2$ is to represent the field by a recursion in λ, i.e., a single parameter (or dimension) rather than multiple dimensions.

The key idea in deriving the telescoping representation is to establish a notion of "time" for Markov random fields. We show that the parameter λ, which corresponds to the telescoping surface, acts as time. In our telescoping representation, we define the *state* to be the field values at the telescoping surfaces. For Gaussian MRFs (GMRFs), the telescoping recursive representation results in a linear stochastic differential equation in the parameter λ and is driven by Brownian motion. For a certain class of *homogeneous isotropic* GMRFs over $\mathbb{R}^2$, for which the covariance is a function of the Euclidean distance between points, we show that the driving noise is 2-D white Gaussian noise. For the Whittle field [102] defined over a unit disc, we show that the driving noise is zero and the field is uniquely determined using the boundary conditions.

Recursive Estimation of MRFs

Using the telescoping recursive representation, we promptly recover recursive algorithms well known for Markov random processes. As an example, for GMRFs, we derive extensions of the Kalman-Bucy filter [40] and the Rauch-Tung-Striebel (RTS) smoother [75]. For the Kalman-Bucy filter, we sweep the observations over the telescoping surfaces starting at the boundary and recursing inwards. For the smoother, we sweep the observations starting from the inside and recursing outwards. Although we use the RTS smoother, other known smoothing algorithms can be used as well, see [6], [26], [37].

2.1.2 Related Work

Markov random fields (MRFs) indexed over continuous indices have been studied extensively in the literature, starting from work by Lévy [54] to subsequent works by McKean [58], Wong [103], Pitt [73], Kallianpur and Mandrekar [38], Rozanov [79], Wong and Zakai [109], and Moura and Goswami [63]. These works have mainly focused on theoretical foundations of MRFs, where the authors have characterized various properties of

MRFs. For MRFs indexed over a one-dimensional domain, called reciprocal processes [9], [32], there has been a lot of work on deriving recursive representations and subsequently recursive estimators. For example, in [1], [2], [7], the authors derived recursive estimators for a class for reciprocal processes characterized by a solution to a stochastic differential equation with mixed boundary conditions. In [88], the authors derived recursive representations and recursive estimators for reciprocal processes characterized by solutions to a second order stochastic differential equation driven by correlated noise, see [45]. However, these representations do not generalize to MRFs indexed over high dimensional continuous domains. Further, algorithms proposed for estimation over discrete indexed MRFs, see [53], [62], [69], [110], do not generalize to continuous indexed MRFs.

Wong and coauthors have studied the problem of recursive estimation of random fields, see [67], [104]–[106], [108]. However, the random fields considered by Wong do not capture spatial variability of noncausal random fields and are causal in some sense. For noncausal *isotropic* Gaussian MRFs (GMRFs) over $\mathbb{R}^2$, the authors in [84] derived recursive representations, and subsequently recursive estimators, by transforming the 2-D problem into a countably infinite number of 1-D problems. This transformation was possible because of the isotropy assumption since isotropic fields over $\mathbb{R}^2$, when expanded in a Fourier series in terms of the polar coordinate angle, the Fourier coefficient processes of different orders are uncorrelated [84]. In this way, the authors derived recursive representations for the Fourier coefficient process. The recursions in [84] are with respect to the radius when the field is represented in polar coordinate form. The algorithm is an approximate recursive estimation algorithm since it requires solving a set of countably *infinite* number of 1-D estimation problems [84].

2.1.3 Chapter Organization

The organization of the Chapter is as follows. Section 2.2 reviews the theory of GMRFs. Section 2.3 introduces the telescoping representation for GMRFs indexed on a unit disc. Section 2.4 generalizes the telescoping representations to arbitrary domains. Section 2.5 extends the telescoping representations to GMRFs pinned to two boundaries. Section 2.6

derives recursive estimation algorithms using the telescoping representation. Section 2.7 summarizes the Chapter.

2.2 Gauss-Markov Random Fields

For a random process $x(s)$, $s \in \mathbb{R}$, the notion of Markovianity corresponds to the assumption that the past $\{x(s) : s < t\}$, and the future $\{x(s) : s > t\}$ are conditionally independent given the present $x(s)$. Higher order Markov processes can be considered when the past is independent of the future given the present and information near the present. The extension of this definition to random fields, *i.e.*, a random process indexed over $\mathbb{R}^d$ for $d \geq 2$, was introduced in [54]. Specifically, a random field $x(s)$, $s \in S \subset \mathbb{R}^d$, is Markov if for any smooth surface ∂G separating S into complementary domains, the field inside is independent of the field outside conditioned on the field on (and near) ∂G. To capture this definition in a mathematically precise way, we use the notation introduced in [58]. On the probability space $(\Omega, \mathcal{F}, \mathcal{P})$, let[1] $x(s) \in \mathbb{R}$ be a zero mean random field for $s \in S \subset \mathbb{R}^d$, where $d \geq 2$ and let $\partial S \subset S$ be the smooth boundary of S. For any set $A \subset S$, denote $x(A)$ as

$$x(A) = \{x(s) : s \in A\}. \tag{2.1}$$

Let $G_- \subset S$ be an open set with smooth boundary ∂G and let G_+ be the complement of $G_- \cup \partial G$ in S. Together, G_- and G_+ are called *complementary sets*. Fig. 2.2(a) shows an example of the sets G_-, G_+, and ∂G on a domain $S \subset \mathbb{R}^2$. For $\epsilon > 0$, define the set of points from the boundary ∂G at a distance less than ϵ

$$\partial G_\epsilon = \{s \in S : d(s, \partial G) < \epsilon\}, \tag{2.2}$$

[1]For ease in notation, we assume $x(s) \in \mathbb{R}$, however our results remain valid for $x(s) \in \mathbb{R}^n$, when $n \geq 2$.

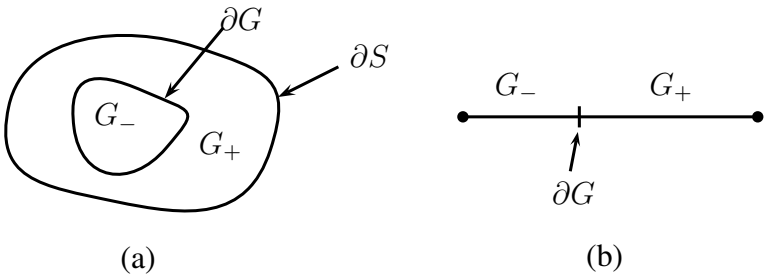

Figure 2.2: (a) An example of complementary sets on a random field defined on S with boundary ∂S. (b) Corresponding notion of complementary sets for a random process.

where $d(t, \partial G)$ is the distance of a point $s \in S$ to the set of points ∂G. On $G_\pm$ and ∂G, define the sets

$$\Sigma_x(G_\pm) = \sigma(x(G_\pm)) \tag{2.3}$$

$$\overline{\Sigma}_x(\partial G) = \bigcap_{\epsilon>0} \sigma(x(\partial G_\epsilon))\,, \tag{2.4}$$

where $\sigma(A)$ stands for the σ-algebra generated by the set A. If $x(s)$ is a *Markov random field*, the conditional expectation of $x(s)$, $s \notin G_-$, given $\Sigma_x(G_-)$ is the conditional expectation of $x(s)$ given $\overline{\Sigma}_x(\partial G)$, i.e., [58], [73]

$$E[x(s)|\Sigma_x(G_-)] = E[x(s)|\overline{\Sigma}_x(\partial G)]\,, \quad s \notin G_-\,. \tag{2.5}$$

Equation (2.5) also holds for Markov random processes for complementary sets defined as in Fig. 2.2(b). In the context of Markov processes, the set G_- in Fig. 2.2(b) is called the "past", G_+ is called the "future", and ∂G is called the "present". The equivalent notions of past, present, and future for random fields is clear from the definition of G_-, G_+, and ∂G in Fig. 2.2(a).

To derive linear stochastic differential equations of MRFs, we assume $x(s)$ is zero mean Gaussian, giving us a Gauss-Markov random field (GMRF), so the conditional expectation in (2.5) becomes a linear projection. Following [73], the key assumptions we make throughout the paper are as follows.

A1. We assume the index set $S \subset \mathbb{R}^d$ is a connected[2] open set with smooth boundary ∂S.

A2. The zero mean GMRF $x(s) \in L^2(\Omega, \mathcal{F}, \mathcal{P})$, which means that $x(s)$ has finite energy.

A3. The covariance of $x(s)$ is $R(t,s)$, where $t, s \in S \subset \mathbb{R}^d$. The function space of $R(t,s)$ is associated with the uniformly strongly elliptic inner product

$$< u, v > = \left\langle D^\alpha u, a_{\alpha,\beta} D^\beta v \right\rangle_T \tag{2.6}$$

$$= \sum_{|\alpha| \le m, |\beta| \le m} \int_T D^\alpha u(s) a_{\alpha,\beta}(s) D^\beta v(s) ds \,, \tag{2.7}$$

where $a_{\alpha,\beta}$ are bounded, continuous, and infinitely differentiable, $\alpha = [\alpha_1, \cdots, \alpha_d]$ is a multi-index of order $|\alpha| = \alpha_1 + \cdots + \alpha_d$ and the operator D^α is the partial derivative operator

$$D^\alpha = D_1^{\alpha_1} \cdots D_d^{\alpha_d} \,, \tag{2.8}$$

where $D_i^{\alpha_i} = \partial^{\alpha_i} / \partial t_i^{\alpha_i}$ for $t = [t_1, \ldots, t_d]$.

A4. Since the inner product in (2.7) is uniformly strongly elliptic, it follows as a consequence of A3 that $R(t,s)$ is jointly continuous, and thus $x(s)$ can be modified to have continuous sample paths. We assume that this modification is done, so the GMRF $x(s)$ has continuous sample paths.

Under Assumptions A1-A4, we now review results on GMRFs we use in this Chapter.

Weak normal derivatives: Let ∂G be a boundary separating complementary sets G_- and G_+. Whenever we refer to normal derivatives, they are to be interpreted in the following weak sense: For every smooth $f(t)$,

$$y(s) = \frac{\partial}{\partial n} x(s)$$

$$\Rightarrow \int_{\partial G} f(s) y(s) dl = \lim_{h \to 0} \frac{\partial}{\partial h} \int_{\partial G} f(s) x(s + h\dot{s}) dl \,, \tag{2.9}$$

[2] A set is connected if it can not be divided into disjoint nonempty closed set.

where dl is the surface measure on ∂G and $\dot{s}$ is the unit vector normal to ∂G at the point s.

GMRFs with order m: Throughout the paper, unless mentioned otherwise, we assume that the GMRF has order m, which can have multiple different equivalent interpretation: (i) the GMRF $x(s)$ has $m-1$ normal derivatives, defined in the weak sense, for each point $s \in \partial G$ for all possible surfaces ∂G, (ii) the σ-algebra $\overline{\Sigma}_x(\partial G)$ in (2.4), called the germ σ-algebra, contains information about $m-1$ normal derivatives of the field on the boundary ∂G [73], or (iii) there exists a symmetric and positive strongly elliptic differential operator $\mathcal{L}_t$ with order $2m$ such that [63]

$$\mathcal{L}_t R(t,s) = \delta(t-s)\,, \tag{2.10}$$

where the differential operator has the form,

$$\mathcal{L}_t u(t) = \sum_{|\alpha|,|\beta| \le m} (-1)^{|\alpha|} D^{\alpha}[a_{\alpha,\beta}(t) D^{\beta}(u(t))]\,. \tag{2.11}$$

Prediction: The following theorem, proved in [73], gives us a closed form expression for the conditional expectation in (2.5).

Theorem 2.2.1 ([73]). *Let $x(s)$, $s \in S \subset \mathbb{R}^d$, be a zero mean GMRF of order m and covariance $R(t,s)$. Consider complementary sets G_- and G_+ with common boundary ∂G. For $s \notin G_-$, the conditional expectation of $x(s)$ given $\Sigma_x(G_-)$ is*

$$E[x(s)|\Sigma_x(G_-)] = \sum_{j=0}^{m-1} \int_{\partial G} b_j(s,r) \frac{\partial^j}{\partial n^j} x(r) dl\,, \tag{2.12}$$

where $\partial^j/\partial n^j$ is the normal derivative, defined in (2.9), dl is a surface measure on the boundary ∂G, and the functions $b_j(s,r)$, $s \notin G_-$ and $r \in \partial G$, are smooth.

Proof. A detailed proof of Theorem 2.2.1 can be found in [73], where the result is proved for the case when $s \in G_+$. To include the case when $s \in \partial G$, we use the fact that $R(t,s)$

is jointly continuous (consequence of A3) and the uniform integrability of the Gaussian measure (see [4]). □

Theorem 2.2.1 says that for each point outside G_-, the conditional expectation given all the points in G_- depends only the field defined on or near the boundary. This is not surprising since, as stated before, $E[x(s)|\Sigma_x(G_-)] = E[x(s)|\overline{\Sigma}_x(\partial G)]$, and we mentioned before that $\overline{\Sigma}_x(\partial G)$ has information about the $m-1$ normal derivatives of $x(s)$ on the surface ∂G. Appendix A.1 shows how the smooth functions $b_j(s,r)$ can be computed and outlines an example of the computations in the context of a Gauss-Markov process. In general, Theorem 2.2.1 extends the notion of a Gauss-Markov *process* of order m (or an autoregressive process of order m) to random fields.

A simple consequence of Theorem 2.2.1 is that we get the following characterization for the covariance of a GMRF of order m.

Theorem 2.2.2. *If $s \in G_-$ and $s \notin G_-$, the covariance $R(t,s)$ can be written as,*

$$R(s,t) = \sum_{j=0}^{m-1} \int_{\partial G} b_j(s,r) \frac{\partial^j}{\partial n^j} R(r,t) dl \,, \tag{2.13}$$

where the normal derivative in (2.13) is with respect to the variable r.

Proof. Since $x(s) - E[x(s)|\Sigma_x(G_-)] \perp x(s)$ for $s \in G_-$, using (2.12), we can easily establish (2.13). □

Theorem 2.2.2 says that the covariance $R(s,t)$ of a GMRF can be written in terms of the covariance of the field defined on a boundary dividing s and t. Both Theorems 2.2.1 and 2.2.2 will be used in deriving the telescoping recursive representation.

2.3 Telescoping Representation: GMRFs on a Unit Disc

In this Section, we present the telescoping recursive representation for GMRFs indexed over a domain $S \subset \mathbb{R}^2$, which is assumed to be a unit disc centered at the origin. The generalization to arbitrary domains is presented in Section 2.4. To parametrize the GMRF,

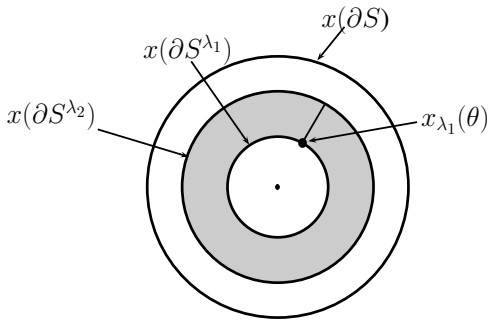

Figure 2.3: A random field defined on a unit disc. The boundary of the field, i.e., the field values defined on the circle with radius 1 is denoted by $x(\partial S)$. The field values at a distance of $1-\lambda$ from the center of the field are given by $x(\partial S^{\lambda})$. Each point is characterized in polar coordinates as $x_{\lambda}(\theta)$, where $1-\lambda$ is the distance to the center and θ denotes the angle.

say $x(s)$ for $s \in S$, we use polar coordinates such that $x_{\lambda}(\theta)$ is defined to be the point

$$x_{\lambda}(\theta) = x((1-\lambda)\cos\theta, (1-\lambda)\sin\theta)\,, \tag{2.14}$$

where $(\lambda, \theta) \in [0,1] \times [-\pi, \pi]$. Thus, $\{x_0(\theta) : \theta \in [-\pi, \pi]\}$ corresponds to the field defined on the boundary of the unit disc, denoted as ∂S. Let ∂S^{λ} denote the set of points in S at a distance $1-\lambda$ from the center of the field. We call ∂S^{λ} a *telescoping surface* since the telescoping representations we derive recurse these surfaces. The notations introduced so far are shown in Fig. 2.3.

2.3.1 Main Theorem

Before deriving our main theorem regarding the telescoping representation, we first define some notation. Let $x(s) \in \mathbb{R}$ be a zero mean GMRF defined on a unit disc $S \subset \mathbb{R}^2$ parametrized as $x_{\lambda}(\theta)$, defined in (2.14). Let $\Theta = [-\pi, \pi]$ and denote the covariance between $x_{\lambda_1}(\theta_1)$ and $x_{\lambda_2}(\theta_2)$ by $R_{\lambda_1,\lambda_2}(\theta_1, \theta_2)$ such that

$$R_{\lambda_1,\lambda_2}(\theta_1, \theta_2) = E[x_{\lambda_1}(\theta_1) x_{\lambda_2}(\theta_2)]\,. \tag{2.15}$$

Define $C_\lambda(\theta_1, \theta_2)$ and $B_\lambda(\theta)$ as

$$C_\lambda(\theta_1, \theta_2) = \lim_{\mu \to \lambda^-} \frac{\partial}{\partial \mu} R_{\mu,\lambda}(\theta_1, \theta_2) - \lim_{\mu \to \lambda^+} \frac{\partial}{\partial \mu} R_{\mu,\lambda}(\theta_1, \theta_2) \tag{2.16}$$

$$B_\lambda(\theta) = \begin{cases} \sqrt{C_\lambda(\theta, \theta)} & C_\lambda(\theta, \theta) \neq 0 \\ K & C_\lambda(\theta, \theta) = 0 \end{cases}, \tag{2.17}$$

where K is any non-zero constant. We will see in (A.31) that $C_\lambda(\theta, \theta)$ is the variance of a random variable and hence it is non-negative. Define F_θ as the integral transform

$$F_\theta[x_\lambda(\theta)] = \sum_{j=0}^{m-1} \int_\Theta \lim_{\mu \to \lambda^+} \frac{\partial}{\partial \mu} b_j((\mu, \theta), (\lambda, \alpha)) \frac{\partial^j}{\partial n^j} x_\lambda(\alpha) d\alpha \,, \tag{2.18}$$

where $b_j((\mu, \theta), (\lambda, \alpha))$ is defined in (2.12) and the index (μ, θ) in polar coordinates corresponds to the point $((1-\mu)\cos\theta, (1-\mu)\sin\theta)$ in Cartesian coordinates. We see that $F_\theta[x_\lambda(\theta)]$ operates on the surface ∂S^λ such that it is a linear combination of all normal derivatives of $x_\lambda(\theta)$ up to order $m-1$. The normal derivative in (2.18) is interpreted in the weak sense as defined in (2.9). We now state the main theorem of the paper.

Theorem 2.3.1 (**Telescoping Recursive Representation**). *For the GMRF parametrized as $x_\lambda(\theta)$, defined in (2.14), we have the following stochastic differential equation*

$$dx_\lambda(\theta) = F_\theta[x_\lambda(\theta)]d\lambda + B_\lambda(\theta) dw_\lambda(\theta) \,, \tag{2.19}$$

where $dx_\lambda(\theta) = x_{\lambda+d\lambda}(\theta) - x_\lambda(\theta)$ for $d\lambda$ small, F_θ is defined in (2.18), $B_\lambda(\theta)$ is defined in (2.17), and $w_\lambda(\theta)$ has the following properties:

i) The driving noise $w_\lambda(\theta)$ is zero mean Gaussian, almost surely continuous in λ, and independent of $x(\partial S)$ (the field on the boundary).

ii) For all $\theta \in \Theta$, $w_0(\theta) = 0$.

iii) For $0 \leq \lambda_1 \leq \lambda_1' \leq \lambda_2 \leq \lambda_2'$ and $\theta_1, \theta_2 \in \Theta$, $w_{\lambda_1'}(\theta_1) - w_{\lambda_1}(\theta_1)$ and $w_{\lambda_2'}(\theta_2) - w_{\lambda_2}(\theta_2)$ are independent random variables.

iv) For $\theta \in \Theta$, we have

$$E[w_\lambda(\theta_1)w_\lambda(\theta_2)] = \int_0^\lambda \frac{C_u(\theta_1,\theta_2)}{B_u(\theta_1)B_u(\theta_2)}du\,. \tag{2.20}$$

v) Assuming the set $\{u \in [0,1] : C_u(\theta,\theta) = 0\}$ has measure zero for each $\theta \in \Theta$, for $\lambda_1 > \lambda_2$ and $\theta_1, \theta_2 \in \Theta$, the random variable $w_{\lambda_1}(\theta_1) - w_{\lambda_2}(\theta_2)$ is Gaussian with mean zero and covariance

$$E\left[\left(w_{\lambda_1}(\theta_1) - w_{\lambda_2}(\theta_2)\right)^2\right] = \lambda_1 + \lambda_2 - 2\int_0^{\lambda_2} \frac{C_u(\theta_1,\theta_2)}{B_u(\theta_1)B_u(\theta_2)}du\,. \tag{2.21}$$

Proof. See Appendix A. □

Theorem 2.3.1 says that $x_{\lambda+d\lambda}(\theta)$, where $d\lambda$ is small, can be computed using the random field defined on the telescoping surface ∂S^λ and some random noise. The dependence on the telescoping surface follows from Theorem 2.2.1. The main contribution in Theorem 2.3.1 is to explicitly compute properties of the driving noise $w_\lambda(\theta)$. We now discuss the telescoping representation and highlight its various properties.

Driving noise $w_\lambda(\theta)$: The properties of the driving noise $w_\lambda(\theta)$ in (2.19) lead to the following theorem.

Theorem 2.3.2 (Driving noise $w_\lambda(\theta)$)**.** *For the collection of random variables*

$$\{w_\lambda(\theta) : (\lambda,\theta) \in [0,1] \times \Theta\}$$

defined in (2.19), for each fixed $\theta \in \Theta$, $w_\lambda(\theta)$ is a standard Brownian motion when the set $\{u \in [0,1] : C_u(\theta,\theta) = 0\}$ has measure zero for each $\theta \in \Theta$.

Proof. For fixed $\theta \in \Theta$, to show $w_\lambda(\theta)$ is Brownian motion, we need to establish the following: (i) $w_\lambda(\theta)$ is continuous in λ, (ii) $w_0(\theta) = 0$ for all $\theta \in \Theta$, (iii) $w_\lambda(\theta)$ has independent increments, *i.e.*, for $0 \le \lambda_1 \le \lambda_1' \le \lambda_2 \le \lambda_2'$, $w_{\lambda_1'}(\theta) - w_{\lambda_1}(\theta)$ and $w_{\lambda_2'}(\theta) - w_{\lambda_2}(\theta)$ are independent random variables, and (iv) for $\lambda_1 > \lambda_2$, $w_{\lambda_1}(\theta) - w_{\lambda_2}(\theta) \sim \mathcal{N}(0, \lambda_1 - \lambda_2)$.

The first three points follow from Theorem 2.3.1. To show the last point, let $\theta_1 = \theta_2$ in (2.21) and use the computations done in (A.39)-(A.42). □

Theorem 2.3.2 says that for each fixed θ, $w_\lambda(\theta)$ in (2.19) is Brownian motion. This is extremely useful since we can use standard Ito calculus to interpret (2.19).

White noise: A useful interpretation of $w_\lambda(\theta)$ is in terms of white noise. Define a random field $v_\lambda(\theta)$ such that

$$w_\lambda(\theta) = \int_0^\lambda v_\gamma(\theta) d\gamma \,. \tag{2.22}$$

Using Theorem 2.3.1, we can easily establish that $v_\lambda(\theta)$ is a generalized process such that for an appropriate function $\Psi(\cdot)$,

$$\int_0^1 \Psi(\gamma) E[v_\gamma(\theta_1) v_\lambda(\theta_2)] d\gamma = \Psi(\lambda) \frac{C_\lambda(\theta_1, \theta_2)}{B_\lambda(\theta_1) B_\lambda(\theta_2)} \,, \tag{2.23}$$

which is equivalent to the expression

$$E[v_{\lambda_1}(\theta_1) v_{\lambda_2}(\theta_2)] = \delta(\lambda_1 - \lambda_2) \frac{C_{\lambda_1}(\theta_1, \theta_2)}{B_{\lambda_1}(\theta_1) B_{\lambda_2}(\theta_2)} \,. \tag{2.24}$$

Using the white noise representation, an alternative form of the telescoping representation is given by

$$\frac{dx_\lambda(\theta)}{d\lambda} = F_\theta[x_\lambda(\theta)] + B_\lambda(\theta) v_\lambda(\theta) \,. \tag{2.25}$$

Boundary Conditions: From the form of the integral transform F_θ in (2.18), it is clear that boundary conditions for the telescoping representation will be given in terms of the field defined at the boundary and its normal derivatives. A general form for the boundary conditions can be given as

$$\sum_{j=0}^{m-1} \int_\Theta c_{k,j}(\theta, \alpha) \frac{\partial^j}{\partial n^j} x_0(\alpha) d\alpha = \beta_k(\theta) \,, \theta \in \Theta \,, k = 1, \ldots, m \,, \tag{2.26}$$

where for each k, $\beta_k(\theta)$ is a Gaussian process in θ with mean zero and known covariance.

Integral Form: The representation in (2.19) is a symbolic representation for the equation

$$x_{\lambda_1}(\theta) = x_{\lambda_2}(\theta) + \int_{\lambda_2}^{\lambda_1} F_\theta[x_\mu(\theta)]d\mu + \int_{\lambda_2}^{\lambda_1} B_\mu(\theta)dw_\mu(\theta)\,, \quad \lambda_1 > \lambda_2\,. \tag{2.27}$$

Since from Theorem 2.3.2, $w_\lambda(\theta)$ is Brownian motion for fixed θ, the last integral in (2.27) is an Wiener integral. Thus, to recursively synthesize the field, we start with boundary values, given by (2.26), and generate the field values recursively on the telescoping surfaces ∂S^λ for $\lambda \in (0, 1]$.

Comparison to [84]: The telescoping recursive representation differs significantly from the recursive representation derived in [84]. Firstly, the representation in [84] is only valid for isotropic GMRFs and does not hold for nonisotropic GMRFs. The telescoping representation we derive holds for arbitrary GMRFs. Secondly, the recursive representation in [84] was derived on the Fourier series coefficients, whereas we derive a representation directly on the field values.

2.3.2 Homogeneous and Isotropic GMRFs

In this Section, we study homogeneous isotropic random fields over $\mathbb{R}^2$ whose covariance only depends on the Euclidean distance between two points. In general, suppose $R_{\mu,\lambda}(\theta_1, \theta_2)$ is the covariance of a homogeneous isotropic random field over a unit disc such that the point (μ, θ_1) in polar coordinates corresponds to the point $((1-\mu)\cos\theta, (1-\mu)\sin\theta)$ in Cartesian coordinates. The Euclidean distance between two points (μ, θ_1) and (λ, θ_2) is given by

$$D_{\mu,\lambda}(\theta_1, \theta_2) = \left[(1-\mu)^2 + (1-\lambda)^2 - 2(1-\mu)(1-\lambda)\cos(\theta_1 - \theta_2)\right]^{1/2}\,. \tag{2.28}$$

If $R_{\mu,\lambda}(\theta_1, \theta_2)$ is the covariance of a homogeneous and isotropic GMRF, we have

$$R_{\mu,\lambda}(\theta_1, \theta_2) = \Upsilon\left(D_{\mu,\lambda}(\theta_1, \theta_2)\right)\,, \tag{2.29}$$

where $\Upsilon(\cdot) : \mathbb{R} \to \mathbb{R}$ is assumed to be differentiable at all points in $\mathbb{R}$. The next Lemma computes $C_\lambda(\theta_1, \theta_2)$ for isotropic and homogeneous GMRFs.

Lemma 2.3.1. *For an isotropic and homogeneous GMRF with covariance given by (2.29), $C_\lambda(\theta_1, \theta_2)$, defined in (2.16), is given by*

$$C_\lambda(\theta_1, \theta_2) = \begin{cases} 0 & \theta_1 \neq \theta_2 \\ -2\Upsilon'(0) & \theta_1 = \theta_2 \end{cases} . \tag{2.30}$$

Proof. For $\theta_1 \neq \theta_2$, we have

$$\frac{\partial}{\partial u} R_{\mu,\lambda}(\theta_1, \theta_2) = -\Upsilon'\left(D_{\mu,\lambda}(\theta_1, \theta_2)\right) \frac{(1-\mu) - (1-\lambda)\cos(\theta_1 - \theta_2)}{D_{\mu,\lambda}(\theta_1, \theta_2)} , \tag{2.31}$$

where $\Upsilon'(\cdot)$ is the derivative of the function $\Upsilon(\cdot)$. Using (2.16), $C_\lambda(\theta_1, \theta_2) = 0$ when $\theta_1 \neq \theta_2$.

For $\theta_1 = \theta_2$, $D_{\mu,\lambda}(\theta_1, \theta_2) = |\mu - \lambda|$, so we have

$$\frac{\partial}{\partial u} R_{\mu,\lambda}(\theta_1, \theta_2) = -\Upsilon'(|\lambda - \mu|) \frac{\lambda - \mu}{|\lambda - \mu|} , \tag{2.32}$$

Using (2.16), $C_\lambda(\theta_1, \theta_2) = -2\Upsilon'(0)$ when $\theta_1 = \theta_2$. □

Using Lemma 2.3.1, we have the following theorem regarding the driving noise $w_\lambda(\theta)$ of the telescoping representation of an isotropic and homogeneous GMRF.

Theorem 2.3.3 (Homogeneous isotropic GMRFs)**.** *For homogeneous isotropic GMRFs, with covariance given by (2.29), such that $\Upsilon(\cdot)$ is differentiable at all points in $\mathbb{R}$ and $\Upsilon'(0) < 0$, the telescoping representation is*

$$dw_\lambda(\theta) = F_\theta x_\lambda(\theta) + \sqrt{-\Upsilon'(0)} dw_\lambda(\theta) . \tag{2.33}$$

For each fixed θ, $w_\lambda(\theta)$ is Brownian motion in λ and

$$E[w_{\lambda_1}(\theta_1) w_{\lambda_2}(\theta_2)] = 0 , \quad \lambda_1 \neq \lambda_2, \theta_1 \neq \theta_2 \tag{2.34}$$

$$E[w_\lambda(\theta_1)w_\lambda(\theta_2)] = 0\,, \quad \theta_1 \neq \theta_2\,. \tag{2.35}$$

Proof. Since we assume $\Upsilon'(0) < 0$, thus $B_\lambda(\theta) = C_\lambda(\theta,\theta) = \sqrt{-\Upsilon'(0)}$, which gives us (2.33). To show (2.34) and (2.35), we simply substitute the value of $C_\lambda(\theta_1,\theta_2)$, given by (2.30), in (2.20) and use the independent increments property of $w_\lambda(\theta)$ given in Theorem 2.3.1. □

Example: We now consider an example of a homogeneous and isotropic GMRF where $\Upsilon'(0) = 0$ and thus the field is uniquely determined by the boundary conditions. Let $\Upsilon(s)$, $s \in [0,\infty)$, be such that

$$\Upsilon(t) = \int_0^\infty \frac{b}{(1+b^2)^2} J_0(bt)db\,, \tag{2.36}$$

where $J_n(\cdot)$ is the Bessel function of the first kind of order n [97]. The derivative of $\Upsilon(t)$ is given by

$$\Upsilon'(t) = -\int_0^\infty \frac{b^2}{(1+b^2)^2} J_1(bt)db\,, \tag{2.37}$$

where we use the fact that $J_0'(\cdot) = -J_1(\cdot)$ [97]. Since $J_1(0) = 0$, $\Upsilon'(0) = 0$ and thus $B_\lambda(\theta) = 0$ in the telescoping representation. This means there is no driving noise in the telescoping representation. The rest of the parameters of the telescoping representation can be computed using the fact [103]

$$(\Delta - 1)^2 R(t,s) = \delta(t-s)\,, \tag{2.38}$$

where $R(t,s)$ corresponds to the covariance associated with $\Upsilon(\cdot)$ written in Cartesian coordinates and Δ is the Laplacian operator. Since the operator associated with $R(t,s)$ in (2.38) has order four, it is clear that the GMRF has order two. The field with covariance satisfying (2.38) is also commonly referred to as the Whittle field [102]. The telescoping recursive representation will be of the form

$$dx_\lambda(\theta) = \int_{-\pi}^{\pi} \lim_{\mu\to\lambda^+} \left[\frac{\partial}{\partial u} b_0((\mu,\theta),(\lambda,\alpha))x_\lambda(\alpha) + \frac{\partial}{\partial u} b_1((\mu,\theta),(\lambda,\alpha))\frac{\partial}{\partial n} x_\lambda(\alpha)\right] d\alpha\, d\lambda\,,$$

where $0 \leq \lambda \leq 1$ with appropriate boundary conditions defined on the unit circle.

2.4 Telescoping Representation: GMRFs on arbitrary domains

In the last Section, we presented telescoping recursive representations for random fields defined on a unit disc. In this Section, we generalize the telescoping representations to arbitrary domains. Section 2.4.1 shows how to define telescoping surfaces using the concept of homotopy. Section 2.4.2 shows how to parametrize arbitrary domains using the homotopy. Section 2.4.3 presents the telescoping representation for GMRFs defined on arbitrary domains.

2.4.1 Telescoping Surfaces Using Homotopy

Informally, a homotopy is defined as a continuous deformation from one space to another. Formally, given two continuous functions f and g such that $f, g : \mathcal{X} \rightarrow \mathcal{Y}$, a homotopy is a continuous function $h : \mathcal{X} \times [0,1] \rightarrow \mathcal{Y}$ such that if $x \in \mathcal{X}$, $h(x,0) = f(x)$ and $h(x,1) = g(x)$ [64]. An example of the use of homotopy in neural networks is shown in [16].

In deriving our telescoping representation for GMRFs on a unit disc in Section 2.3, we saw that the recursions started at the boundary, which was the unit circle, and telescoped inwards on concentric circles and ultimately converged to the center of the unit disc. To parametrize these recursions, we can define a homotopy from the unit circle to the center of the unit disc. In general, for a domain $S \subset \mathbb{R}^d$ with smooth boundary ∂S, the telescoping surfaces can be defined using a homotopy, $h : \partial S \times [0,1] \rightarrow c$, from the boundary ∂S to a point $c \in S$ such that

P1. $\{h(s,0) : s \in \partial S\} = \partial S$ and $\{h(s,1) : s \in \partial S\} = c$.

P2. For $0 < \lambda \leq 1$, $\{h(s,\lambda) : s \in \partial S\} \subset S$ is the boundary of the region $\{h(s,\mu) : (s,\mu) \in \partial S \times (\lambda, 1)\}$.

P3. For $\lambda_1 < \lambda_2$, $\{h(s,\lambda_1), s \in \partial S\} \subset \{h(s,\mu), s \in \partial S, 0 \leq \mu \leq \lambda_2\}$.

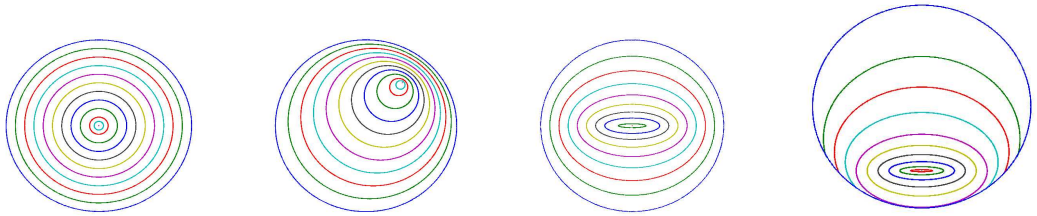

(a) (b) (c) (d)

Figure 2.4: Telescoping surfaces defined using different homotopies.

P4. $\bigcup_\lambda \{h(s,\lambda), s \in \partial S\} = S$.

Property 1 says that, for $\lambda = 0$, we get the boundary ∂S and for $\lambda = 1$, we get the point $c \in S$, which we choose arbitrarily. Property 2 says that for each λ, we want the telescoping surfaces to be in S and it should be a boundary of another region. Property 3 restricts the surfaces to be contained within each other, and Property 4 says that the homotopy must sweep the whole index set S.

Using the homotopy, for each λ, we can define a telescoping surface ∂S^λ such that

$$\partial S^\lambda = \{h(\theta,\lambda) : \theta \in \partial S\}\,, \tag{2.39}$$

where ∂S is the boundary of the field. As an example, we consider defining different telescoping surfaces for the field defined on a unit disc. The boundary of the unit disc can be parametrized by the set of points

$$\partial S = \{(\cos\theta, \sin\theta), \theta \in [-\pi, \pi]\}\,. \tag{2.40}$$

We consider four different kinds of telescoping surfaces:

a) The telescoping surfaces in Fig 2.4(a) are generated using the homotopy

$$h((\cos\theta,\sin\theta),\lambda) = ((1-\lambda)\cos\theta, (1-\lambda)\sin\theta)\,. \tag{2.41}$$

b) The telescoping surfaces in Fig 2.4(b) can be generated by the homotopy

$h((\cos\theta, \sin\theta), \lambda)$

$$= ((1-\lambda)(\cos\theta - c_1) + c_1, (1-\lambda)(\sin\theta - c_2) + c_2)\,, \tag{2.42}$$

$$= ((1-\lambda)\cos\theta + c_1 - (1-\lambda)c_1, \tag{2.43}$$

$$(1-\lambda)\cos\theta + c_2 - (1-\lambda)c_2)\,,$$

where (c_1, c_2) is inside the unit disc, *i.e.*, $c_1^2 + c_2^2 < 1$. For the homotopy in (2.41), each telescoping surface is centered about the origin, whereas the telescoping surfaces in (2.43) are centered about the point $(c_1 - (1-\lambda)c_1, c_2 - (1-\lambda)c_2)$.

c) In Fig 2.4(a)-(b), the telescoping surfaces are circles, however, we can also have other shapes for the telescoping surface. Fig 2.4(c) shows an example in which the telescoping surface is an ellipse, which we generate using the homotopy

$$h((\cos\theta, \sin\theta), \lambda) = (a_\lambda \cos\theta, b_\lambda \sin\theta) \tag{2.44}$$

where a_λ and b_λ are continuous functions chosen in such a way that P1-P4 are satisfied for h. In Fig 2.4(c), we choose $a_\lambda = \lambda$ and $b_\lambda = \lambda^2$.

d) Another example of a set of telescoping surfaces is shown in Fig 2.4(d). From here, we notice that two telescoping surfaces may have common points.

Apart from the telescoping surfaces for a unit disc shown in Fig 2.4(a)-(d), we can define many more telescoping surfaces. The basic idea in obtaining these surfaces, which is compactly captured by defining a homotopy, is to continuously deform the boundary of the index set until we converge to a point within the index set. In the next Section, we provide a characterization of continuous index sets in $\mathbb{R}^d$ for which we can easily find telescoping surfaces by simply scaling and translating the points on the boundary.

2.4.2 Generating Similar Telescoping Surfaces

From Section 2.4.1, it is clear that, for a given domain, many different telescoping surfaces can be obtained by defining different homotopies. In this Section, we identify domains on which we can easily generate a set of telescoping surfaces, which we call *similar telescoping surfaces*.

Definition 1 (Similar Telescoping Surfaces)**.** *Two telescoping surfaces are* similar *if there exists an affine map between them,* i.e.*, we can map one to another by scaling and translating of the coordinates. A set of telescoping surfaces are similar if each pair of telescoping surfaces in the set are similar.*

As an example, the set of telescoping surfaces in Fig 2.4(a)-(b) are similar since all the telescoping surfaces are circles. On the other hand, the telescoping surfaces in Fig 2.4(c)-(d) are not similar since each telescoping surfaces has a different shape. The following theorem shows that, for certain index sets, we can always find a set of similar telescoping surfaces.

Theorem 2.4.1. *For a domain $T \in \mathbb{R}^d$ with boundary ∂S if there exists a point $c \in S$ such that, for all $s \in S \cup \partial S$ and $\lambda \in [0,1]$, $(1-\lambda)t + \lambda c \in S$, we can generate similar telescoping surfaces using the homotopy*

$$h(\theta, \lambda) = (1-\lambda)\theta + \lambda c\,, \quad \theta \in \partial S\,. \tag{2.45}$$

Proof. Given the homotopy in (2.45), the telescoping surfaces are given by $\partial S^\lambda = \{h(\theta,\lambda) : \theta \in \partial S\}$. Using (2.45), it is clear that $\partial S^0 = \partial S$ and $\partial S^1 = c$. Given the assumption, we have that $\partial S^\lambda \subset S$ for $0 < \lambda \leq 1$. Since the distance of each point on ∂S^λ to the point c is $(1-\lambda)||\theta - c||$, it is clear that, for $\lambda_1 < \lambda_2$, $\partial S^{\lambda_1} \subset \{\partial S^\mu : 0 \leq \mu \leq \lambda_2\}$. This shows that the homotopy in (2.45) defines a valid telescoping surface. The set of telescoping surfaces is similar since we are only scaling and translating the boundary ∂S. □

Examples of similar telescoping surfaces generated using the homotopy in (2.45) are shown in Fig 2.5(a) and Fig 2.5(c). Choosing an appropriate c is important to generate

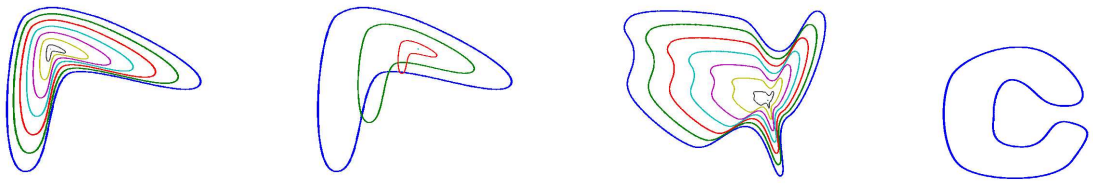

(a) (b) (c) (d)

Figure 2.5: Telescoping surfaces defined using different homotopies on arbitrary regions.

similar telescoping surfaces. For example, Fig 2.5(b) shows an example where telescoping surfaces are generated using (2.45). It is clear that these surfaces do not satisfy the desired properties of telescoping surfaces. Fig 2.5(d) shows an example of an index set for which similar telescoping surfaces do not exist since there exists no point c for which $(1-\lambda)s + \lambda c \in S$ for all $\lambda \in [0,1]$ and $s \in S \cup \partial S$.

2.4.3 Telescoping Representations

We now generalize the telescoping representation to GMRFs defined on arbitrary domains. Let $x(s)$ be a zero mean GMRF, where $s \in S \subset \mathbb{R}^d$ such that the smooth boundary of S is ∂S. Define a set of telescoping surfaces ∂S^λ constructed by defining a homotopy $h(\theta, \lambda)$, where $\theta \in \partial S$ and $\lambda \in [0,1]$. We parametrize the GMRF $x(s)$ as $x_\lambda(\theta)$ such that

$$x_\lambda(\theta) = x(h(\theta, \lambda))\,. \tag{2.46}$$

Denote $\Theta = \partial S$ and define $C_\lambda(\theta_1, \theta_2)$, $B_\lambda(\theta)$, and F_θ by (2.16), (2.17), and (2.18), respectively. Although the initial definition for these values was for $\Theta = [-\pi, \pi]$ and $x_\lambda(\theta)$ parametrized in polar coordinates, assume the definitions in (2.16), (2.17), and (2.18) are in terms of the parameters defined in this Section. The normal derivatives in the definition of F_θ for a point $x_\lambda(\theta)$ will be computed in the direction normal to the telescoping surface ∂S^λ at the point $h(\theta, \lambda)$. The telescoping representation is given by

$$dx_\lambda(\theta) = F_\theta[x_\lambda(\theta)]d\lambda + B_\lambda(\theta)dw_\lambda(\theta) \tag{2.47}$$

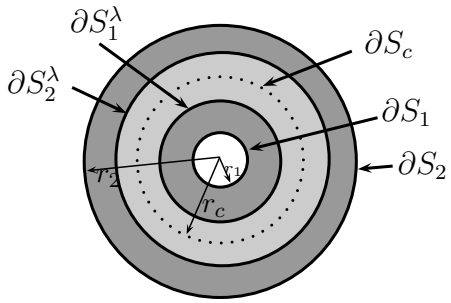

Figure 2.6: An example of a random field pinned to two boundaries.

where the $w_\lambda(\theta) = w(h(\theta, \lambda))$ is the driving noise with the same properties as outlined in Theorem 2.3.1. It is clear from (2.47), that the recursions for the GMRF initiate at the boundary and recurse inwards along the telescoping surfaces defined using the homotopy $h(\theta, \lambda)$. Thus, the recursions are effectively captured by the parameter λ.

2.5 GMRFs Pinned to Two Boundaries

So far we have considered GMRFs that are pinned to a single boundary. In this Section, we show that the telescoping representations extend to GMRFs pinned to two boundaries. An example of where such models can be used is in modeling the temperature distribution of a thick pipe with appropriate boundary conditions on the inside and outside wall. Let $x(s) \in \mathbb{R}$ be an MRF of order m on a domain $S = \text{int}(S_2 \backslash S_1)$, where $\text{int}(A)$ is the interior of the set A and $S_1 \subset S_2 \subset \mathbb{R}^d$, $d \geq 2$. Denote the smooth boundaries of S_1 and S_2 as ∂S_1 and ∂S_2, respectively. We assume that the field is driven by boundary conditions on ∂S_1 and ∂S_2. The telescoping representations derived for GMRFs pinned to a single boundary do not directly apply to GMRFs pinned to multiple boundaries since we need to take into account the effect of both boundary values. For example, if we could write down recursive equations that initiate at the boundary ∂S_2 and recurse inwards to the boundary ∂S_1, this representation would not be consistent with the original distribution since it would not use the initial conditions on ∂S_1. Thus, we need to derive recursive representations that capture the boundary conditions on both ∂S_1 and ∂S_2.

For notational simplicity, we assume S_1 and S_2 are discs in $\mathbb{R}^2$. The representations derived can be easily generalized to arbitrary domains using homotopy. We assume S_1 (S_2) is a disc of radius r_1 (r_2), where $r_1 < r_2$. Consider a disc S_c of radius r_c, as shown in Fig. 2.6, such that $r_1 < r_c < r_2$ and denote its boundary as ∂S_c. We parametrize the GMRF using polar coordinates such that

$$x_\mu(\theta) = x(\mu\cos\theta, \mu\sin\theta), r_1 < \mu < r_2, \theta \in [0, 2\pi)\,. \tag{2.48}$$

For $0 \leq \lambda \leq 1$, let ∂S_1^λ be the boundary of the disc S_1^λ with radius $r_1 + \lambda(r_c - r_1)$ and let ∂S_2^λ be the boundary of the disc S_2^λ with radius $r_2 + \lambda(r_c - r_2)$. We see that S_1^λ lies between S_1 and S_c and S_2^λ lies between S_2 and S_c. The notations introduced so far are shown in Fig. 2.6. Define $z_\lambda^c(\theta) \in \mathbb{R}^2$ on ∂S_1^λ and ∂S_2^λ such that

$$z_\lambda^c(\theta) = \begin{bmatrix} x_{r_1+\lambda(r_c-r_1)}(\theta) \\ x_{r_2+\lambda(r_c-r_2)}(\theta) \end{bmatrix}, 0 \leq \lambda \leq 1\,, \theta \in [0, 2\pi)\,. \tag{2.49}$$

Thus, we have embedded the original random field, which takes values in $\mathbb{R}$ into another random field which takes values in $\mathbb{R}^2$. For $\lambda = 0$, $z_0^c(\theta)$ corresponds to the boundary values of the random field $x(s)$. As λ increases, we approach the circle of radius r_c from the inner and outer boundary. Thus, we have converted the boundary valued problem into an initial value problem with initial conditions given by $z_0^c(\theta)$ for $\theta \in [0, 2\pi)$, where

$$z_0^c(\theta) = \begin{bmatrix} x_{r_1}(\theta) \\ x_{r_2}(\theta) \end{bmatrix}\,. \tag{2.50}$$

Another way to visualize the construction of $z_\lambda^c(\theta)$ is through an Origami type folding of the index set, which is outlined in Fig. 2.7. The idea is to fold the index set in such a way that the boundaries are combined into one state. We have the following Lemma that characterizes the recursions on the GMRF.

Lemma 2.5.1. *For the random field $\widehat{z}_\lambda^c(\theta)$ defined in (2.49), let $\widehat{z}_{\lambda+d\lambda|\lambda}^c(\theta)$ denote the conditional expectation of $z_{\lambda+d\lambda}^c(\theta)$ given the σ-algebra generated by the field $\{z_\mu^c(\alpha)$:*

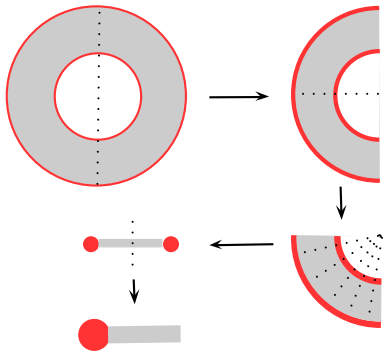

Figure 2.7: Starting with the original domain with two boundaries (shown in red), we first fold along the diameter (shown as a dotted line). This leads to a semi-circle. In the semi-circle, we observe that the boundaries are shown in thicker lines. This corresponds to the overlapping of boundaries when folding. Next, we fold along the radius shown as a dotted line. After this, we continually fold the domain in the radial direction. We then fold from the middle of the line so that both boundary values now overlap and the random field that was pinned to two boundaries can now be interpreted as pinned to one boundary.

$(\mu, \alpha) \in [0, \lambda] \times \Theta\}$. *There exists a* 2×2 *matrix* $b_j^z\left((\lambda + d\lambda, \theta), (\lambda, \alpha)\right)$ *such that*

$$\widehat{z}^c_{\lambda+d\lambda|\lambda}(\theta) = \sum_{j=0}^{m-1} \int_0^{2\pi} b_j^z((\lambda + d\lambda, \theta), (\lambda, \alpha)) \frac{d^j}{dn^j} z^c_\lambda(\alpha) d\alpha \,. \tag{2.51}$$

Proof. Since $x(s)$ is a GMRF, the result follows from Theorem 2.2.1. □

Using Lemma 2.5.1 and following similar steps as in the proof of the telescoping representation in (2.19), we can derive the following representation for $z^c_\lambda(\theta)$:

$$dz^c_\lambda(\theta) = F^z_\theta[z^c_\lambda(\theta)]d\lambda + B^z_\lambda(\theta) w^c_\lambda(\theta) \,, \tag{2.52}$$

where F^z_θ and $B^z_\lambda(\theta)$ can be defined in similar manner as in (2.18) and (2.17), respectively. Note that the coefficient in (2.19) are scalar, whereas the coefficients in (2.52) are matrices (since $z^c_\lambda(\theta) \in \mathbb{R}^2$). Thus, the recursions start at both the boundaries and recursive towards the surface ∂S_c.

2.6 Recursive Estimation of GMRFs

Using the telescoping representation, we now derive recursive equations for estimating GMRFs. Let $x(s)$ be the zero mean GMRF defined on an index set $S \subset \mathbb{R}^d$ with smooth boundary ∂S. Assume the parametrization $x_\lambda(\theta) = x(h(\theta, \lambda))$, where $h(\theta, \lambda)$ is an appropriate homotopy and $\theta \in \Theta = \partial S$. The corresponding telescoping representation is given in (2.47).

Consider the observations, written in parametric form, as

$$dy_\lambda(\theta) = G_\lambda(\theta)x_\lambda(\theta)d\lambda + D_\lambda(\theta)dn_\lambda(\theta)\,,\ 0 \le \lambda \le 1\,, \tag{2.53}$$

where $G_\lambda(\theta)$ and $D_\lambda(\theta)$ are known functions with $D_\lambda(\theta) \neq 0$, $y_0(\theta) = 0$ for all $\theta \in \Theta$, $n_\lambda(\theta)$ is standard Brownian motion for each fixed θ such that

$$E[n_{\lambda_1}(\theta_1)n_{\lambda_2}(\theta_2)] = 0\,, \quad \lambda_1 \neq \lambda_2, \theta_1 \neq \theta_2\,, \tag{2.54}$$

and $n_\lambda(\theta)$ is independent GMRF $x_\lambda(\theta)$.

We consider the filtering and smoothing problem for GMRFs. For random fields, because of the multidimensional index set, it is not clear how to define the filtered estimate. For Markov processes, the filtered estimate sweeps the data in a causal manner, because the process itself admits a causal representation. To define the filtered estimate for GMRFs, we sweep the observations over the telescoping surfaces defined in the telescoping recursive representation in (2.47). Define the filtered estimate $\widehat{x}_{\lambda|\lambda}(\theta)$, error $\widetilde{x}_{\lambda|\lambda}(\theta)$, and error covariance $S_\lambda(\alpha, \beta)$ such that

$$\widehat{x}_{\lambda|\lambda}(\theta) \triangleq E\left[x_\lambda(\theta)|\sigma\{y_\mu(\theta)\,, 0 \le \mu \le \lambda, \theta \in \Theta\}\right] \tag{2.55}$$

$$\widetilde{x}_{\lambda|\lambda}(\theta) \triangleq x_{\lambda|\lambda}(\theta) - \widehat{x}_{\lambda|\lambda}(\theta) \tag{2.56}$$

$$S_\lambda(\alpha, \beta) \triangleq E[\widetilde{x}_{\lambda|\lambda}(\alpha)\widetilde{x}_{\lambda|\lambda}(\beta)]\,. \tag{2.57}$$

The set $\{y_\mu(\theta)\,, 0 \le \mu \le \lambda, \theta \in \Theta\}$ consists of the region between the boundary of the

field, ∂S, and the surface ∂S^{λ}. A stochastic differential equation for the filtered estimate $\widehat{x}_{\lambda|\lambda}(\theta)$ is given in the following theorem.

Theorem 2.6.1 (**Recursive Filtering of GMRFs**). *For the GMRF $x_\lambda(\theta)$ with observations $y_\lambda(\theta)$, a stochastic differential equation for the filtered estimate $\widehat{x}_{\lambda|\lambda}(\theta)$, defined in (2.55), is given as follows:*

$$d\widehat{x}_{\lambda|\lambda}(\theta) = F_\theta[\widehat{x}_{\lambda|\lambda}(\theta)]d\lambda + K_\theta[de_\lambda(\theta)]\,, \tag{2.58}$$

where $e_\lambda(\theta)$ is the innovation field such that

$$D_\lambda(\theta)de_\lambda(\theta) = dy_\lambda(\theta) - G_\lambda(\theta)\widehat{x}_{\lambda|\lambda}(\theta)d\lambda\,, \tag{2.59}$$

F_θ is the integral transform defined in (2.18) and K_θ is an integral transform such that

$$K_\theta[de_\lambda(\theta)] = \int_\Theta \frac{G_\lambda(\alpha)}{D_\lambda(\alpha)} S_\lambda(\alpha,\theta)de_\lambda(\alpha)d\alpha\,, \tag{2.60}$$

where $S_\lambda(\alpha,\theta)$ satisfies the equation

$$\frac{\partial}{\partial\lambda}S_\lambda(\alpha,\theta) = F_\alpha[S_\lambda(\alpha,\theta)] + F_\theta[S_\lambda(\alpha,\theta)] + C_\lambda(\theta,\alpha) - \int_\Theta \frac{G_\lambda^2(\beta)}{D_\lambda^2(\beta)} S_\lambda(\alpha,\beta)S_\lambda(\theta,\beta)d\beta\,. \tag{2.61}$$

Proof. See Appendix A.3. □

We show in Lemma A.3.1 (Appendix B) that $e_\lambda(\theta)$ is Brownian motion. Thus, (2.58) can be interpreted using Ito calculus. Since we do not observe the field on the boundary, we assume that the boundary conditions in (2.58) are zero such that:

$$\frac{\partial^j}{\partial n^j}\widehat{x}_{\lambda|\lambda}(\theta) = 0\,,\ j = 1\ \ldots, m-1\,,\ \theta\in\Theta\,. \tag{2.62}$$

The boundary equations for the partial differential equation associated with the filtered

error covariance is computed using the covariance of the field at the boundary such that

$$\frac{\partial^j}{\partial n^j} S_0(\alpha,\theta) = \frac{\partial^j}{\partial n^j} R_{0,0}(\alpha,\theta)\,,\ \alpha,\theta \in \Theta\,. \tag{2.63}$$

The filtering equation in (2.58) is similar to the Kalman-Bucy filtering equations derived for Gauss-Markov processes. The differences arise because of the telescoping surfaces. Using (2.58), let Θ be a single point instead of $[-\pi,\pi]$. In this case, the integrals in (2.18) and (2.60) disappear and we easily recover the Kalman-Bucy filter for Gauss-Markov processes.

Using the filtered estimates, we now derive equations for smoothing GMRFs. Define the smoothed estimate $\widehat{x}_{\lambda|T}(\theta)$, error $\widetilde{x}_{\lambda|T}(\theta)$, and error covariance $S_{\lambda|T}(\alpha,\beta)$ as follows:

$$\widehat{x}_{\lambda|T}(\theta) \triangleq E[x_{\lambda|T}|\sigma\{y(T)\}] \tag{2.64}$$

$$\widetilde{x}_{\lambda|T}(\theta) \triangleq x_\lambda(\theta) - \widehat{x}_{\lambda|T}(\theta) \tag{2.65}$$

$$S_{\lambda|T}(\alpha,\beta) = E[\widetilde{x}_{\lambda|T}(\alpha)\widetilde{x}_{\lambda|T}(\beta)]\,. \tag{2.66}$$

A recursive smoother for GMRFs, similar to the Rauch-Tung-Striebel (RTS) smoother, is given as follows.

Theorem 2.6.2 (**Recursive Smoothing for GMRFs**). *For the GMRF $x_\lambda(\theta)$, assuming $S_\lambda(\theta,\theta) > 0$, the smoothed estimate is the solution to the following stochastic differential equation:*

$$d\widehat{x}_{\lambda|T}(\theta) = F_\theta[\widehat{x}_{\lambda|T}(\theta)]d\lambda + \frac{C_\lambda(\theta,\theta)}{S_\lambda(\theta,\theta)}[\widehat{x}_{\lambda|T}(\theta) - \widehat{x}_{\lambda|\lambda}(\theta)]\,,\ 1 \geq \lambda \geq 0\,, \tag{2.67}$$

where $\widehat{x}_{\lambda|\lambda}(\theta)$ is calculated using Theorem 2.6.1 and the smoother error covariance is a solution to the partial differential equation,

$$\begin{aligned}\frac{\partial S_{\lambda|T}(\alpha,\theta)}{\partial\lambda} &= \widetilde{F}_\theta S_{\lambda|T}(\alpha,\theta) + \widetilde{F}_\alpha S_{\lambda|T}(\alpha,\theta) + C_\lambda(\alpha,\theta) \\ &\quad - \frac{C_\lambda(\alpha,\alpha)S_\lambda(\alpha,\theta)}{S_\lambda(\alpha,\alpha)} - \frac{C_\lambda(\theta,\theta)S_\lambda(\alpha,\theta)}{S_\lambda(\theta,\theta)}\,,\end{aligned} \tag{2.68}$$

where

$$\widetilde{F}_\beta = F_\beta + C_\lambda(\beta,\beta)/S_\lambda(\beta,\beta)\,. \tag{2.69}$$

Proof. See Appendix A.4 □

The equations in Theorem 2.6.2 are similar to the Rauch-Tung-Striebel smoothing equations for Gauss-Markov processes [75]. Other smoothing equations for Gauss-Markov processes can be extended to apply to GMRFs.

2.7 Summary

We derived a recursive representation for noncausal Gauss-Markov random fields (GMRFs) indexed over regions in $\mathbb{R}^d$ or $\mathbb{Z}^d$, $d \geq 2$. We called the recursive representation *telescoping* since it initiated at the boundary of the field and telescoped inwards. Although the representations were derived assuming $x(s)$ is scalar, we can easily generalize the results for $x(s) \in \mathbb{R}^n$, $n \geq 1$. Our recursions are on hypersurfaces in $\mathbb{R}^d$, which we call telescoping surfaces. For fields indexed over $\mathbb{R}^d$, we saw that the set of telescoping surfaces is not unique and can be represented using a homotopy from the boundary of the field to a point within the field (not on the boundary). Another way to interpret our results is to reparameterize the field on on the telescoping surfaces which leads to a tree or *chain like structure* for processing GMRFs. Using the telescoping representations, we recovered recursive algorithms for recursive filtering and smoothing. Besides the RTS smoother that we derived, other recursive smoothers can be derived using the results in [6], [26], [37].

We note although the results derived in this paper assumed Gaussianity, recursive representations on telescoping surfaces can be derived for general non-Gaussian Markov random fields. In this case, the representation will no longer be given by linear stochastic differential equation, but instead be transition probabilities.

Chapter 3

Block-Tree Structures in Markov Random Fields Over Graphs

3.1 Introduction

In Chapter 2, we studied Markov random fields that are indexed over continuous indices and derived a tree like representation that initiated at the boundary and recursed inwards. In this Chapter, we study Markov random fields indexed over graphs. In particular, we are given a finite collection of random variables such that the Markov properties amongst random variables is determined by a graph. In the literature, such random fields are also known as *graphical models*. Informally, a graphical model is a random vector defined on a graph such that each node represents a random variable (or multiple random variables), and edges in the graph represent conditional independencies [48]. The underlying graph structure in a graphical model leads to a factorization of the joint probability distribution. This property has lead to graphical models being used in many applications such as sensor networks, image processing, computer vision, bioinformatics, speech processing, and ecology [80], [96], to name a few.

The structure of the graph plays an important role in determining the computational complexity of performing various tasks over graphical models. For example, given a probability distribution $p(\mathbf{x})$ of a graphical model $\mathbf{x} = \{x_1, \ldots, x_n\}$, it is of interest in many

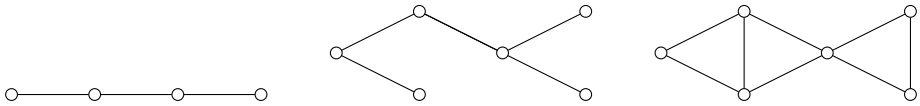

(a) Chain structured (b) Tree structured (c) Graph with cycles

Figure 3.1: Types of Graph Structures

applications to compute the marginal distribution $p_s(x_s)$. We refer to this problem as *inference*. Inference over chain or tree-structured graphical models, shown in Fig. 3.1(a) and Fig. 3.1(b), respectively, is computationally tractable due to the belief propagation algorithm [69]. However, belief propagation does not work for undirected graphs with cycles, an example of which is shown in Fig. 3.1(c). Since undirected graphs with cycles have superior modeling capability [83], it is desirable to find efficient algorithms for performing inference.

A popular method for inference in graphs with cycles is to perform variable elimination, where the joint probability distribution is marginalized according to a chosen elimination order, which is a permutation of the nodes in the graph. Frameworks for variable elimination have been proposed in [19], [21], [117]. A general framework for variable elimination is achieved by constructing a *junction-tree* [49], [77], which is a tree-structured graph with edges between clusters of nodes.

Our main contribution in this Chapter is to propose the use of *block-trees* for constructing tree-structured graphs from undirected graphs with cycles. A block-tree is a generalization of a tree-structured graph such that each node in the graph is a cluster of multiple nodes and edges in the graph are between clusters. The key difference between block-trees and junction-trees is that the clusters in a block-tree are disjoint, whereas, clusters in a junction-tree have common nodes. We show that constructing block-trees is much faster than constructing junction-trees and give trade-offs for using block-trees as opposed to junction-trees when performing inference over graphical models.

The rest of the Chapter is organized as follows. Section 3.2 reviews relevant theory necessary for this and Chapter and Chapter 4. Section 3.3 outlines algorithms for

constructing block-trees given a graph. Section 3.4 shows how the belief propagation algorithm can be extended for inference over block-trees. Section 3.5 discusses the advantages of using block-trees vs. junction-trees for inference over graphical models. Section 3.6 summarizes the Chapter.

3.2 Background and Problem Statement

Section 3.2.1 reviews properties and definitions related to graphs and graphical models necessary for this Chapter. For a more complete study, we refer to [48]. Section 3.2.2 defines the problem of inference over graphical models. Section 3.2.3 outlines the belief propagation algorithm for inference over tree-structured graphical models. Section 3.2.4 outlines the junction-tree algorithm for inference over undirected graphs with cycles. Section 3.2.5 outlines our problem statement for constructing block-trees.

3.2.1 Graphs and Graphical Models

Let $\mathbf{x} = \{x_s \in \mathbb{R}^d : s \in V\}$ be a random vector defined on a graph $G = (V, E)$, where $V = \{1, 2, \ldots, n\}$ is the set of nodes and $E \subset V \times V$ is the set of edges. For notational simplicity we assume that $d = 1$, so that each node in the graph is a random variable. Our results easily generalize to the case when $d > 1$. Given any subset $W \subset V$, let

$$x_W = \{x_s : s \in W\}$$

denote the set of random variables in W. An edge between two nodes can either be *directed*, denoted by $s \to t$, or *undirected*, denoted by $s - t$. One way of representing the edge set is via an $n \times n$ *adjacency matrix* A such that

$$A(i, j) = 1 \quad \text{if} \quad (i, j) \in E\,, \tag{3.1}$$

where we assume $A(i, i) = 1$ for all $i = 1, \ldots, n$. If (s, t) is a directed edge, x_s is called a *parent* of x_t and x_t is called a *child* of x_s. Denote the set of all parents of a node x_s

as $\text{pa}(x_s)$ and the set of all children of a node x_t as $\text{ch}(x_t)$. A graph with only directed edges is called a directed graph. A directed graph with no cycles, i.e., if we start from a node and move from one node to another along the directed edges and never end up going back to the starting position, is called a directed acyclic graph (DAG). For $\mathbf{x}$ defined on DAGs, we have a factorization of the probability distribution as

$$p(\mathbf{x}) = \prod_{s=1}^{n} p\left(x_s|\text{pa}(x_s)\right) . \tag{3.2}$$

For example, the factorization of a random vector defined on the directed graphical model in Fig. 3.2(a) is

$$p(\mathbf{x}) = p(x_1)p(x_2|x_1)p(x_3|x_1)p(x_4|x_2)p(x_5|x_3)p(x_6|x_4, x_5) . \tag{3.3}$$

A graph with only undirected edges is called an undirected graph. An undirected graph has *cycles* if we start from one node and move from node to node along the edges and end up going back to the starting position. For any $s \in V$,

$$\mathcal{N}(s) = \{t \in V : (s, t) \in E\} \tag{3.4}$$

defines the *neighborhood* of s in the undirected graph $G = (V, E)$. The *degree* of a node s, denoted $d(s)$, is the number of neighbors of s. A set of nodes $\mathcal{C}$ in an undirected graph is a *clique* if all the nodes in $\mathcal{C}$ are connected to each other, i.e., all nodes in $\mathcal{C}$ have an undirected edge. A random vector $\mathbf{x}$ defined on an undirected graph G is referred to as an *undirected graphical model*.

Given a directed acyclic graph G, we can form an undirected graph by computing its moralized graph G^m in the following manner:

i) Convert all directed edges into undirected edges.

ii) For each node s, connect all the nodes in $\text{pa}(x_s)$ with undirected edges.

For example, the moralized graph for the DAG given in Fig. 3.2(a) is shown in Fig. 3.2(b).

Because of this property, in this Chapter, unless mentioned otherwise, we only consider undirected graphical models. The associated analysis for directed graphical models can be done by moralizing the graph.

The edges in an undirected graphical model are used to specify a set of conditional independencies in the random vector $\mathbf{x}$. For any disjoint subsets A, B, C of V, we say that B separates A and C if all the paths between A and C pass through B. For undirected graphical models, we have the following equivalent Markov properties:

Definition 2 (Pairwise Markov Property)**.** *Any two non-adjacent nodes are conditionally independent given all other nodes:* $x_s \perp x_t | x_{V\setminus\{s,t\}}$ *if* $(s,t) \notin E$.

Definition 3 (Local Markov Property)**.** *A node is conditionally independent of all other nodes given its neighbors:* $x_s \perp x_{V\setminus\{s,N(s)\}} | x_{N(s)}$.

Definition 4 (Global Markov Property)**.** *For subsets* A, B, C *of* V *such that* B *separates* A *and* C, x_A *is conditionally independent of* x_C *given* x_B*:* $x_A \perp x_C | x_B$.

From the Hammersley-Clifford theorem, the probability distribution $p(\mathbf{x})$ of graphical models factors in terms of cliques as [11]

$$p(\mathbf{x}) = \frac{1}{Z} \prod_{C \in \mathcal{C}} \psi_C(x_C)\,, \tag{3.5}$$

where $\{\psi_C(x_C)\}_{C\in\mathcal{C}}$ are positive potential functions, also known as clique functions, that depend only on the variables in the clique $C \in \mathcal{C}$ and Z, the partition function, is a normalization constant. For example, Fig. 3.2(b) shows an undirected graph with cliques $\{1,2\}, \{1,3\}, \{2,4\}, \{3,5\}, \{4,5,6\}$; thus the joint distribution factorizes as

$$p(\mathbf{x}) = \frac{1}{Z}\psi_{1,2}(x_1,x_2)\psi_{1,3}(x_1,x_3)\psi_{2,4}(x_2,x_4)\psi_{3,5}(x_3,x_5)\psi_{4,5,6}(x_4,x_5,x_6)\,. \tag{3.6}$$

(a) Directed graph (b) Undirected graph

Figure 3.2: Different examples of graphical models

3.2.2 Inference Algorithms

Inference in graphical models corresponds to finding marginal distributions, say $p_s(x_s)$, given the probability distribution $p(\mathbf{x})$ for $\mathbf{x} = \{x_1, \ldots, x_n\}$. Assuming x_s is a discrete random variable taking values in Ω such that $|\Omega| = K$, we have

$$p_s(x_s) = \sum_{x_k \in \Omega, k=1,\ldots,n, k \neq s} p(\mathbf{x})\,. \tag{3.7}$$

Computing $p_s(x_s)$ using (3.7) requires K^{n-1} additions since there are $n-1$ joint summations over K possible states of x_s. Further, these additions must be done for each state of x_s, thus the total complexity is $O(K^n)$. Even for small K, for example if Ω is binary, i.e., $\Omega = \{0, 1\}$, computing marginals becomes computationally challenging. For graphical models, this problem is simplified since $p(\mathbf{x})$ admits a factorization, such as in (3.2) or (3.5). As an example, consider the undirected graph in Fig. 3.2(b), and suppose we want to compute $p_6(x_6)$. Given $p(\mathbf{x})$ as in (3.6), we have

$$p_6(x_6) = \frac{1}{Z} \sum_{x_1, x_2, x_3, x_4, x_5} \psi_{1,2}\psi_{1,3}\psi_{2,4}\psi_{3,5}\psi_{4,5,6}\,, \tag{3.8}$$

where $\psi_A(x_A)$ is shortened as ψ_A. We can distribute the computations in (3.8) as follows:

$$p_6(x_6) = \sum_{x_4, x_5} \left[\psi_{4,5,6} \left(\sum_{x_3} \psi_{3,5} \right) \left(\sum_{x_2} \psi_{2,4} \left(\sum_{x_1} \psi_{1,2}\psi_{1,3} \right) \right) \right]. \tag{3.9}$$

Using (3.8) for computing $p_6(x_6)$ requires K^6 additions, whereas, using (3.9) requires $4K^3$ additions. Using (3.9) to compute marginals is known as *variable elimination* and

general frameworks for doing this have been proposed in [21], [117]. The key step in variable elimination over graphs is to choose an *elimination order*, which is a permutation of nodes. For example, in (3.9), the elimination order is $\{1, 2, 3, 4, 5, 6\}$. The marginal computed is always at the end of the order. The complexity of the variable elimination algorithm depends on the elimination order. An *optimal* elimination order is the one that results in the least number of summations. The problem of finding an optimal elimination order can be mapped to finding the treewidth (see Definition 6) of a graph, which is an NP-hard problem [5]. The variable elimination algorithm has a hidden step where we triangulate a graph. A triangulated graph, also known as a chordal graph, is defined as follows [101]:

Definition 5 (Triangulated graph)**.** *A graph is triangulated if all cycles of length four or more have an edge connecting non-adjacent nodes in the cycle.*

For example, in (3.9), when summing over x_1, the resulting term $\sum_{x_1} \psi_{1,2}\, \psi_{1,3}$ is a function of the nodes x_2 and x_3 and thus creating an edge between these two nodes. Each summation in the variable elimination algorithm creates intermediate factors. We can capture these factors graphically using the triangulation algorithm, which has the following steps [8]:

1. Choose an elimination order, which is a permutation of nodes in the graph.
2. For each node in the elimination order, form an edge between all the nodes in its neighbors and update the edge set.
3. Remove the node and all its edges to other nodes and repeat step 2 until we exhaust all the nodes in the elimination order.

The resulting graph after steps 1-3 will be triangulated. Using the triangulated graph, we define the width and treewidth as follows [77].

Definition 6 (Width and Treewidth)**.** *Width of a triangulated graph is the size of the largest clique minus 1. Treewidth, tw(G), of a graph G is the minimum width among all possible triangulations of the graph G.*

The complexity of variable elimination, given an elimination order, is exponential in the width. So, finding an optimal elimination order corresponds to finding the treewidth of a given graph, which is an NP-hard problem. Thus, it is desirable to have a low treewidth graph to recover computationally tractable algorithms on graphical models. An example of a low treewidth graph are trees, that have treewidth of one.

A limitation of the variable elimination algorithm is that it does not scale well when more than one marginal density needs to be computed. For this purpose, message passing algorithms have been proposed in the literature. For tree-structured graphs, we review the belief propagation algorithm next in Section 3.2.3.

3.2.3 Belief Propagation

The belief propagation algorithm consists of the following steps [69]:

1. Identify a root node, say x_r, and find all the nodes other than x_r which have degree one. These are called the leaves of the tree.

2. Starting from the leaves, pass messages along edges in the graph until we reach the root node x_r:
$$m_{i\to j} = \sum_{x_i} \psi_{i,j}(x_i, x_j) \prod_{e\in\mathcal{N}(i)\setminus j} m_{e\to j}\,, \tag{3.10}$$
where $m_{i\to j}$ indicates the message passed from node x_i to x_j.

3. Once all the messages reach the root node x_r, pass messages starting from x_r to all the leaves in the same way as done in step 2 using (3.10).

Fig. 3.3 shows an example of how the belief propagation algorithm works. The marginal probability distribution of each node is the product of all messages received from its neighbors, i.e.,
$$p(x_s) = \frac{1}{Z} \prod_{t\in\mathcal{N}(s)} m_{t\to s}\,. \tag{3.11}$$
In this way, we avoid the need to do variable elimination repeatedly for computing the marginal distribution of each node in the graph. The above algorithm only works for

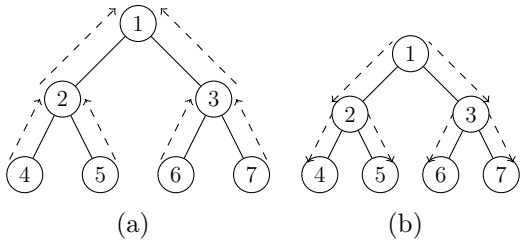

Figure 3.3: Belief propagation on trees: (a) messages, shown via dashed lines, are first passed from the leaves to the root, (b) and then passed from the root to the leaves.

tree and chain structured distributions. For graphs with cycles, a popular method is to construct a junction-tree and then apply belief propagation, which we discuss in the next Section.

3.2.4 Junction-Tree

Junction-trees were introduced in [77] for representing graphs with cycles as tree-structured graphs. In [49], the authors showed that inference in graphical models with cycles can be achieved efficiently using junction-trees. Formally, a junction-tree is defined as follows.

Definition 7 (Junction-Tree)**.** *For a graph $G = (V, E)$, a junction-tree $\mathcal{J} = (\mathcal{C}, \mathcal{E})$ is a graph over clusters of nodes in V so that*

1. *Each node in V is associated with at least one cluster in $\mathcal{C}$.*
2. *For every edge $(v_1, v_2) \in E$, there exists a cluster $C_k \in \mathcal{C}$ such that $\{v_1, v_2\} \in C_k$.*
3. *$\mathcal{J}$ satisfies the running intersection property: For all clusters C_i, C_k, and C_j such that C_k separates C_i and C_j, $C_i \cap C_j \subset C_k$.*

The idea behind using junction-trees for inference in graphical models is to cluster nodes in the graph and then form a tree-structured graph over the clusters. Given a tree-structured graph, we can now apply variants of the belief propagation algorithm so that the message passing is between clusters of nodes (instead of individual nodes) [34], [82]. The running intersection property ensures that inference over the junction-tree is

Algorithm 1: Constructing a Junction-Tree: JunctionTree(G,W)

Data: A graph $G = (V, E)$ and an elimination order W.
Result: A junction-tree $\mathcal{J} = (\mathcal{C}, \mathcal{E})$

1 Triangulate the graph G using the elimination order W.
2 Identify the set of cliques $\mathcal{C}$ in the triangulated graph.
3 For all tuples $C_i, C_j \in \mathcal{C}$, construct a weighted graph with weights $w(i, j) = |C_i \cap C_j|$.
4 $\mathcal{E} \leftarrow \arg\max_{\mathcal{E}} \sum_{(i,j)\in\mathcal{E}} w(i, j)$.

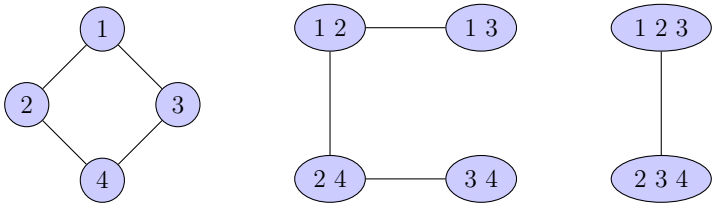

(a) (b) (c)

Figure 3.4: (a) An undirected graph, (b) Not a valid junction-tree since $\{1, 2\}$ separates $\{1, 3\}$ and $\{3, 4\}$,but $3 \notin \{1, 2\}$. In other words, the running intersection property says that for two clusters with a common node, all the clusters on the path between the two clusters must have that common node. (c) A valid junction-tree for the graph in (a).

consistent so that if a node s is in two clusters, the marginal distribution of x_s computed from each cluster after running message passing is the same. Fig. 3.4 illustrates an example of the running intersection property.

The next natural question to ask is how do we construct junction-trees and whether there exists a junction-tree given an undirected graph. Note that if we simply assume that the cluster in the junction-tree is all the nodes V of the original graph, we get a valid junction-tree. This shows that a junction-tree always exists. An algorithm to construct a junction-tree is outlined in Algorithm 1. In summary, we first triangulate a graph using an elimination order, then find the cliques in the triangulated graph, and then use a maximum weight spanning tree (MWST) algorithm to find an appropriate tree over the cliques.

Theorem 3.2.1. *Given a graph $G = (V, E)$, the complexity of constructing a junction-*

tree (Algorithm 1) given an elimination order W is $O(|E| + |\mathcal{C}|^2)$, where $\mathcal{C}$ are the cliques in the triangulated graph computed using the elimination order W.

Proof. Triangulation has complexity $O(|E|)$ [78]. Given a triangulated graph with $|\mathcal{C}|$ number of clusters, we need to find the weighted graph, which has complexity $O(|\mathcal{C}|^2)$ and the MWST algorithm has a worst case complexity of $O(|\mathcal{C}|^2)$ [33]. □

To do inference using the junction tree, we first associate potential functions with each clique. This is done by grouping potentials from the original joint distribution and mapping them to their respective cliques. Having defined potential functions for each clique, a message passing scheme, similar in spirit to the belief propagation algorithm outlined in Section 3.2.3, can be formulated to compute marginal distributions for each clique [34], [49], [82]. The marginal distribution of each node can be subsequently computed by marginalizing the distribution of the cliques. The following theorem summarizes the complexity of performing belief propagation over graphical models using junction-trees.

Theorem 3.2.2 (Complexity of inference using junction tree)**.** *For a random vector $\mathbf{x} \in \Omega^n$, where $|\Omega| = K$, defined on an undirected graph $G = (V, E)$, the complexity of message passing using a junction-tree $\mathcal{J} = (\mathcal{C}, \mathcal{E})$ is*

$$O\left(\sum_{(i,j)\in\mathcal{E}} K^{|\mathcal{C}_i|} + K^{|\mathcal{C}_j|}\right). \tag{3.12}$$

In Theorem 3.2.2, when K is large compared to $|\mathcal{C}|$, the complexity of inference will be dominated by the clique with maximum size. Thus, an optimal junction-tree can be defined as the junction-tree with minimal maximal clique size. In Definition 6, we saw that this is equivalent to defining the treewidth of a graph, which in turn corresponds to finding an optimal elimination order. Further, since finding the optimal elimination order is an NP-hard problem, finding an optimal junction tree is also NP-hard.

We now consider some examples of how junction-trees are constructed. The examples presented here will be used later to show how our proposed framework for using block-trees compares to that of using junction-trees.

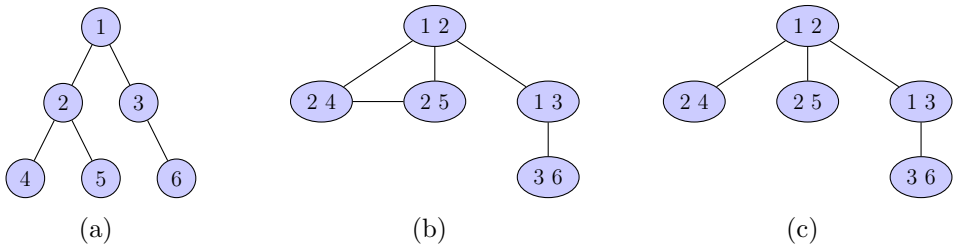

Figure 3.5: (a) Tree-structured graph (b) The graph over cliques (c) A junction-tree for (a).

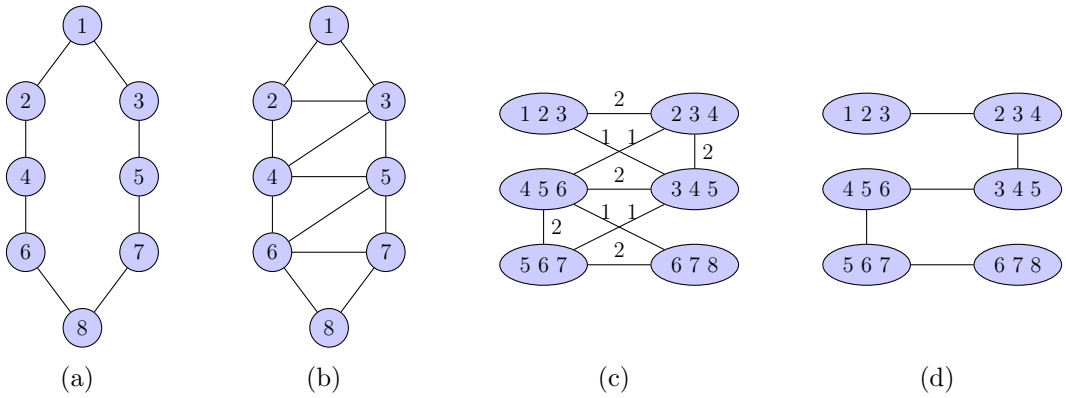

Figure 3.6: (a) Original single cycle graph. (b) Triangulated graph of (a). (c) Weighted graph over cliques. (d) Final junction-tree.

Example: We start with an example of constructing a junction-tree for the tree-structured graph in Fig. 3.5(a). Notice that the graph is already triangulated, however, this information may not be given a priori. Thus, the first step of the algorithm is to determine an elimination order that does not change the graph structure, i.e., does not introduce extra edges or cliques in the graph. This can be done in $O(|V|)$ time using lexicographic bread-first search [78]. Next, we identify the cliques in Fig. 3.5(a), which are shown in Fig. 3.5(b). The graph over the cliques is shown in Fig. 3.5(b), where all the edges have weight one. Thus, any spanning tree of the graph over cliques will be a valid junction-tree, an example of which is shown in Fig. 3.5(c).

Example: Fig. 3.6(a) shows an example of a graph with one cycle. Using an elimination order $W = \{1, 2, 3, 4, 5, 6, 7, 8\}$, we get the triangulated graph in Fig. 3.6(b). The weighted graph over the cliques is shown in Fig. 3.6(c). Using a MWST algorithm, such as Prim's

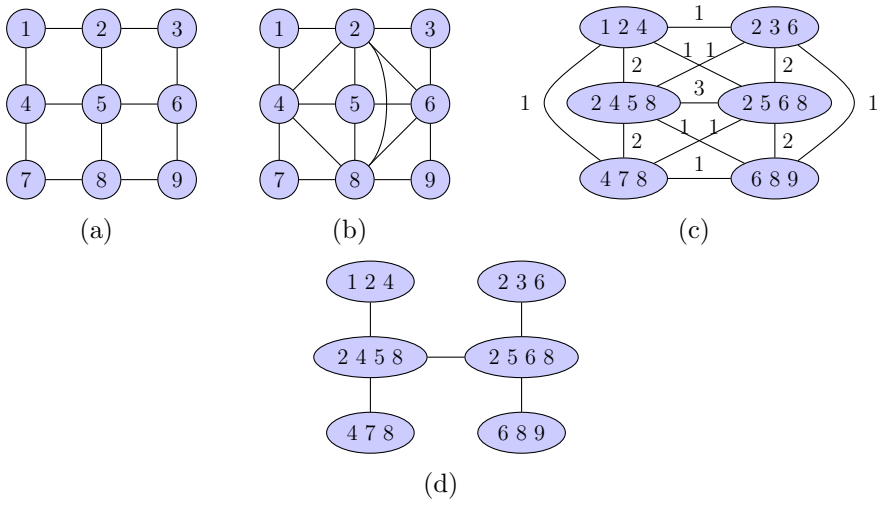

Figure 3.7: (a) A grid graph (b) Triangulated graph of (a). (c) Weighted graph over cliques. (d) Junction-tree

[74] or Kruskal's [47], we get the junction-tree in Fig. 3.6(d). It can easily be shown that this junction-tree is optimal, i.e., there exists no other junction-tree with smaller maximal clique size.

Example: Consider the 3×3 grid graph in Fig. 3.7(a). A triangulated graph, constructed using the elimination order $\{1, 3, 7, 9, 4, 5, 2, 6, 8\}$, is shown in Fig. 3.7(b). It can be shown that the elimination order chosen is optimal. The weighted graph over cliques is shown in Fig. 3.7(c). The junction tree constructed using the triangulated graph is shown in Fig. 3.7(d). The width of the triangulated graph in Fig. 3.7(c) is three. Since the elimination order is optimal, the treewidth of the graph in Fig. 3.7(a) is also three.

Example: By deleting the edge between node 1 and 2 in Fig. 3.7(a), we consider the partial grid graph in Fig. 3.8(a). Fig. 3.8(b) shows the triangulated graph using an optimal elimination order $\{1, 3, 7, 9, 4, 5, 2, 6, 8\}$. The weighted graph over cliques is shown in Fig. 3.8(c). Using this weighted graph, two possible junction-trees can be constructed, which are shown in Fig. 3.8(d) and Fig. 3.8(e), respectively. This example shows that given an elimination order, the corresponding junction-tree may not be unique.

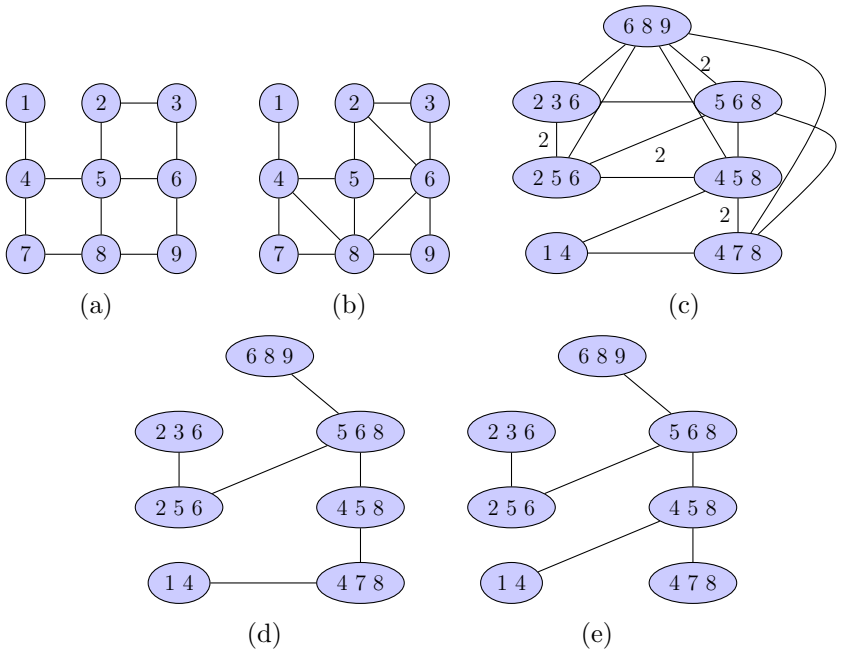

Figure 3.8: (a) Partial grid graph. (b) Triangulated graph from (a). (c) Weighted graph over cliques. The weightless edges all have weight one. (d) One possible junction-tree from (c). (e) Another possible junction-tree from (c).

3.2.5 Problem Statement

In this Chapter, we consider an alternative to junction-trees for deriving efficient inference algorithms over graphical models. Instead of using junction-trees, we propose block-trees, that are defined as follows.

Definition 8 (Block-Tree)**.** *For a graph $G = (V, E)$, a block-tree $\mathcal{G} = (\mathcal{V}, \mathcal{E})$ is a graph over clusters of nodes in V such that*

1. *Each node in V is associated with only one cluster in $\mathcal{V}$. In other words, the clusters in $\mathcal{V}$ are disjoint.*

2. *The edges $\mathcal{E} \subset |\mathcal{V}| \times |\mathcal{V}|$ form a tree-structured graph.*

Note that the main difference between a block-tree and junction-tree is that a junction-tree is a tree-structured graph on overlapping clusters, whereas the clusters in a block-tree are disjoint. Further, in defining edges in a junction-tree, it is important to satisfy the running intersection property, whereas, there is no such requirement for defining block-trees.

We propose an $O(|E|)$ algorithm for constructing block-trees. This makes constructing block-trees faster than constructing junction-trees, thus making block-trees a practical alternative to junction-trees when solving inference problems over graphical models. Numerically, we show that for a certain class of graphs, using block-trees for inference is computationally faster than using junction-trees. This is mainly true for graphical models in which exact inference is computationally tractable. In Chapter 4, we will show how block-trees can be used to derive efficient approximate inference algorithms over arbitrary graphical models.

There has been work in deriving efficient algorithms on graphical models using disjoint clusters. In fact, it is well known that inference over graphical models can be performed using disjoint clustering, and researchers often refer to this as the clustering algorithm and credit the book by J.D. Pearl [69]. Specific applications of using disjoint clustering in medical diagnostics can be found in [17] and [71]. In the engineering literature, [110]

and [62] derive recursive representations by scanning the lattice horizontally (or vertically) and thereby forming disjoint clusters of nodes. To our knowledge, previous work has not addressed the question of constructing a block-tree given an arbitrary graph. Further, our analysis shows how block-trees compare to junction-trees and how block-trees can lead to computationally faster algorithms for inference over a certain class of graphical models.

3.3 Tree Structures in Graphs Using Block-Trees

In this Section, we show how block-trees can be used to find tree structures in arbitrary graphs and present various examples of this construction. Section 3.3.1 outlines an algorithm for constructing block-trees given an arbitrary graphs. Section 3.3.2 shows how to construct block-trees in linear time. Section 3.3.3 compares block-trees to junction-trees.

3.3.1 Constructing Block-Trees

Suppose we are given an undirected graph $G = (V, E)$, where $|V| = n$. Given G, we want to find a block-tree $\mathcal{G} = (\mathcal{V}, \mathcal{E})$ such that $\mathcal{V} = \{\mathcal{V}_1, \mathcal{V}_2, \ldots, \mathcal{V}_l\}$ is a set of disjoint clusters and $\mathcal{E}$ is a set of edges such that $(i, j) \in \mathcal{E}$ if there exists an edge $e \in E$ between any node in $\mathcal{V}_i$ and any node in $\mathcal{V}_j$.

Our proposed algorithm for constructing $\mathcal{G}$ is shown in Algorithm 2. The input to the algorithm is the original graph G and a set of nodes $V_1 \subset V$. The output of the algorithm is the block-tree $\mathcal{G}$. We refer to V_1 as the *root cluster*. The various steps in the algorithm are explained as follows:

- **Forward step** (Line 1): We find clusters $V_1, V_2, \ldots, V_r$ using breadth-first search (BFS). These clusters serve as initial clusters for the block-tree.
- Let E' be a copy of the edges E (Line 2) and let denote $G' = (V, E')$.
- Split V_r into its connected components $\{V_r^1, \ldots, V_r^{m_r}\}$ using the subgraph $G(V_r)$, which denotes the graph only over the nodes in V_r (Line 3).

Algorithm 2: Constructing Block-Trees: BlockTree(G,V_1)

Data: A graph $G = (V, E)$ and a set of nodes V_1.
Result: A block-tree $\mathcal{G} = (\mathcal{C}, \mathcal{E})$

1 Find successive neighbors of V_1 to construct a sequence of r clusters $V_1, V_2, \ldots, V_r$ such that $V_2 = \mathcal{N}(V_1)$, $V_3 = \mathcal{N}(V_2) \backslash \{V_1 \cup V_2\}, \ldots, V_r = \mathcal{N}(V_r) \backslash \{V_{r-2} \cup V_{r-1}\}$.
2 $E' \leftarrow E$
3 $\{V_r^1, \ldots, V_r^{m_r}\} \leftarrow$ Find m_r connected components of V_r using subgraph $G(V_r)$.
4 **for** $i = r, r-1, \ldots 2$ **do**
5 **for** $j = 1, 2, \ldots m_i$ **do**
6 $C(V_i^j) \leftarrow \mathcal{N}(V_i^j) \cap V_{i-1}$; All nodes in V_i connected to V_i^j.
7 Update E' with all the edges between nodes in $C(V_i^j)$.
8 $\{V_{i-1}^1, \ldots, V_{i-1}^{m_{i-1}}\} \leftarrow$ Find m_{i-1} connected components of V_{i-1} using subgraph $G'(V_{i-1})$.
9 $\{V_1^1, \ldots, V_1^{m_1}\} \leftarrow$ Find m_1 connected components of V_1 using subgraph $G(V_1)$.
10 $\mathcal{V} \leftarrow \bigcup_{k=1}^{r} \{V_k^1, V_k^2, \ldots, V_k^{m_k}\}$
11 $\mathcal{E} \leftarrow$ edges between all the clusters in $\mathcal{C}$

- **Backwards step** (Lines 3-7): We now recursively split other clusters. Starting at $k = r$, for each connected component V_r^j of V_r, find the set of nodes $C(V_r^j)$ that are connected to V_{r-1} (Line 6). Next, we find all possible edges over the nodes $C(V_r^j)$ and add these edges to E' (Line 7). These edges indicate the nodes in V_{r-1} that should belong to the same cluster, i.e., if there exists an edge between $v, v' \in V_{r-1}$, v and v' would belong to the same cluster in the final block-tree. Find all connected components of V_{r-1} (Line 8). Repeat the above steps for $k = r - 1$ till $k = 2$.

- Split V_1 into connected components using the graph $G(V_1)$ (Line 9).

- After splitting the clusters V_k for $k = 1, 2, \ldots, r$, we find the associated block-tree (Lines 10 and 11).

We illustrate Algorithm 2 using some examples.

Example: Consider the tree-structured graph in Fig. 3.5(a). Suppose we choose $V_1 = \{1\}$. Using the structure of the graph, we have that $V_2 = \{2, 3\}$, $V_3 = \{4, 5, 6\}$. We now find the components of V_3 in $G(V_3)$. It is clear that $G(V_3)$ is edgeless, so that

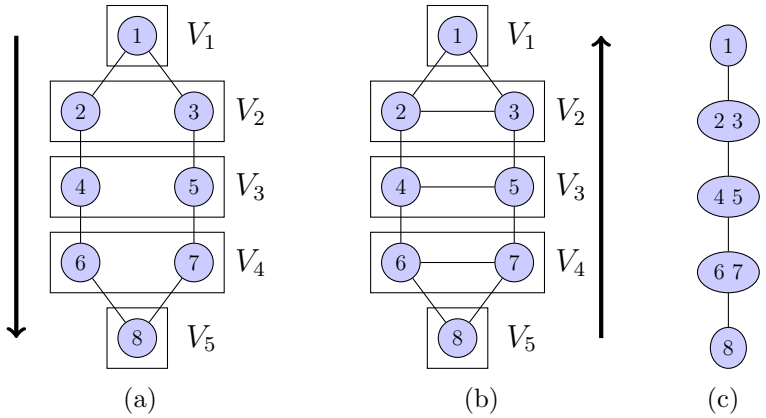

Figure 3.9: (a) Initial estimates of the clusters. (b) Final estimates of the clusters. (c) Final block-tree.

$V_3^1 = \{4\}, V_3^2 = \{5\}$, and $V_3^3 = \{6\}$. The neighbor of V_3^1 and V_3^2 in V_2 is $\{2\}$, so we introduce no new edges in the graph. The neighbor of V_3^2 in V_2 is $\{3\}$ and thus again we introduce no new edges in the graph. Finding the components of $G(V_2)$, we have that $V_2^1 = \{2\}$ and $V_2^2 = \{3\}$. Since V_1 has a single node, we do not need to consider splitting this. Thus, after invoking Algorithm 2 on the tree-structured graph, the graph remains unchanged. It is easy to see that this will be the case no matter what V_1 we start with.

Example: Consider the graph with a single loop in Fig. 3.6(a). Choosing $V_1 = \{1\}$, we can get the initial estimates of the clusters as shown in Fig. 3.9(a). To get the final estimates, which coincides with the initial estimates of the clusters, we run the backwards step of Algorithm 2. See Fig. 3.9(b) for the resulting graph. The final block-tree is shown in Fig. 3.9(c). Notice the difference between the junction-tree in Fig. 3.9(d) and the block-tree.

Example: Now consider the grid graph of Fig. 3.7(a). Choosing $V_1 = \{1\}$, we get the initial estimates of the clusters as shown in Fig. 3.10(a). Running the backwards step to identify the final clusters (see Fig. 3.10(b)), we get the block-tree in Fig. 3.10(c).

Example: In the examples considered so far, the initial estimates of the clusters matched the final estimates and the final block-tree was a chain-structured graph. We now consider

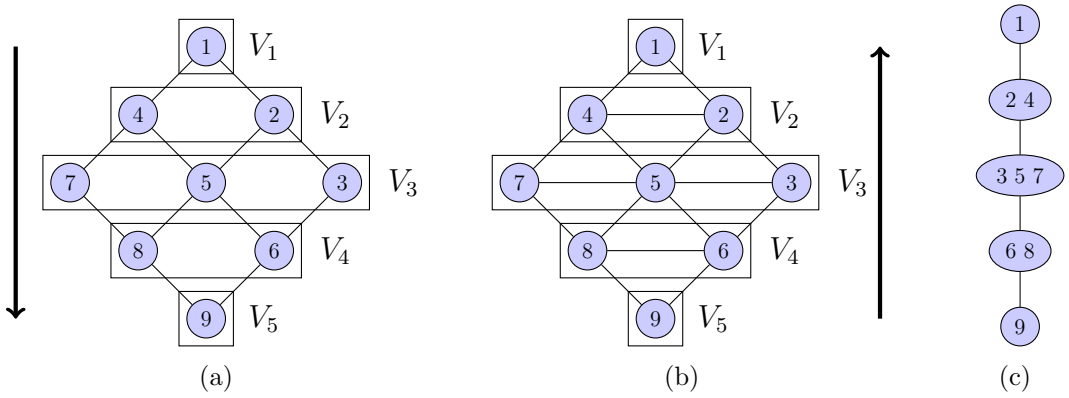

Figure 3.10: (a) Original estimates of the clusters in the grid graph when running the forward pass of Algorithm 2 (b) The final clusters after running the backwards pass of Algorithm 2 (c) Final block-tree.

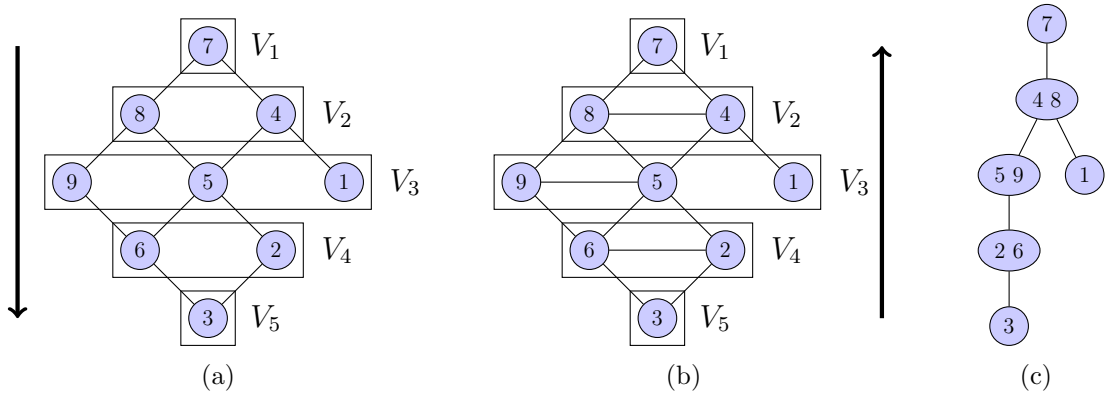

Figure 3.11: (a) Original estimates of the clusters in the partial grid when running the forward pass of Algorithm 2 (b) The final clusters after running the backwards pass of Algorithm 2 (c) Final block-tree.

an example where the final block-tree will in fact be tree-structured. Consider the partial grid graph of Fig. 3.8(a). Choosing $V_1 = \{7\}$, we get the initial estimates of the clusters in Fig. 3.11(a). We now run the backwards step of the algorithm. Since V_5 has only one node, we do not need to find its components. Now, V_5 is connected to 2 and 6, so $C(V_5) = \{2, 6\}$. We introduce an edge between 2 and 6 to show that both 2 and 6 should be in the same cluster in the final block-tree. Next, we find the components of V_4 using the additional edges and the component is V_4 itself. Now, V_4 is connected to both 5 and 9 in V_3, so $C(V_4) = \{5, 9\}$. We introduce an edge between 5 and 9 and then find the connected components of V_3. Notice that 1 is not connected to 5 and 9, so we can split V_3 as $V_3^1 = \{5, 9\}$ and $V_3^2 = \{1\}$. Continuing the algorithm we find the rest of the clusters as shown in Fig. 3.11(c). The final block-tree is shown in Fig.3.11(d).

The examples above illustrate how to construct block-trees given an undirected graph. As mentioned in Section 3.2.1, directed graphs can be converted to undirected graphs, so the algorithm for constructing block-trees also extends to directed graphs.

3.3.2 A Linear Time Block-Tree Construction Algorithm

Algorithm 2 for constructing block-trees served as a way to explain the block-tree construction algorithm. In this Section, we present an $O(|E|)$ algorithm for constructing a block-tree given an undirected graph $G = (V, E)$ and an initial root cluster V_1.

Step 1. Use a breadth-first-search (BFS) algorithm to construct clusters $V_1, V_2, \ldots, V_r$ as in Line 1 of Algorithm 2. For each cluster V_k, split V_k into m_k disjoint clusters $\{V_k^1, \ldots, V_k^{m_k}\}$ such that $\bigcup V_k^k = V_k$ and there are no edges between V_k^i and V_k^j for $i \neq j$. This partitioning of the nodes can be done in $O(|E|)$ time using standard BFS algorithms.

Step 2. We now merge clusters to find the final block-tree. The key intuition in this step is that each cluster in V_k should be connected to a single cluster in V_{k-1}. If this is not the case, we merge clusters in V_{k-1} accordingly. Starting at $V_r = \{V_r^1, V_r^2, \ldots, V_r^{m_r}\}$, for each V_r^j, $j = 1, \ldots, m_r$, find all clusters $C(V_r^j)$ in V_{r-1}

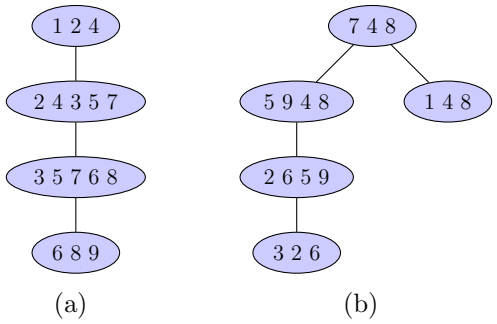

Figure 3.12: (a) Junction-tree for the block-tree in Fig. 3.10(c) (b) Junction-tree for the block-tree in Fig. 3.11(c)

that are connected to V_r^j. Combine all clusters in $C(V_r^j)$ into a single cluster and update the clusters in V_{r-1}^j accordingly. Repeat the above steps for all clusters in $V_{r-1}, V_{r-2}, \ldots, V_3$. This step can be done in $O(|E|)$ time since we only need to iterate over the edges in the graph.

Comparing the complexity of constructing block-trees to that of constructing junction-trees (Theorem 3.2.1), we clearly see that constructing block-trees is faster. The main reason for the reduction in complexity for constructing block-trees is that we do not have to perform a MWST step.

3.3.3 Block-Trees Vs. Junction-Trees

In this Section, we take a closer look at the structure of block-trees and compare them to junction-trees. Since a block-tree is a tree-structured graph, we can apply Algorithm 1, using an appropriate elimination order, to the block-tree to construct a junction-tree. For example, the junction-tree representation for the block-trees in Fig. 3.10(c) and Fig. 3.11(c) are given in Fig. 3.12(a) and Fig. 3.12(b), respectively. However, given a junction-tree, it is not necessary that we can find an equivalent block-tree. For example, for the junction-tree in Fig. 3.7(c), we can not construct an equivalent block-tree. This suggests that junction-trees are a broader class of representations for graphs than block-trees and we thus get the relationship between the class of block-trees and the class of junction-trees

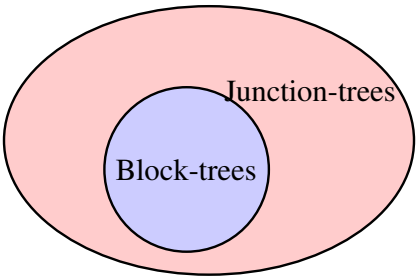

Figure 3.13: The relationship between the set of all block-trees and the set of all junction-trees for a given graph G.

in Fig. 3.13. This relationship can also be seen from the way the graphs were constructed since the block-tree only required an initial cluster of nodes V_1, whereas the junction-tree required an elimination order, which is a permutation of the nodes $V \supseteq V_1$, for construction. Note that although junction-trees are a broader class of representations, we have seen in previous Sections that constructing block-trees is computational faster.

3.4 Inference of Graphical Models Using Block-Trees

In this Section, we show how to use block-trees for inference over graphical models. Section 3.4.1 outlines the inference algorithm. Section 3.4.2 studies the problem of finding optimal block-trees.

3.4.1 Belief Propagation on Block-Trees

Since block-trees are tree-structured graphs, we can use belief propagation algorithms for inference. Let $\mathbf{x}$ be an undirected graphical model on $G = (V, E)$ with probability distribution $p(\mathbf{x})$. For simplicity, we assume that $\mathbf{x}$ is discrete valued so that $\mathbf{x} \in \Omega$, where $|\Omega| = K$, however, the inference algorithm easily extends to continuous valued distributions. Recall from (3.5) that the probability distribution factorizes over the cliques of the graph so that

$$p(\mathbf{x}) = \frac{1}{Z} \prod_{C \in \mathcal{C}} \psi_C(x_C)\,, \tag{3.13}$$

where the functions $\psi_C(x_C)$ are known a priori. Suppose we construct a block-tree $\mathcal{G} = (\mathcal{V}, \mathcal{E})$ from G using a root cluster V_1. To capture the structure of the original graph G in the block-tree $\mathcal{G}$, we introduce some notation. For every edge $(i, j) \in \mathcal{E}$ connecting two clusters $\mathcal{V}_i$ and $\mathcal{V}_j$, associate a label $(\overline{\mathcal{V}}_i, \overline{\mathcal{V}}_j)$ so that in the original graph G, the nodes in $\overline{\mathcal{V}}_i$ are not connected to the nodes in $\overline{\mathcal{V}}_j$. As an example, in Fig. 3.11(c), all the edge labels will be empty, except the label between $\{1\}$ and $\{4, 8\}$, which will have a label $(\{\}, \{4\})$. The steps involved in inference over graphical models using block-trees are summarized as follows.

Step 1. Construct a block-tree $\mathcal{G}$ from the undirected graph G using a root cluster V_1.

Step 2. The cliques in the block-tree $\mathcal{G}$ are the edges, so we can write down an alternative factorization for the probability distribution in $p(\mathbf{x})$ as

$$p(\mathbf{x}) = \prod_{k=1}^{l} \phi_k(x_{\mathcal{V}_k}) \prod_{(i,j)\in\mathcal{E}} \Psi_{i,j}(x_{\mathcal{V}_i \setminus \overline{\mathcal{V}}_i}, x_{\mathcal{V}_j \setminus \overline{\mathcal{V}}_j}), \tag{3.14}$$

where we map each potential function in the original factorization in (3.13) to an appropriate factor without repeating.

Step 3. Using an arbitrary root node in the block-tree, identify the leaves and pass messages starting at the leaves up to the root:

$$m_{i\to j}(x_{\mathcal{V}_j}) = \sum_{x_{\mathcal{V}_i \setminus \overline{\mathcal{V}}_i}} \Psi_{i,j}(x_{\mathcal{V}_i \setminus \overline{\mathcal{V}}_i}, x_{\mathcal{V}_j \setminus \overline{\mathcal{V}}_j}) \sum_{x_{\overline{\mathcal{V}}_i}} \prod_{k \in \mathcal{N}(x_{\mathcal{V}_i}) \setminus x_{\mathcal{V}_j}} \phi_i(x_{\mathcal{V}_i}) m_{k\to i}(x_{\mathcal{V}_i}) \tag{3.15}$$

Step 4. Once all messages have reached the root, pass messages from the root back to the leaves using the same message passing equation in (3.15).

Step 5. The joint distribution for each cluster is given by

$$p_{\mathcal{V}_i}(x_{\mathcal{V}_i}) = \prod_{j \in \mathcal{N}(\mathcal{V}_i)} m_{j\to i}(x_{\mathcal{V}_i}) \phi_i(x_{\mathcal{V}_i}) \tag{3.16}$$

Step 6. Marginilize the distribution of each cluster to find the distribution of each node.

The complexity of the message passing algorithm is given as follows.

Theorem 3.4.1. *For an undirected graphical model* $\mathbf{x}$ *defined on a graph* $G = (V, E)$*, let* $\mathcal{G} = (\mathcal{V}, \mathcal{E})$ *be the block-tree constructed using a root cluster* V_1*. The complexity of message passing over the block-tree is*

$$O\left(\sum_{(i,j)\in\mathcal{E}} K^{|\overline{\mathcal{V}}_i|} + K^{|\overline{\mathcal{V}}_j|} + 2K^{|\mathcal{V}_i\backslash\overline{\mathcal{V}}_i|+|\mathcal{V}_j\backslash\overline{\mathcal{V}}_j|}\right). \tag{3.17}$$

Proof. From (3.15), the complexity of passing messages from cluster $\mathcal{V}_i$ to cluster $\mathcal{V}_j$ is $O\left(K^{|\overline{\mathcal{V}}_i|} + K^{|\mathcal{V}_i\backslash\overline{\mathcal{V}}_i|+|\mathcal{V}_j\backslash\overline{\mathcal{V}}_j|}\right)$. Summing over all edges and using the fact that we pass messages twice on an edge (i, j), we get the desired result. □

An alternative way to derive a message passing algorithm over block-trees is to transform the block-tree into a junction-tree and then use popular junction-tree based inference algorithms [34], [82]. The complexity of the inference algorithm will be the same, however, by directly using the block-tree, we avoid the step of constructing a junction-tree. In the next Section, we consider the problem of finding optimal block-trees.

3.4.2 Optimal Block-Trees

From Theorem 3.4.1, we see that the complexity of message passing over block-trees is dominated by the term in (3.17) whose exponent is maximum. Thus, an optimal block-tree can be defined such that the width

$$w(\mathcal{G}, V_1) = \max_{(i,j)\in\mathcal{E}} \left\{\max\left\{|\overline{\mathcal{V}}_i|, |\overline{\mathcal{V}}_j|, |\mathcal{V}_i\backslash\overline{\mathcal{V}}_i| + |\mathcal{V}_j\backslash\overline{\mathcal{V}}_j|\right\}\right\} \tag{3.18}$$

is minimized. Notice that (3.18) depends on the choice of the root cluster V_1 in constructing the block-tree. Thus, finding the optimal block-tree is equivalent to finding an optimal root cluster. This problem is computationally intractable since we need to search over all possible combinations of root clusters V_1.

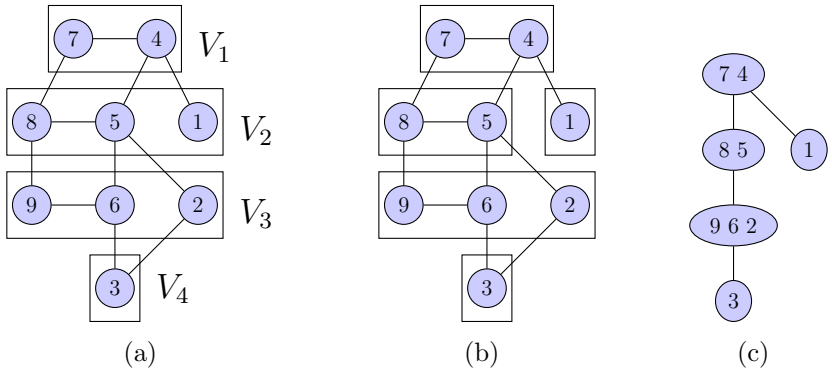

Figure 3.14: (a) Original estimates of the clusters in the partial grid using $V_1 = \{7, 4\}$ as the root cluster (b) Splitting of clusters (c) Final block-tree.

As an example illustrating how the choice of V_1 alters the block-tree, consider finding block-trees for the partial grid in Fig. 3.11. In Fig. 3.11(c), we construct a block-tree using $V_1 = \{7\}$ as the root cluster. The complexity of inference in this graph is $O(K^4)$ because of the message passing between the cluster $\{5, 9\}$ and $\{4, 8\}$ and between cluster $\{2, 6\}$ and $\{5, 9\}$. Instead of choosing $V_1 = \{7\}$, let $V_1 = \{7, 4\}$. The initial estimate of the clusters are shown in Fig. 3.14(a). The final block-tree is shown in Fig. 3.14(c). It is clear that message passing on the block-tree in Fig. 3.14(c) will have complexity $O(K^5)$ because of the message passing between the cluster $\{9, 6, 2\}$ and the cluster $\{8, 5\}$.

3.4.3 Greedy Algorithms For Finding Optimal Block-Trees

In this Section, we discuss some greedy algorithms for finding optimal block-trees.

- **Minimal degree node:** In this approach, which we call MinDegree, we find the node with minimal degree and use that node as the root cluster. The intuition behind this is that the minimal degree node may lead to the smallest number of nodes being added in the clusters. The complexity of this approach is $O(n)$, where n is the number of nodes in the graph.

- **Using an elimination order:** Recall from Section 3.3.3 that a block-tree can be converted into a junction-tree by joining clusters connected via edges. This means

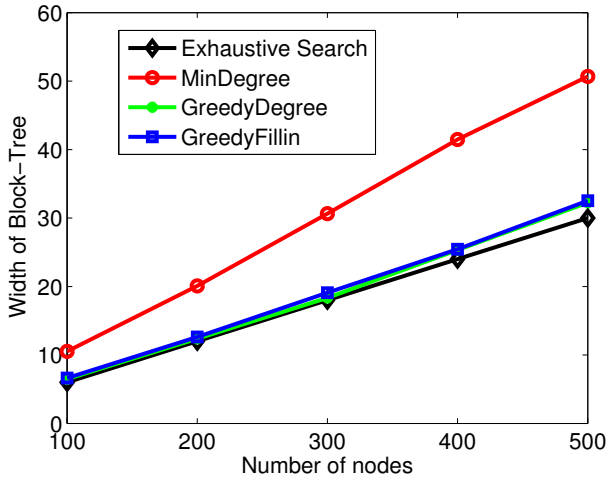

Figure 3.15: Plot showing the performance of three different greedy heuristics for finding optimal block-trees.

that an optimal junction-tree may be used to find an approximate optimal block-tree. To do this, we first use a greedy heuristic to find an optimal elimination order that leads to the cliques of the junction-tree. We then search over a constant number of cliques to find a root cluster that leads to the minimal width as defined in (3.18). The complexity of this step depends on the complexity of finding the optimal elimination order. One of the simplest algorithms for doing this is known as GreedyDegree [10], [56], where the elimination order corresponds to the sorted list of nodes in increasing degree. The complexity of GreedyDegree algorithm is $O(n \log n)$ since we just need to sort the nodes. Another popular greedy algorithm is to find an elimination order such that at each step in the triangulation algorithm, we choose a node that adds a minimal number of extra edges in the graph. This is known as GreedyFillin [42] and has polynomial complexity and is in general slower than GreedyDegree, but does lead to slightly better elimination orders on average.

We evaluate the three different greedy heuristics for finding optimal block-trees in Fig. 3.15. To do this, we create clusters of size k such that the total number of nodes is n (one cluster may have less than k nodes). We then form a tree over the clusters

and associate a clique between two clusters connected to each other. We then remove a certain fraction of edges over the graph (not the block-tree), but make sure that the graph is still connected. By construction, the width of the graph constructed will be at most $2k$. Fig. 3.15 shows the performance of MinDegee, GreedyDegree, and GreedyFillin over graphs with different number of nodes and different values of k. We clearly see that both GreedyDegree and GreedyFillin compute widths that are close to optimal. The main point is that we can use various known algorithms for finding optimal junction-trees to final optimal block-trees.

3.5 Inference Over Graphical Models: Block-Tree Vs. Junction-Tree

In this Section, we show how block-trees can lead to computational savings when used for inference over graphical models. The main idea is that for certain graphical models, the complexity of constructing the junction-tree can dominate the complexity of the inference algorithm, thus in these cases, we can use block-trees instead of junction-trees for inference. Section 3.5.1 considers a simple example of a graphical model with a single cycle and Section 3.5.2 considers more general graphical models.

3.5.1 Example: Single Cycle Graphical Models

Let $G = (V, E)$ be a graphical model on a graph with a single cycle, as in Fig. 3.6(a). The complexity of inference using a junction-tree is

$$O\left(n + n^2 + 2nK^3\right) \approx O\left(n^2 + 2nK^3\right) , \tag{3.19}$$

where $O(n + n^2)$ is the complexity of constructing the junction-tree (see Theorem 3.2.1) and $O(nK^3)$ is the complexity of belief propagation (see Theorem 3.2.2) since all the cliques in the junction-tree will have size three (see Fig. 3.6(c) for an example). The

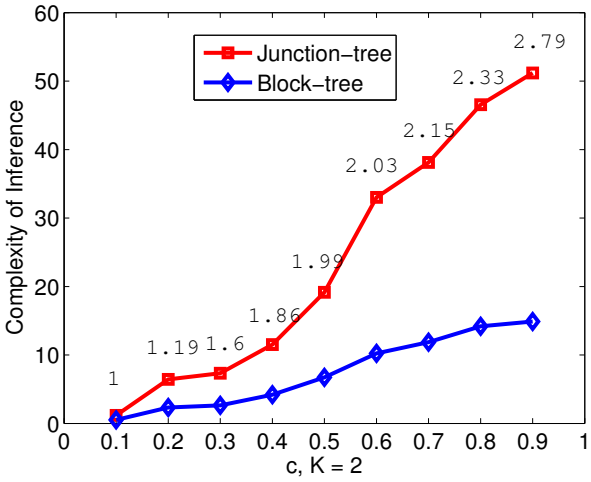

Figure 3.16: Complexity of inference

complexity of inference using a block-tree is

$$O\left(n + nK^4\right) \approx O\left(nK^4\right) , \tag{3.20}$$

where $O(n)$ is the complexity of constructing the block-tree (see Section 3.3.2) and $O(nK^4)$ is the approximate complexity of inference over the block-tree (see Fig. 3.9(c) for an example). It is clear that there exists some constant $c > 0$ such that if $n > cK^4$, the complexity of inference using the junction-tree will dominate the complexity of inference using the block-tree. Recall that K is the number of states each random variable can take, so this number remains fixed as n increases.

3.5.2 Example: Erdős-Rényi Graph

In this Section, we assume that the graph $G = (V, E)$ is a realization of the Erdős-Rényi [24], [29] graph, denoted by $G(n, c/n)$. Here n is the number of nodes and c/n is the probability that an edge appears in the graph (independent of all other edges). Many naturally occurring networks, such as large social networks, have been modeled using Erdős Rényi graphs [31], [66]. Recently, authors have also studied the problem of

learning graphical models on sparse random graphs [3].

It is well known that for $c < 1$ and for *large* n, the treewidth of a graph realized using an Erdős-Rényi model is at most two [23]. Thus, for graphical models defined on such random graphs, inference is tractable. The comparison of the complexity of inference using block-trees and junction-trees on a 1000 node graph is shown in Fig. 3.16. The results shown are over 100 randomly generated graphs for c chosen between 0 and 1. The average treewidth over the 100 graphs is also shown in the graph. We clearly see the benefits of using block-trees over junction-trees. Note that, when reporting complexity results, we factor in the complexity of constructing the junction-tree or the block-tree, in addition to the complexity of performing message passing in the graph. For $c > 1$, the graph realized using an Erdős-Rényi model no longer has low treewidth and the treewidth is known to be of the order $c'n$, where c' is some constant and n is the number of nodes in the graph [50]. Thus, in this case, the complexity of inference will dominate the complexity of constructing the junction-tree, so the block-tree framework will no longer be faster.

3.5.3 Discussion

From the examples presented in this Section, we see that, for a certain class of graphical models, the complexity of using block-trees over junction-trees leads to complexity benefits when performing inference over graphical models. The main computational gains are in constructing the block-tree. We note that for some applications, the junction-tree or the block-tree only needs to be computed once. In these cases, the complexity of inference will be dominated by the message passing algorithm. Thus, the main advantage of the block-tree framework is in studying inference problems where the graph structure varies over time and the inference algorithm needs to compute a new tree-decomposition at each time instant.

Fig. 3.17 outlines an algorithm for deciding between choosing the junction-tree or block-tree for inference. In the first step of the algorithm, we compute an elimination order from the graph. As outlined in Section 3.4.3, this can be done using standard algorithms in the literature to compute optimal elimination orders, see [12] for a review

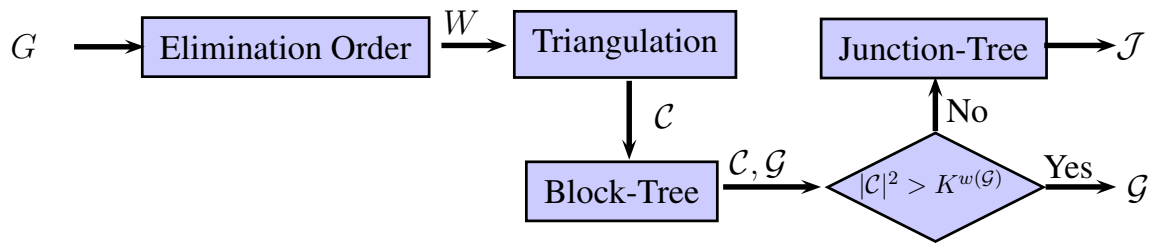

Figure 3.17: Algorithm to choose between a block-tree and a junction-tree for inference over graphical models.

of such algorithms. Using the elimination order, we compute a triangulated graph and find the set of cliques $\mathcal{C}$. We use the set of cliques to find a block-tree as outlined in Section 3.4.3. From the block-tree, we determine if the complexity of constructing the junction-tree dominates the complexity of inference over the block-tree. If this is the case, we use the block-tree for inference, otherwise we construct the junction-tree.

3.6 Summary

We introduced an alternative framework for performing inference over graphical models using block-trees as opposed to using the popular approach of constructing junction-trees. The key difference between a block-tree and junction-tree is that a block-tree is a tree over disjoint clusters of nodes, whereas a junction-tree is a tree connecting overlapping clusters of nodes. We showed that the complexity of constructing block-trees is linear in the number of edges in the graph. This makes the construction of block-trees faster than the construction of junction-trees. We derived message passing algorithms for inference over block-trees that allowed us to define optimal block-trees. We proposed a greedy heuristic for finding optimal block-trees that uses the cliques in the junction-tree. Finally, we compared the complexity of using block-trees and junction-trees for inference. We concluded that, when the complexity of constructing a junction-tree dominates the complexity of performing inference using block-trees, the block-tree is a computationally better framework for performing inference over graphical models. Further, this lead to an algorithm for choosing between junction-trees and block-trees given the task of performing

inference over a graphical model on a graph G.

Chapter 4

Generalizing Algorithms on Graphical Models Using Block-Graphs

4.1 Introduction

In Chapter 3 we saw that exact inference over graphical models is computationally tractable only for a particular class of graphical models with small treewidth. This severely restricts the use of exact inference algorithms in real-world problems. For example, in image processing, it is common to represent images as graphical models over lattices for applications such as denoising and segmentation. However, the treewidth of an $n \times n$ lattice is n and thus for large images, exact inference is intractable. In general, it has been shown that inference over graphical models is NP-hard [18]. Further, recent results have shown that treewidth is the only factor that determines the complexity of inference in graphical models [15]. Thus, for graphical models with large treewidth, there exists no computationally tractable algorithm for exact inference. This has lead to much work in deriving approximate inference algorithms.

The class of approximate inference algorithms can be divided into two categories: stochastic and deterministic. Stochastic methods make use of Markov chain Monte Carlo

(MCMC) algorithms for sampling from a joint probability distribution, see [55] for some examples of these methods. Although sampling based methods are simple and theoretically appealing, they suffer from slow convergence. Deterministic algorithms include loopy belief propagation (LBP) [69], tree-based reparameterization belief propagation (TRP-BP) [83], [94], and tree-reweighted belief propagation (TRW-BP) [95]. These algorithms can be categorized into iterative algorithms or message passing algorithms where nodes in the graph exchange statistical information until convergence. Although message passing algorithms are efficient and have been used effectively in many applications, in many cases, there are no guarantees for the convergence of the algorithm or the quality of estimates. Many researchers have studied and analyzed properties and conditions under which message passing algorithms converge, see [96] for a review of such work.

In this Chapter, we propose a framework for generalizing various algorithms over graphical models so that the message passing occurs between clusters of nodes instead of individual nodes themselves. In the context of inference, it is well known that extending message passing algorithms to cluster based message passing leads to faster convergence and improved estimators [115]. However, frameworks for such extensions are limited and have been proposed in the context of choosing overlapping clusters and only for some specific algorithms. Our main contribution is to propose a general framework for message between clusters where the clusters are disjoint. We propose a simple and efficient algorithm for finding such clusters, where the algorithm modifies the block-tree construction algorithm proposed in Section 3.3.2 to find an appropriate set of disjoint clusters. We call the resulting graph over the disjoint clusters a block-graph.

Section 4.2 presents our framework for generalizing algorithms using block-graphs and applies it to the problem of approximate inference over graphical models. Section 4.3 discusses our algorithm for constructing block-graphs. Section 4.4 presents experimental results. Section 4.5 discusses how our work relates to other works on generalizing algorithms on graphical models. Section 4.6 summarizes this Chapter.

4.2 Generalized Algorithms Using Block-Graphs

Let $\mathbf{x} = \{x_s \in \Omega : s \in V\}$ be a graphical model defined on a graph $G = (V, E)$, where $|V| = n$ and $|\Omega| = K$. For simplicity, we assume that $\mathbf{x}$ is a pairwise graphical model so that the distribution of $\mathbf{x}$ factorizes as

$$p(\mathbf{x}) = \frac{1}{Z} \prod_{i \in V} \phi_i(x_i) \prod_{(i,j) \in E} \psi_{ij}(x_i, x_j)\,, \tag{4.1}$$

where $\phi_i(x_i)$ and $\psi_{ij}(x_i, x_j)$ are positive functions. As shown in [98], any graphical model that factorizes over higher order cliques (as in (3.5) in Chapter 3) can be written in terms of an equivalent graphical model. Thus, the algorithms we derive in this Chapter can be extended to arbitrary graphical models.

The focus in this Chapter is to characterize graphical models using block-graphs. We formally define a block-graph as follows.

Definition 9. *A block-graph is a tuple $\mathcal{G} = (\mathcal{V}, \mathcal{E})$, where $\mathcal{V} = \{\mathcal{V}_1, \mathcal{V}_2, \ldots, \mathcal{V}_l\}$ is a set of non-overlapping clusters and $\mathcal{E}$ are edges connecting clusters so that if $(i, j) \in \mathcal{E}$, $\mathcal{V}_i$ and $\mathcal{V}_j$ are connected by an edge.*

From the definition, it is clear that block-graphs generalize graphs so that each node in the graph contains multiple nodes. Suppose we cluster nodes in the graph $G = (V, E)$ to obtain a block-graph $\mathcal{G} = (\mathcal{V}, \mathcal{E})$, where an edge between $\mathcal{V}_i$ and $\mathcal{V}_j$ means that there exists a node in $\mathcal{V}_i$ that is connected to a node in $\mathcal{V}_j$ in the original graph G. We can now write an alternative factorization of $p(\mathbf{x})$ over the clusters $\mathcal{V}$ such that

$$p(\mathbf{x}) = \frac{1}{Z} \prod_{\mathcal{V}_i \in \mathcal{V}} \Phi_i(x_{\mathcal{V}_i}) \prod_{(i,j) \in \mathcal{E}} \Psi_{ij}(x_{\mathcal{V}_i}, x_{\mathcal{V}_j})\,, \tag{4.2}$$

where we map each factor in (4.1) to an appropriate factor without repeating. The factors $\Psi_{ij}(x_{\mathcal{V}_i}, x_{\mathcal{V}_j})$ only depend on the nodes in $\mathcal{V}_i$ and $\mathcal{V}_j$ that are connected to each other. This dependence was highlighted when we studied block-trees. However, since we will assume that each cluster $\mathcal{V}_i$ has small cardinality, in most of the cases all nodes in $\mathcal{V}_i$ will

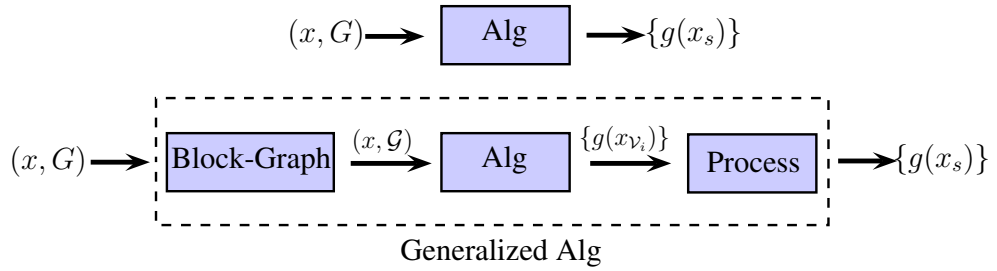

Figure 4.1: A framework for generalizing algorithms on graphical models.

be connected to all nodes in $\mathcal{V}_j$ if $(i, j) \in \mathcal{E}$.

4.2.1 General Theory

Suppose we are given an algorithm **Alg** that operates on the random vector $\mathbf{x}$ that is indexed by the nodes of the graph $G = (V, E)$. Let the output of **Alg** be a functional on each node $g(x_s)$. For inference problems, this output can be the marginal distribution of each node in the random vector $\mathbf{x}$. Our proposed framework for generalizing **Alg** is shown in Fig. 4.1. The various steps are explained as follows.

- From the graph G, we first construct a block-graph $\mathcal{G}$. Algorithms for doing this will be discussed in Section 4.3.
- We then reparameterize the graphical model $\mathbf{x}$ on the block-graph $\mathcal{G}$ using (4.2).
- We now run **Alg** on the reparameterized version of $\mathbf{x}$ defined on $\mathcal{G}$. The output of **Alg** will be functionals over each cluster in the block-graph. For inference problems, this will correspond to finding the joint distribution of $g(x_{\mathcal{V}_i})$ for each cluster $\mathcal{V}_i$ in the block-graph.
- Since we are actually interested in functionals over each node, we process each $g(x_{\mathcal{V}_i})$ to get these functions.

An example illustrating the framework to generalize algorithms on graphical models is shown in Fig. 4.2. We are given a graphical model on a 3×3 grid graph. Instead of

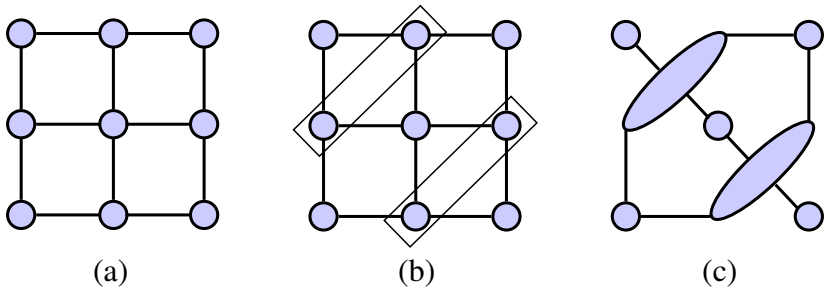

Figure 4.2: Example illustrating how to generalize algorithms on graphical models.

running an algorithm on the grid graph, we cluster some nodes and obtain the block-graph in Fig. 4.2(c).

4.2.2 Approximate Inference Using Block-Graphs

In this Section, we review the loopy belief propagation (LBP) algorithm [69] applied to block-graphs. The algorithm uses the same message passing updates as in the normal belief propagation (see Section 3.2.3) applied to tree-structured graphs, but ignores the fact that the graph is not tree-structured.

Let $\mathcal{G} = (\mathcal{V}, \mathcal{E})$ be the block-graph and suppose we have reparametrized the graphical model $\mathbf{x}$ on $\mathcal{G}$ using (4.2). Let $m^t_{i\to j}(x_{\mathcal{V}_j})$ denote the message passed from cluster $\mathcal{V}_i$ to $\mathcal{V}_j$. Assume the initial messages at $t = 0$ are unity, i.e., $m^0_{i\to j}(x_{\mathcal{V}_j}) = 1$ for all $x_{\mathcal{V}_j} \in \Omega^{|\mathcal{V}_j|}$ and $(i, j) \in \mathcal{E}$. For each iteration, the message passing updates are given as follows:

$$m^t_{i\to j}(x_{\mathcal{V}_j}) = \sum_{x_i} \Phi_i(x_{\mathcal{V}_i})\Psi_{ij}(x_{\mathcal{V}_i}, x_{\mathcal{V}_j}) \prod_{k\in\mathcal{N}(i)\setminus j} m^{t-1}_{k\to i}(x_{\mathcal{V}_i})\,, \tag{4.3}$$

where $\mathcal{N}(i)$ denotes the neighbors of the cluster $\mathcal{V}_i$. Note that for each edge $(i, j) \in \mathcal{E}$, we pass messages from $\mathcal{V}_i$ to $\mathcal{V}_j$ and from $\mathcal{V}_j$ to $\mathcal{V}_i$. After T iterations, the joint distribution of each cluster $\mathcal{V}_i$ is given as

$$p_{\mathcal{V}_i}(x_{\mathcal{V}_i}) = \frac{1}{Z_i} \prod_{j\in\mathcal{N}(i)} \Phi_i(x_{\mathcal{V}_i}) m^t_{j\to i}(x_{\mathcal{V}_i})\,. \tag{4.4}$$

To find the final marginal distribution of each node, we marginalize the distribution $p_{\mathcal{V}_i}(x_{\mathcal{V}_i})$. The following theorem summarizes the complexity of LBP using block-graphs for computing the marginal distribution of each node.

Theorem 4.2.1. *Given a graphical model* $\mathbf{x}$ *parameterized on a block-graph* $\mathcal{G}$*, the complexity of inference using the loopy belief propagation algorithm is*

$$O\left(2T\sum_{(i,j)\in\mathcal{E}} K^{|\mathcal{V}_i|+|\mathcal{V}_j|}\right) + O\left(\sum_{\mathcal{V}_i\in\mathcal{V},|\mathcal{V}_i|>1} |\mathcal{V}_i|\, K^{|\mathcal{V}_i|}\right), \tag{4.5}$$

where the first term corresponds to the complexity of passing $2T$ *messages between edges in the block-graph using (4.3) and the second term corresponds to the complexity of marginalizing the distribution of each cluster.*

The complexity of LBP on the original graph is $O(2T|V|K^2)$, where T is again the number of iterations. The next Section discusses an algorithm to find the block-graph $\mathcal{G}$ given the original graph G.

4.3 Constructing Block-Graphs

From (4.5), we know that the complexity of message passing between two disjoint clusters $\mathcal{V}_i$ and $\mathcal{V}_j$ is at most exponential in $|\mathcal{V}_i|+|\mathcal{V}_j|$. We assume a user defined maximal message passing complexity m so that the complexity of message passing between any two clusters is at most $O(K^m)$, where K is the number of states each random variable can take. In general, m will be chosen to be sufficiently small so that inference is tractable. We modify the linear time block-tree construction algorithm in Section 3.3.2 to construct a block-graph using the following steps.

Step 1. Using an initial cluster of nodes V_1, find clusters $V_1, V_2, \ldots, V_r$ using breadth-first search (BFS) such that $V_2 = \mathcal{N}(V_1), V_3 = \mathcal{N}(V_2)\backslash\{V_1 \cup V_2\}, \ldots, V_r = \mathcal{N}(V_r)\backslash\{V_{r-2} \cup V_{r-1}\}$. While doing the BFS, write V_k as the set of all connected components in the subgraph $G(V_k)$. Thus, V_k is a set of clusters.

Step 2. To ensure that the user defined maximal message passing complexity is satisfied, for k odd, we split the clusters in V_k so that each cluster has maximal cardinality $\lceil m/2 \rceil$ and for k even, we split clusters in V_k so that each cluster has maximal cardinality $\lfloor m/2 \rfloor$. This ensures that for all messages passed between clusters in different V_k, the message passing complexity is at most $O(K^m)$.

Step 3. For V_r, if there exists any cluster that has cardinality greater than $\lceil m/2 \rceil$ or $\lfloor m/2 \rfloor$, depending on whether r is odd or even, partition those components. Let $V_r = \{V_r^1, V_r^2, \ldots, V_r^{m_r}\}$ be the final set clusters.

Step 4. We perform the next steps for each $k = r-1, r-2, \ldots, 1$, starting at $k = r-1$. Let $\widetilde{V}_k$ be the set of all clusters V_k that have cardinality greater than $\lceil m/2 \rceil$ or $\lfloor m/2 \rfloor$, dependending on whether k is odd or even.

Step 5. Partition all clusters in $\widetilde{V}_k$ into appropriate size clusters of size $\lceil m/2 \rceil$ or $\lfloor m/2 \rfloor$ and also ensuring that the message passing complexity between clusters created is at most $O(K^m)$.

Step 6. We now merge the clusters in the set $V_k \backslash \widetilde{V}_k$. The idea used in merging clusters is that if two clusters are connected to the same cluster in V_{k+1}, then by merging these two clusters, we reduce one edge in the final block-graph. Further, if two clusters in V_k are not connected to the same cluster in V_{k+1}, we do not merge these two clusters, since the number of edges in the final block-graph will remain the same. The final clusters constructed using the above rules are denoted as $V_k = \{V_k^1, \ldots, V_k^{m_k}\}$.

Step 7. The block-graph is given by the clusters $\mathcal{V} = \bigcup_{k=1}^{r} \{V_k^1, V_k^2, \ldots, V_k^{m_k}\}$ and the set of edges $\mathcal{E}$ between clusters.

The key step in the above algorithm is Step 6, where we cluster nodes appropriately. Fig. 4.3 explains the intuition behind merging clusters with an example. Suppose, we use the block-graph construction algorithm up to Step 5 and now we want to merge clusters

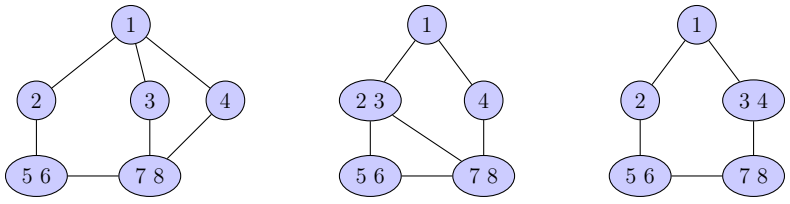

Figure 4.3: Explaining Step 6 in the block-graph construction algorithm. Given the block-graph in (a), if we merge nodes 2 and 3, we get the block-graph in (b). If we merge nodes 3 and 4, we get the block-graph in (c). Notice that the block-graph in (c) has just one loop.

in $V_2 = \{2, 3, 4\}$. If we ignore Step 6 and merge clusters randomly, we might get the block-graph in Fig. 4.3(b) on merging nodes 2 and 3. If we use Step 6, then since nodes 3 and 4 are connected to the same node, we merge these to get the block-graph in Fig. 4.3(c). Notice that Fig. 4.3(c) is a graph with a single cycle with five edges, whereas Fig. 4.3(b) is a graph two cycles of size four and three. It has been observed that inference over graphs with longer cycles is more accurate than inference over graphs with shorter cycles [25]. Thus our proposed algorithm leads to block-graphs that are favorable for inference.

4.4 Numerical Simulations

In this Section, we provide numerical simulations to show the performance gains when using block-graphs for inference over graphical models. We primarily study the problem of performing inference over binary valued graphical models over grid graphs. For each random variable, let $x_s \in \{-1, +1\}$. We consider the following node and edge potentials when running simulations:

$$\phi_i(x_i) = \exp(-a_i x_i) \tag{4.6}$$

$$\text{Repulsive: } \phi_i(x_i, x_j) = \exp(-|b_{ij}| x_i x_j) \tag{4.7}$$

$$\text{Attractive: } \phi_i(x_i, x_j) = \exp(|b_{ij}| x_i x_j) \tag{4.8}$$

$$\text{Mixed: } \phi_i(x_i, x_j) = \exp(-b_{ij} x_i x_j)\,, \tag{4.9}$$

where $a_i \sim \mathcal{N}(0, (0.25^2)$ and $b_{ij} \sim \mathcal{N}(0, 1)$. For distributions with attractive (repulsive) potentials, neighboring random variables are more likely to take the same (opposite) value. For distributions with mixed potentials, some neighbors are attractive, whereas some are repulsive. We consider three types of graphs: 7×7 grid graphs, 8×8 grid graphs, and 30×30 grid graphs. The analysis of the results from the numerical simulations are as follows:

- Notation: LBP refers to running loopy belief propagation on the original graph. LBPm refers to running LBP on a block-graph constructed using our proposed algorithm in Section 4.3 such that the maximal message passing complexity is $O(K^m)$. LBPm-Rand refers to using a modification of the algorithm in Section 4.3 so that instead of merging clusters in a structured manner using Step 5 and Step 6, we instead merge clusters randomly. Note that each iteration of the LBP algorithm has complexity $O(2|E|K^2)$. On the other hand, running LBP on block-graphs has higher complexity (see Theorem 4.5). To objectively compare results on the number of iterations, we rescale the values. Thus, if the LBP on a block-graph converges in T iterations, we rescale this number by $T \cdot C'/C$, where C' is the complexity of inference using the block-graph and C is the complexity of using just the graph. We declare convergence if the absolute difference between the messages passed in successive iterations is less than a threshold of $\epsilon = 10^{-4}$. If the algorithm does not converge in 3000 iterations, we say the algorithm failed to converge. Given the true marginal distribution $p_s(x_s)$ of each node and an estimate $\widehat{p}_s(x_s)$, the accuracy is measured by

$$\text{Accuracy} = \frac{1}{2|V|} \sum_{x_s \in \{-1,+1\}} \left| p_s(x_s) - \widehat{p}_s(x_s) \right|. \tag{4.10}$$

- 7×7 grid graph: Fig. 4.4 shows results of running LBP on block-graphs and running LBP on the original 7×7 grid graph. The first three columns report the number of times the algorithm converged out of 500 runs. LBP using mixed potentials converged only 60% of the time, whereas LBP4 and LBP4-Rand converged on all

	Number of runs that converged			Number of Iterations for conv.			Accuracy		
	R	A	M	R	A	M	R	A	M
LBP	500	500	302	22.7	24.9	142.4	0.213	0.219	0.065
LBP4	500	500	500	35.1	37.2	128.9	0.189	0.189	0.046
LBP4-Rand	500	500	500	43.7	44.1	225.7	0.187	0.185	0.058

Figure 4.4: Comparison of convergence and accuracy of using LBP on graphs vs. using LBP on block-graphs for a 7×7 grid graph. Results are over 500 runs. The iterations and accuracy results are when all the algorithms converge.

	Number of runs that converged			Number of Iterations for conv.			Accuracy		
	R	A	M	R	A	M	R	A	M
LBP	200	200	72	25.3	24.8	220.7	0.217	0.214	0.073
LBP4	200	200	200	38.1	37.7	191.1	0.199	0.191	0.052
LBP6	200	200	200	69.2	66.5	192.8	0.174	0.157	0.037
LBP6-Rand	200	200	200	64.4	62.7	368.5	0.178	0.182	0.073

Figure 4.5: Comparison of convergence and accuracy of using LBP on graphs vs. using LBP on block-graphs for a 8×8 grid graph. Results are over 200 runs. The iterations and accuracy results are when all the algorithms converge.

500 runs. This suggests that mixed potentials cause Ising models to sometimes not converge. Comparing the mean number of iterations (which are rescaled) required for convergence, we note that for both attractive and repulsive potentials, LBP converges faster. However, for mixed potentials, block-graphs converge faster. Comparing LBP4 and LBP4-Rand, we see the benefits of merging clusters in a structured manner rather than merging clusters randomly since LBP4 converges faster than LBP4-Rand. For mixed potentials, the convergence speed is almost twice as that of LBP4-Rand. Comparing the accuracy, we see that using block-graphs leads to smaller errors. Comparing LBP4 and LBP4-Rand, for repulsive and attractive potentials there is almost no difference between the error, however, for mixed potentials, LBP4 has lower error.

- 8×8 grid graph: Fig. 4.4 shows results of running LBP on block-graphs and running LBP on the original 8×8 grid graph. The interpretation of the results are similar to that of the results for the 7×7 grid graph. We notice that increasing the message passing complexity to 6, compared to 4, improves the estimates of the

node potentials at the cost of higher computational cost. Comparing LBP6-Rand to LBP4, we notice that for mixed potentials LBP4 performs better suggesting and LBP6-Rand performs as good as LBP.

- 30×30 grid graph: Fig. 4.4 shows results of running LBP on block-graphs and running LBP on the original 30×30 grid graph. In this case, over 100 runs, the LBP failed to converge in 3000 iterations. The interpretation of the results is the same as before. We note that to compare the quality of the estimates, we did not have the true estimates available since it is computationally intractable to find these since the graph has high treewidth. Instead we ran LBP on a block-graph with maximal message passing complexity $O(K^{10})$ and used these estimates as the ground truth. Note that even though LBP did not get converge in 3000 iterations, the quality of the estimate is almost the same as that of using LBP8-Rand.

From the numerical simulations presented above, it is clear that using LBP on block-graphs leads to more accurate estimates of the marginal distributions. For repulsive and attractive node potentials, we observed that higher accuracy comes at the cost of more computations. For mixed potentials, we observed that using block-graphs was more accurate and faster than using the original graph. Further, we evaluated our proposed algorithm for constructing block-graphs and noticed that our proposed algorithm leads to more accurate estimates when compared to an approach of randomly selecting clusters. This shows the advantage of using the block-tree as an initial estimate of the block-graph.

4.5 Related Work

There has been a lot of work in extending the BP algorithm of message passing between nodes to message passing between clusters. It is known that the true marginal distributions of a graphical model minimizes the Gibbs free energy [35]. In [114], [115], the authors showed that the fixed points of the BP algorithm minimize the Bethe free energy, which is an approximation to the Gibbs free energy. This motivated the Generalized Be-

	Number of runs that converged			Number of Iterations for conv.			Accuracy*		
	R	A	M	R	A	M	R	A	M
LBP	100	100	0	86.85	83.74	-	0.232	0.243	0.114
LBP4	100	100	100	126.6	120.2	1971.8	0.157	0.181	0.078
LBP8	100	100	100	454.1	512.2	7769.9	0.083	0.068	0.059
LBP8-Rand	100	100	100	493.9	491.5	5574	0.258	0.257	0.101

Figure 4.6: Comparison of convergence and accuracy of using LBP on graphs vs. using LBP on block-graphs for a 30×30 grid graph. Results are over 100 runs. Since finding the true node potentials is computatinally intractable, we use a higher order block-graph to estimate the ground truth.

lief Propagation (GBP) algorithm that minimized the Kikuchi free energy [41], a better approximator to the Gibbs free energy. In GBP, the message passing is between clusters of nodes in the graph. A more general approach to GBP is proposed in [116] using region graphs and in [70] using the cluster variation method. Further, region graphs have been used in [93], [94] to extend the TRP based method for inference in graphical models.

Although [93], [116] show that approximate inference can be improved using clustering, they do not address the problem of choosing regions or clusters in arbitrary graphs over which we want to perform message passing. As shown in our experimental results, arbitrarily choosing clusters may not result in better inference algorithms. In [99], [100], the authors have considered methods for choosing regions, however, their algorithms are limited to a small class of graphical models. In [57], the authors propose Iterative Join-Graph Propagation (IJGP), which is a class of GBP algorithms. The IJGP algorithm first computes a junction-tree and then randomly splits appropriate clusters into smaller clusters to build a join-graph (or cluster-graph). However, since IJGP uses junction-trees, the clusters chosen are overlapping and thus it is important to assign edges over these clusters so that the running intersection property (see Definition 7) is satisfied. This constraint, combined with the fact that we are constructing a junction-tree, makes the construction of a join-graph computationally hard. Thus, for problems where the graph structure changes over time, using junction-tree based algorithms can be computationally infeasible. Another restriction of the IJGP based approach is that it does not generalize other algorithms for message passing such as TRP-BP or TRW-BP.

Our proposed approach of using non-overlapping clusters for approximate inference has been considered before. In the original paper describing GBP [114], the authors gave an example of how disjoint clusters can be used, however, there have been no algorithms in the literature that show how such clusters can be chosen. In [111], [112], the authors use disjoint clusters to generalize mean field algorithms for approximate inference. Although we don't demonstrate the use of our algorithm for mean field methods, the clustering algorithm used in [112] is based on standard graph partitioning algorithms that are computationally intensive for large graphs. Our approach to forming clusters is simple, efficient, and motivated by observations that inference over graphs with longer cycles is easier than inference over graphs with shorter cycles.

4.6 Summary

We proposed a framework for generalizing algorithms over graphical models using the notion of block-graphs, defined as a graph where each node is a cluster of nodes and the clusters are disjoint. We proposed a simple and efficient algorithm for constructing block-graphs that relied on block-trees to construct an initial estimate of the disjoint cluster of nodes. Our numerical simulations showed the advantages of using block-graphs for approximate inference over graphical models. We also showed that our proposed algorithm for constructing block-graphs leads to more accurate estimates of marginal distributions than an algorithm that randomly selects clusters to form a block-graph.

Chapter 5

Conclusion and Future Work

5.1 List of Contributions

In this thesis, we studied the problem of finding tree-structured like representations for Markov random fields (MRFs). Our main contributions are as follows:

1. For MRFs over continuous indices, we showed that tree-structured like representations can be derived over a collection of hypersurfaces. This reparameterization of the field allowed us to study MRFs as Markov processes, thereby allowing us to extend algorithms like the Kalman-Bucy filter to random fields.

2. For MRFs over graphs, we showed that tree-structured like representations can be derived by clustering nodes in the original graph to construct a tree-structured graph over the cluster of nodes. We called the resulting tree over the clusters a block-tree and showed how the belief propagation algorithm for inference (computing marginal distribution given a joint distribution) over MRFs can be extended to MRFs characterized by block-trees.

3. Finally, we proposed an algorithm for generalizing various algorithms over graphical models using the notion of a block-graph, defined as a graph over disjoint cluster of nodes. We proposed an efficient algorithm for constructing block-graphs and showed how our framework for generalization can be used for generalized belief propagation.

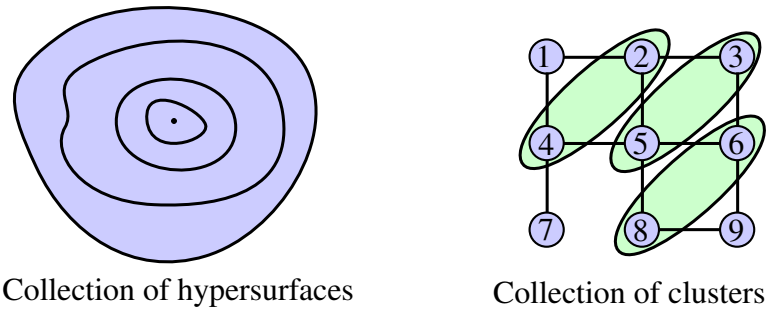

Figure 5.1: An example of the tree-structures we derive in this thesis. For MRFs over continuous indices, we derive tree representations over hypersurfaces. For MRFs over graphs, we derive tree representations over a disjoint collection of clusters over nodes.

5.2 Chapter Summaries

5.2.1 Chapter 2: Tree-Structures in MRFs over Continuous Indices

In Chapter 2, we derived tree-structured like representations for MRFs indexed over continuous indices. Although these MRFs were introduced in 1956 by Lévy, there had been no prior work on finding recursive representations that can enable the extension of Kalman filters to random fields. We showed that a natural tree like representation for MRFs exists on a collection of hypersurfaces starting at the boundary and telescoping inwards. See Fig. 5.1 for an example for an example.

To derive recursive representations, we parameterized the field indexed over some region $S \in \mathbb{R}^d$, $d > 1$, by a tuple (λ, θ), where $\lambda \in [0, 1]$ is the parameter over which we derive recursions and $\theta \in \Theta \subset \mathbb{R}^{d-1}$ parameterizes the hypersurfaces over which we define recursions. For Gaussian MRFs (GMRFs), we showed that a representation over the hypersurfaces is given by a linear stochastic differential equation of the form

$$dx_\lambda(\theta) = F_\theta[x_\lambda(\theta)] + B_\lambda(\theta) w_\lambda(\theta)\,, \tag{5.1}$$

where $F_\theta[x_\lambda(\theta)]$ is a functional over the field defined on $x_\lambda(\theta)$ for all $\theta \in \Theta$ and the driving noise $w_\lambda(\theta)$ can be interpreted as Brownian motion for each fixed θ. Equation (5.1)

generalizes known state-space models for Gaussian Markov random processes to GMRFs. Using (5.1), we derived extensions of the Kalman-Bucy filter [40] and Rauch-Tung-Striebel smoother [75]. The recursions for the Kalman filter initiated at the boundary and telescoped inwards and the recursions for the smoother telescoped inwards and outwards.

5.2.2 Chapter 3: Block-Tree Structures in MRFs over Graphs

In Chapter 3, we studied MRFs indexed over graphs, often referred to as graphical models. Our main contribution was to show that a tree-structured representation for arbitrary graphical models can be derived by clustering nodes in the graph to form a tree over disjoint clusters of nodes. Our proposed algorithm for constructing such graphs, which we call block-trees, is simple and efficient with a complexity linear in the number of edges. See Fig. 5.1 for an example of a block-tree for a 3×3 grid graph.

We compared block-trees to junction-trees [77], a tree-structured graph over clusters that are overlapping. We showed that constructing block-trees is faster than constructing junction-trees. Further, in the context of inference over graphical models (computing marginal distributions given a joint probability distribution), we showed the advantages of using block-trees vs. using junction-trees. Finally, we proposed an algorithm for choosing between a junction-tree and a block-tree when performing inference over graphical models.

5.2.3 Chapter 4: Generalizing Algorithms on Graphical Models

In Chapter 4, we proposed a framework for generalizing algorithms over graphical models. The main idea is to cluster nodes in the graph to form a block-graph and then run algorithms over the block-graph instead of the original graph. As an example, we showed how loopy belief propagation (LBP) [69], an approximate inference algorithm for computing marginal distributions, can be easily generalized using block-graphs. The need for approximate inference algorithm arises because for many graphs, the clusters in a block-tree or a junction-tree can be large, so performing exact inference is intractable.

Our main contribution is to propose an algorithm for constructing block-graphs that

modifies the algorithm for constructing block-trees. The main idea is to split larger clusters in a block-tree so that there are minimal number of edges in the block-graph. Numerically, we observed that using LBP on block-graphs leads to better estimates than using LBP on the original graph. Further, we also observed that using our proposed algorithm for constructing block-graphs leads to better estimates than using a block-graph constructed by randomly clustering nodes.

5.3 Suggestions for Future Work

The work in this thesis naturally leads to other research ideas that we briefly discuss here.

5.3.1 Estimation of Random Fields Over Continuous Indices

In this thesis, we showed that a natural recursive representation for Markov random fields (MRFs) is in terms of tree-structured like representations over a collection of hypersurfaces. In reality, a random field may not necessarily be an MRF. For such cases, it is of interest to find efficient algorithms for processing data. To do this, we can study the problem of finding an approximate telescoping representation given an arbitrary Gaussian random field. Further, since there is flexibility in choosing the hypersurfaces in the telescoping representation, there can exist multiple different approximate telescoping representations. Thus, one way to proceed is to model the underlying random field as a mixture of telescoping representations on various collections of hypersurfaces. This approach to finding stochastic models is in concept similar to work done in [60], where the authors model an arbitrary distribution using a mixture of tree-structured graphical models.

5.3.2 Other Applications of Using Block-Graphs

In this thesis, we proposed a framework for generalizing current algorithms on graphical models. As an example, we consider the problem of generalizing loopy belief propagation and showed numerical simulations to validate that the generalized algorithm leads to bet-

ter estimates. It is easy to see that other known algorithms can also be generalized. It will be interesting to see what kinds of improvements one can get by running the generalized algorithm on other algorithms. Further, our approach to generalizing algorithms is not only limited to inference algorithms, but can also be applied to problems such as MAP inference [96] and computing the partition function for graphical models [95].

5.3.3 Learning Graphical Models Using Block-Graphs

In this thesis, we considered the problem of deriving algorithms on graphical models. Another problem of interest in graphical models is to derive algorithms for learning the structure and parameters of a graphical models given observed samples. This problem in general is NP-hard, however, there are works in the literature [61], [76] that propose consistent algorithms for learning graphical models under some conditions. In recent work, we have derived theoretical conditions under which algorithms for learning graphical models can be improved [91] using ideas from list decoding [22]. We have also applied the idea of clustering nodes towards a problem on approximating high-dimensional distributions [20]. One interesting question that can be asked is whether graphical model selection algorithms can be improved if we cluster nodes and apply current algorithms for learning graphical model to the cluster of nodes instead of individual nodes themselves. This approach can be thought of as the extension of the generalized algorithm we proposed in Chapter 4.

Appendix A

Appendix to Chapter 2

A.1 Computing $b_j(s,r)$ in Theorem 2.2.1

We show how the coefficients $b_j(s,r)$ are computed for a GMRF $x(t)$, $t \in T \subset \mathbb{R}^d$. Let G_- and G_+ be complementary sets in $T \subset \mathbb{R}^d$ as shown in Fig. 2.2. Following [73], define a function $h_s(t)$ such that

$$h_s(t) = \begin{cases} R(s,t) & t \in G_- \cup \partial G \\ h_s(t) : \mathcal{L}_t h_s(t) = 0\,, & \\ h_s(\partial G) = R(s,\partial G) & t \in G_+ \\ h_s(t) \in H_0^m(T) & \end{cases}, \tag{A.1}$$

where $\mathcal{L}_r$ is defined in (2.11) and $H_0^m(T)$ is the completion of $C_0^\infty(T)$, the set of infinitely differentiable function with compact support in T, under the norm Sobolov norm order m. From (2.10), it is clear that $h_s(r) \neq R(s,r)$ when $r \in G_+$. Let $u(r) \in C_0^\infty(T)$ and consider the following steps for computing $b_j(s,r)$:

$$\sum_{|\alpha|,|\beta|\leq m} \int_T D^\alpha u(t) a_{\alpha\beta}(t) D^\beta h_s(t) dt$$

$$= \sum_{|\alpha|,|\beta|\leq m} \int_{G_-} D^\alpha u(t) a_{\alpha,\beta}(t) D^\beta R(s,t) dr \sum_{|\alpha|,|\beta|\leq m} \int_{G_+} D^\alpha u(t) a_{\alpha,\beta}(t) D^\beta h_s(t) dr \tag{A.2}$$

$$= \sum_{j=0}^{m-1} \int_{\partial G} b_j(s,r) \frac{\partial^j}{\partial n^j} u(r) dl + \int_{G_-} u(r) L_t R(s,t) dt + \int_{G_+} u(t) L_t h_s(t) dt \tag{A.3}$$

$$= \sum_{j=0}^{m-1} \int_{\partial G} b_j(s,r) \frac{\partial^j}{\partial n^j} u(r) dl \,. \tag{A.4}$$

To get (A.2), we split the integral integral on the left hand side over G_- and G_+. In going from (A.2) to (A.3), we use integration by parts and the fact that $u(r) \in C_0^\infty(T)$. We get (A.4) using (2.10) and (A.1). Thus, to compute $b_j(s,r)$, we first need to find $h_s(r)$ using (A.1) and then use the steps in (A.2)−(A.4). We now present an example where we compute $b_j(s,r)$ for a Gauss-Markov process.

Example: Let $x(t) \in \mathbb{R}$ be the Brownian bridge on $T = [0,1]$ such that

$$x(t) = w(t) - tw(1) \,, \tag{A.5}$$

where $w(t)$ is a standard Brownian motion. Since covariance of $w(t)$ is $\min(t,s)$, the covariance of $x(t)$ is given by

$$R(t,s) = \begin{cases} s(1-t) & t > s \\ t(1-s) & t < s \end{cases} \,. \tag{A.6}$$

Using the theory of reciprocal processes, see [46], [52], it can be shown that the operator $\mathcal{L}_t$ is

$$L_t R(t,s) = -\frac{\partial^2 R(t,s)}{\partial t^2} = \delta(t-s) \,. \tag{A.7}$$

Thus, the inner product associated with $R(t,s)$ is given by

$$< u, v >= \langle Du, Dv \rangle_T = \int_0^1 \frac{\partial}{\partial s} u(s) \frac{\partial}{\partial s} v(s) ds \,. \tag{A.8}$$

Following (A.1), for $r < 1$ and $s \in [r,1]$, $h_s(t) = R(s,t)$ for $t \in [0,r]$ and

$$-\frac{\partial^2}{\partial t^2} h_s(t) = 0 \,, \quad t > r \tag{A.9}$$

$$h_s(r) = r(1-s)\,, \quad h_s(1) = 0\,. \tag{A.10}$$

We can trivially show that $h_s(t)$ is given by

$$h_s(t) = \frac{r(1-s)}{1-r}(1-t)\,, \quad t \geq r\,. \tag{A.11}$$

We now follow the steps in (A.2)-(A.4):

$$\begin{aligned}
\int_0^1 \frac{\partial}{\partial t}u(t)\frac{\partial}{\partial t}h_s(t)dt &= \int_0^r \frac{\partial}{\partial t}u(t)\frac{\partial}{\partial t}R(s,t)dt + \int_r^1 \frac{\partial}{\partial t}u(t)\frac{\partial}{\partial t}h_s(t)dt \\
&= u(t)\frac{\partial}{\partial t}R(s,t)\Big|_0^r + u(t)\frac{\partial}{\partial t}h_s(t)\Big|_r^1 \\
&= \left(\frac{\partial}{\partial t}R(s,r) - \frac{\partial}{\partial r}h_s(r)\right)u(r)\,. \\
&= \frac{1-s}{1-r}u(r)\,.
\end{aligned}$$

Using Theorem 2.2.1, we can compute $E[x(s)|\sigma\{x(t) : 0 \leq t \leq r\}]$ as

$$E[x(s)|\sigma\{x(t) : 0 \leq t \leq r\}] = E[x(s)|x(r)] = \left(\frac{1-s}{1-r}\right)x(r)\,. \tag{A.12}$$

We note that since $x(t)$ is a Gauss-Markov process, it is known that, [107],

$$E[x(s)|x(r)] = R(s,r)R^{-1}(r,r)x(r)\,. \tag{A.13}$$

Using the expression for $R(s,r)$, we can easily verify that (A.12) and (A.13) are equivalent.

A.2 Proof of Theorem 2.3.1: Telescoping Representation

Let $\widehat{x}_{\lambda+d\lambda|\lambda}(\theta)$ denote the conditional expectation of $x_{\lambda+d\lambda}(\theta)$ given the σ-algebra generated by the field $\{x_\mu(\alpha) : (\mu,\alpha) \in [0,\lambda] \times \Theta\}$. From Theorem 2.2.1, we have

$$\widehat{x}_{\lambda+d\lambda|\lambda}(\theta) = \sum_{j=0}^{m-1} \int_\Theta b_j((\lambda+d\lambda,\theta),(\lambda,\alpha)) \frac{d^j}{dn^j} x_\lambda(\alpha) d\alpha \,. \tag{A.14}$$

It is clear that $x_\lambda(\theta) = \widehat{x}_{\lambda|\lambda}(\theta)$. Taking the limit in (A.14) as $d\lambda \to 0$, we have

$$x_\lambda(\theta) = \sum_{j=0}^{m-1} \int_\Theta b_j((\lambda,\theta),(\lambda,\alpha)) \frac{d^j}{dn^j} x_\lambda(\alpha) d\alpha \,. \tag{A.15}$$

Define the error as $\xi_{\lambda+d\lambda}(\theta)$ such that

$$\xi_{\lambda+d\lambda}(\theta) = x_{\lambda+d\lambda}(\theta) - \widehat{x}_{\lambda+d\lambda}(\theta) \,. \tag{A.16}$$

Adding and subtracting $x_\lambda(\theta)$ in (A.16) and using (A.15), we have

$$\begin{aligned} x_{\lambda+d\lambda}(\theta) - x_\lambda(\theta) = \sum_{j=0}^{m-1} \int_\Theta & [b_j((\lambda+d\lambda,\theta),(\lambda,\alpha)) \\ & - b_j((\lambda,\theta),(\lambda,\alpha))] \frac{d^j}{dn^j} x_\lambda(\alpha) d\alpha + \xi_{\lambda+d\lambda}(\theta) \,. \end{aligned} \tag{A.17}$$

Assuming $d\lambda$ is small, we can write $b_j((\lambda+d\lambda,\theta),(\lambda,\alpha)) - b_j((\lambda,\theta),(\lambda,\alpha))$ as

$$\begin{aligned} & b_j((\lambda+d\lambda,\theta),(\lambda,\alpha)) - b_j((\lambda,\theta),(\lambda,\alpha)) \\ & = \frac{b_j((\lambda+d\lambda,\theta),(\lambda,\alpha)) - b_j((\lambda,\theta),(\lambda,\alpha))}{d\lambda} d\lambda & \text{(A.18)} \\ & = \left(\lim_{\mu \to \lambda^+} \frac{\partial}{\partial \mu} b_j((\mu,\theta),(\lambda,\alpha)) \right) d\lambda \,, & \text{(A.19)} \end{aligned}$$

where in going from (A.18) to (A.19), we use the assumption that $d\lambda$ is close to zero.

Writing $dx_\lambda(\theta) = x_{\lambda+d\lambda}(\theta) - x_\lambda(\theta)$ and substituting (A.19) in (A.17), we get

$$dx_\lambda(\theta) = F_\theta[x_\lambda(\theta)]d\lambda + \xi_{\lambda+d\lambda}(\theta)\,, \tag{A.20}$$

where F_θ is given in (2.18). To get the final form of the telescoping representation, we need to characterize $\xi_{\lambda+d\lambda}(\theta)$. To do this, we write $\xi_{\lambda+d\lambda}(\theta)$ as

$$\xi_{\lambda+d\lambda}(\theta) = B_\lambda(\theta)dw_\lambda(\theta) = B_\lambda(\theta)[w_{\lambda+d\lambda}(\theta) - w_\lambda(\theta)]\,. \tag{A.21}$$

We now prove the properties of $w_\lambda(\theta)$:

i) Since $\xi_\lambda(\theta) = x_\lambda(\theta) - \widehat{x}_{\lambda|\lambda}(\theta)$ and $\widehat{x}_{\lambda|\lambda}(\theta) = x_\lambda(\theta)$ by definition, we have

$$\lim_{d\lambda\to 0} \xi_{\lambda+d\lambda}(\theta) = \xi_\lambda(\theta) = 0\,, a.s..$$

Thus, using (A.21), since $B_\lambda(\theta) \neq 0$, we have

$$\lim_{d\lambda\to 0} w_{\lambda+d\lambda}(\theta) - w_\lambda(\theta) = 0, a.s. \tag{A.22}$$

$$\lim_{d\lambda\to 0} w_{\lambda+d\lambda}(\theta) = w_\lambda(\theta), a.s. \tag{A.23}$$

Equation (A.23) shows that $w_\lambda(\theta)$ is almost surely continuous in λ.

ii) Since the driving noise at the boundary of the field can be captured in the boundary conditions, without loss in generality, we can assume that $w_0(\theta) = 0$ for all $\theta \in \Theta$.

iii) For $0 \leq \lambda_1 \leq \lambda_1' \leq \lambda_2 \leq \lambda_2'$ and $\theta_1, \theta_2 \in \Theta$, let $d\lambda_1 = \lambda_1' - \lambda_1$ and $d\lambda_2 = \lambda_2' - \lambda_2$. Consider the covariance

$$E[\xi_{\lambda_1+d\lambda_1}(\theta_1)\xi_{\lambda_2+d\lambda_2}(\theta_2] = E\left[\left(x_{\lambda_1+d\lambda_1}(\theta_1) - \widehat{x}_{\lambda_1+d\lambda_1}(\theta_1)\right)\xi_{\lambda_2+d\lambda_2}(\theta_2)\right] \tag{A.24}$$

$$= E[x_{\lambda_1+d\lambda_1}(\theta_1)\xi_{\lambda_2+d\lambda_2}(\theta_2)] \tag{A.25}$$

$$- E[\widehat{x}_{\lambda_1+d\lambda_1}(\theta_1)\xi_{\lambda_2+d\lambda_2}(\theta_2)]$$

$$= 0\,, \tag{A.26}$$

where to go from (A.24) to (A.25), we use the orthogonality of the error. Using the definition of $\xi_{\lambda+d\lambda}(\theta)$ in (A.21), we have that $w_{\lambda_1'}(\theta_1) - w_{\lambda_1}(\theta_1)$ and $w_{\lambda_2'}(\theta_2) - w_{\lambda_2}(\theta_2)$ are independent random variables.

iv) We now compute $E[\xi_{\lambda+d\lambda}(\theta_1)\xi_{\lambda+d\lambda}(\theta_2)]$:

$E[\xi_{\lambda+d\lambda}(\theta_1)\xi_{\lambda+d\lambda}(\theta_2)]$

$$
\begin{aligned}
&= E[\xi_{\lambda+d\lambda}(\theta_1)(x_{\lambda+d\lambda}(\theta_2) - \widehat{x}_{\lambda+d\lambda|\lambda}(\theta_2))] \\
&= E[(x_{\lambda+d\lambda}(\theta_1) - \widehat{x}_{\lambda+d\lambda|\lambda}(\theta_1))x_{\lambda+d\lambda}(\theta_2)] \\
&= R_{\lambda+d\lambda,\lambda+d\lambda}(\theta_1,\theta_2) - \sum_{j=0}^{m-1}\int_\Theta b_j((\lambda+d\lambda,\theta_1),(\lambda,\alpha))\frac{\partial^j}{\partial n^j}R_{\lambda,\lambda+d\lambda}(\alpha,\theta_2)d\alpha \\
&= R_{\lambda+d\lambda,\lambda+d\lambda}(\theta_1,\theta_2) - R_{\lambda,\lambda+d\lambda}(\theta_1,\theta_2) + R_{\lambda,\lambda+d\lambda}(\theta_1,\theta_2) \qquad \text{(A.27)} \\
&- \sum_{j=0}^{m-1}\int_\Theta b_j((\lambda+d\lambda,\theta_1),(\lambda,\alpha))\frac{\partial^j}{\partial n^j}R_{\lambda,\lambda+d\lambda}(\alpha,\theta_2)d\alpha\,.
\end{aligned}
$$

Using (A.15), we have

$$
\begin{aligned}
R_{\lambda,\lambda+d\lambda}(\theta_1,\theta_2) &= E[x_\lambda(\theta_1)x_{\lambda+d\lambda}(\theta_2)] \qquad \text{(A.28)} \\
&= \sum_{j=0}^{m-1}\int_\Theta b_j((\lambda,\theta_1),(\lambda,\alpha))\frac{\partial^j}{\partial n^j}R_{\lambda,\lambda+d\lambda}(\alpha,\theta_2)d\alpha\,. \qquad \text{(A.29)}
\end{aligned}
$$

Substituting (A.29) in (A.27), we have

$E[\xi_{\lambda+d\lambda}(\theta_1)\xi_{\lambda+d\lambda}(\theta_2)]$

$$
\begin{aligned}
&= R_{\lambda+d\lambda,\lambda+d\lambda}(\theta_1,\theta_2) - R_{\lambda,\lambda+d\lambda}(\theta_1,\theta_2) - \sum_{j=0}^{m-1}\int_\Theta [b_j((\lambda+d\lambda,\theta_1),(\lambda,\alpha)) \qquad \text{(A.30)} \\
&\quad - b_j((\lambda,\theta_1),(\lambda,\alpha))]\frac{\partial^j}{\partial n^j}R_{\lambda,\lambda+d\lambda}(\alpha,\theta_2)d\alpha \\
&= \left[\frac{R_{\lambda+d\lambda,\lambda+d\lambda}(\theta_1,\theta_2) - R_{\lambda,\lambda+d\lambda}(\theta_1,\theta_2)}{d\lambda}\right]d\lambda \\
&- \left[\sum_{j=0}^{m}\int_\Theta\left(\frac{b_j((\lambda+d\lambda,\theta_1),(\lambda,\alpha)) - b_j((\lambda,\theta_1),(\lambda,\alpha))}{d\lambda}\right)\frac{\partial^j}{\partial n^j}R_{\lambda,\lambda+d\lambda}(\alpha,\theta_2)d\alpha\right]d\lambda
\end{aligned}
$$

$$
\begin{aligned}
&= \left(\lim_{\mu \to \lambda^-} \frac{\partial}{\partial \mu} R_{\mu,\lambda}(\theta_1, \theta_2) - \lim_{\mu \to \lambda^+} \frac{\partial}{\partial \mu} \sum_{j=0}^{m-1} \int_\Theta b^j_{\mu,\lambda}(\theta_1, \alpha) \frac{\partial^j}{\partial n^j} R_{\lambda,\lambda}(\alpha, \theta_2) d\alpha \right) d\lambda \\
&= \left(\lim_{\mu \to \lambda^-} \frac{\partial}{\partial \mu} R_{\mu,\lambda}(\theta_1, \theta_2) - \lim_{\mu \to \lambda^+} \frac{\partial}{\partial \mu} R_{\mu,\lambda}(\theta_1, \theta_2) \right) d\lambda \\
&= C_\lambda(\theta_1, \theta_2) d\lambda \,. \qquad \text{(A.31)}
\end{aligned}
$$

Thus, for $d\lambda$ small, we have

$$
E\left[(w_{\lambda + d\lambda}(\theta_1) - w_\lambda(\theta_1))(w_{\lambda + d\lambda}(\theta_2) - w_\lambda(\theta_2)) \right] = \frac{C_\lambda(\theta_1, \theta_2)}{B_\lambda(\theta_1) B_\lambda(\theta_2)} d\lambda \,. \qquad \text{(A.32)}
$$

Since $w_0(\theta) = 0$, we can use (A.32) to compute $E[w_\lambda(\theta_1) w_\lambda(\theta_2)]$ as follows:

$$
\begin{aligned}
&E[(w_\lambda(\theta_1) - w_0(\theta_1))(w_\lambda(\theta_2) - w_0(\theta_2))] \\
&= \lim_{N \to \infty} E\left[\sum_{k=0}^{N+1} (w_{\gamma_k}(\theta_1) - w_{\gamma_{k-1}}(\theta_2)) \sum_{k=0}^{N+1} (w_{\gamma_k}(\theta_2) - w_{\gamma_{k-1}}(\theta_2)) \right], \gamma_0 = \lambda, \gamma_{N+1} = 0 \qquad \text{(A.33)} \\
&= \lim_{N \to \infty} E\left[\sum_{k=0}^{N+1} (w_{\gamma_k}(\theta_1) - w_{\gamma_{k-1}}(\theta_1))(w_{\gamma_k}(\theta_2) - w_{\gamma_{k-1}}(\theta_2)) \right] \qquad \text{(A.34)} \\
&= \lim_{N \to \infty} \sum_{k=0}^{N+1} \frac{C_{\gamma_{k-1}}(\theta_1, \theta_2)}{B_{\gamma_{k-1}(\theta_1) B_{\gamma_{k-1}}(\theta_2)}} (\gamma_k - \gamma_{k-1}) \qquad \text{(A.35)} \\
&= \int_0^\lambda \frac{C_u(\theta_1, \theta_2)}{B_u(\theta_1) B_u(\theta_2)} du \,. \qquad \text{(A.36)}
\end{aligned}
$$

We get (A.34) using the orthogonal increments property in (iii). We use (A.32) to get (A.35). We use the definition of the Riemann integrals to go from (A.35) to (A.36).

v) For $\lambda_1 > \lambda_2$, the covariance of $w_{\lambda_1}(\theta) - w_{\lambda_2}(\theta)$ is computed as follows:

$$
E[(w_{\lambda_1}(\theta) - w_{\lambda_2}(\theta))^2] = E[w^2_{\lambda_1}(\theta)] + E[w^2_{\lambda_2}(\theta)] - 2E[w_{\lambda_1}(\theta) w_{\lambda_2}(\theta)] \qquad \text{(A.37)}
$$

$$= \lambda_1 + \lambda_2 - 2\int_0^{\lambda_2} \frac{C_u(\theta_1,\theta_2)}{B_u(\theta_1)B_u(\theta_2)}\,du\,, \tag{A.38}$$

where

$$E[w_\lambda^2(\theta)] = \int_0^\lambda \frac{C_u(\theta,\theta)}{B_u^2(\theta)}du \tag{A.39}$$

$$= \int_{\{u\in[0,\lambda]:C_u(\theta,\theta)=0\}} \frac{C_u(\theta,\theta)}{B_u^2(\theta)}du + \int_{\{u\in[0,\lambda]:C_u(\theta,\theta)\neq 0\}} \frac{C_u(\theta,\theta)}{B_u^2(\theta)}du \tag{A.40}$$

$$= \int_{\{u\in[0,\lambda]:C_u(\theta,\theta)\neq 0\}} du \tag{A.41}$$

$$= \lambda\,. \tag{A.42}$$

To go from (A.40) to (A.41), we use (2.17) since $C_u(\theta,\theta) \neq 0$. To go from (A.41) to (A.42), we use the given assumption that the set $\{u \in [0,1] : C_u(\theta,\theta) = 0\}$ has measure zero.

A.3 Proof of Theorem 2.6.1: Recursive Filter

The steps involved in deriving the recursive filter are the same as deriving the Kalman-Bucy filtering equations, see [68]. The only difference is that we need to take into account the dependence of each point in the random field on its neighboring telescoping surface (which is captured in the integral transform F_θ), instead of a neighboring point as we do for Gauss-Markov processes. The steps in deriving the recursive filter are summarized as follows. In Step 1, we define the innovation process and show that it is Brownian motion and equivalent to the observation space. Using this, we find a relationship between the filtered estimate and the innovation, see Lemma A.3.1. In Step 2, we find a representation for the field $x_\lambda(\theta)$, see Lemma A.3.4. Using Lemma A.3.1 and Lemma A.3.4, we find a closed form expression for $\widehat{x}_{\lambda|\lambda}(\theta)$ in Step 3. We differentiate this to derive the equation for the filtered estimate in Step 4. Finally, Step 5 computes the equation for the error covariance.

Step 1. [**Innovations**] Define $q_\lambda(\theta)$ such that

$$q_\lambda(\theta) = y_\lambda(\theta) - \int_0^\lambda G_\mu(\theta)\widehat{x}_{\mu|\mu}(\theta)d\mu\,.$$

Define the innovation field $e_\lambda(\theta)$ such that

$$de_\lambda(\theta) = \frac{1}{D_\lambda(\theta)}\,dv_\lambda(\theta) \tag{A.43}$$

$$= \frac{G_\lambda(\theta)}{D_\lambda(\theta)}\,\widetilde{x}_{\lambda|\lambda}(\theta)d\lambda + dn_\lambda(\theta)\,, \tag{A.44}$$

where we have used (2.53) to get the final expression in (A.44) and assume that $D_\lambda(\theta) \neq 0$.

Lemma A.3.1. *The field $e_\lambda(\theta)$ is Brownian motion for each fixed θ and $E[e_{\lambda_1}(\theta_1)e_{\lambda_2}(\theta_2)] = 0$ when $\lambda_1 \neq \lambda_2, \theta_1 \neq \theta_2$.*

Proof. Note that $E[\widetilde{x}_{\lambda|\lambda}(\theta)|\sigma\{e_\mu(\theta) : 0 \leq \mu \leq \lambda\}] = 0$ since $\widetilde{x}_{\lambda|\lambda}(\theta) \perp y_\mu(\alpha)$ for $\alpha \in \Theta$, $0 \leq \mu \leq \lambda$. Thus, using Corollary 8.4.5 in [68], we establish that $e_\lambda(\theta)$ is Brownian motion for each fixed θ. Assume $\lambda_1 > \lambda_2$ and consider $\gamma < \lambda_2$. Then, using the orthogonality of error, $\widetilde{x}_\mu(\theta_1) \perp y_\gamma(\alpha)$ for $\gamma < \mu$, and the fact that $n_\lambda(\theta) \perp e_\gamma(\alpha)$ for $\gamma < \lambda$, we have

$$E[(e_{\lambda_1}(\theta_1) - e_{\lambda_2}(\theta_2))e_\gamma(\alpha)] = \int_{\lambda_2}^{\lambda_1} \left(\frac{G_\mu(\theta)}{D_\mu(\theta)}\right) E[\widetilde{x}_{\mu|\mu}(\theta_1)e_\gamma(\alpha)]d\mu$$

$$+ E[(n_{\lambda_1}(\theta_1) - n_{\lambda_2}(\theta_1))e_\gamma(\alpha)] \tag{A.45}$$

$$= 0\,. \tag{A.46}$$

Now we compute $E[de_{\lambda_1}(\theta_1)de_{\lambda_2}(\theta_2)]$ for $\lambda_1 > \lambda_2$:

$$E[de_{\lambda_1}(\alpha_1)de_{\lambda_2}(\theta_2)] = E\left[\left(\frac{G_{\lambda_1}(\alpha_1)}{D_{\lambda_1}(\theta_1)}\widetilde{x}_{\lambda_1|\lambda_1}(\theta_1)d\lambda_1 + dn_{\lambda_1}(\theta_1)\right)de_{\lambda_2}(\theta_2)\right] \tag{A.47}$$

$$= E[dn_{\lambda_1}(\theta_1)de_{\lambda_2}(\theta_2)] \tag{A.48}$$

$$= \frac{1}{D_{\lambda_2}(\theta_2)}E\left[dn_{\lambda_1}(\theta_1)\left(dy_{\lambda_2}(\theta_2) - G_{\lambda_2}(\theta_2)\widehat{x}_{\lambda_2|\lambda_2}(\theta_2)d\lambda_2\right)\right] \tag{A.49}$$

$$= \frac{1}{D_{\lambda_2}(\theta_2)} E[dn_{\lambda_1}(\theta_1) dy_{\lambda_2}(\theta_2)] \tag{A.50}$$

$$= \frac{1}{D_{\lambda_2}(\theta_2)} E[dn_{\lambda_1}(\theta_1) \left(G_{\lambda_2}(\theta_2) x_{\lambda_2}(\theta_2) d\theta_2 + D_{\lambda_2}(\theta_2) dn_{\lambda_2}(\theta_2)\right)] \tag{A.51}$$

$$= E[dn_{\lambda_1}(\theta_1) dn_{\lambda_2}(\theta_2)] = 0\,. \tag{A.52}$$

To go from (A.47) to (A.48), we use that $\widetilde{x}_{\lambda_1|\lambda_1}(\theta_1)$ is independent of $de_{\lambda_2}(\theta_2)$, since $de_{\lambda_2}(\theta_2)$ is a linear combination on the observations $\{y(\partial T^s), s \in [0, \lambda_2]\}$. We get (A.49) using the definition of $de_{\lambda_2}(\theta_2)$ in (A.44). To go from (A.49) to (A.50), we use that $dn_{\mu_1}(\theta_1)$ is independent of $\widehat{x}_{\lambda_2|\lambda_2}(\theta_2)$ for $\lambda_1 > \lambda_2$. We get (A.51) using the equation for the observations in (2.53). To go from (A.51) to (A.52), we use the assumption that $n_{\lambda_1}(\theta_1)$ is independent of the GMRF $x_\lambda(\theta)$. In a similar manner, we can get the result for $\lambda_1 < \lambda_2$.

For $\lambda_1 \neq \lambda_2$ and $\theta_1 \neq \theta_2$, $E[e_{\lambda_1}(\theta_1) e_{\lambda_2}(\theta_2)] = 0$ follows from similar computations as done in (A.33)−(A.36). □

Lemma A.3.1 says that the innovation has the properties as the noise observation $n_\lambda(\theta)$. We now use the innovation to find a closed form expression for the filtered estimate $\widehat{x}_{\lambda|\lambda}(\theta)$.

Lemma A.3.2. *The filtered estimate $\widehat{x}_{\lambda|\lambda}(\theta)$ can be written in terms of the innovation as*

$$\widehat{x}_{\lambda|\lambda}(\theta) = \int_0^\lambda \int_\Theta g_{\lambda,\mu}(\theta, \alpha) de_\mu(\alpha) d\alpha \tag{A.53}$$

$$g_{\lambda,\mu}(\theta, \alpha) = \frac{\partial}{\partial \mu} E[x_\lambda(\theta) e_\mu(\alpha)]\,. \tag{A.54}$$

Proof. Using the methods in [68] or [37], we can establish the equivalence between the innovations and the observations. Because of this equivalence, we can write the filtered estimate as in (A.53). We now compute $g_{\lambda,\mu}(\theta, \alpha)$. We know that

$$\left(x_\lambda(\theta) - \widehat{x}_{\lambda|\lambda}(\theta)\right) \perp e_\mu(\alpha)\,, \quad \mu \leq \lambda, \alpha \in \Theta\,.$$

Thus, we have

$$E[x_\lambda(\theta)e_\mu(\alpha)] = E[\widehat{x}_{\lambda|\lambda}(\theta)e_\mu(\alpha)] \tag{A.55}$$

$$= \int_0^\lambda \int_\Theta g_{\lambda,s}(\theta,\beta)E[de_s(\beta)e_\mu(\alpha)]d\beta \tag{A.56}$$

$$= \int_0^\lambda \int_\Theta \int_0^\mu g_{\lambda,s}(\theta,\beta)E[de_s(\beta)de_r(\alpha)]d\beta \tag{A.57}$$

$$= \int_0^\lambda \int_0^\mu \int_\Theta g_{\lambda,s}(\theta,\beta)\delta(s-r)\delta(\beta-\alpha)dsdrd\beta \tag{A.58}$$

$$= \int_0^\mu g_{\lambda,r}(\theta,\alpha)dr\,. \tag{A.59}$$

To go from (A.57) to (A.58), we use Lemma A.3.1. Differentiating (A.59) with respect to μ, we get the expression for $g_{\lambda,\mu}(\theta,\alpha)$ in (A.54). □

Step 2. [**Formula for** $x_\lambda(\theta)$] Before deriving a closed form expression for $x_\lambda(\theta)$, we first need the following Lemma.

Lemma A.3.3. *For any function $\Psi_{\lambda,\gamma}(\theta_1,\theta_2)$ with $m-1$ normal derivatives, we have*

$$\int_0^\lambda F_{\theta_1}[\Psi_{\lambda,\gamma}(\theta_1,\theta_2)]d\gamma = F_{\theta_1}\left[\int_0^\lambda \Psi_{\lambda,\gamma}(\theta_1,\theta_2)d\gamma\right]. \tag{A.60}$$

Proof. Using the definition of F_{θ_1}, we have

$\int_0^\lambda F_{\theta_1}[\Psi_{\lambda,\gamma}(\theta_1,\theta_2)]d\gamma$

$$= \int_0^\lambda \sum_{j=0}^{m-1} \int_\Theta \lim_{\mu\to\lambda^+} \frac{\partial}{\partial\mu} b_j((\mu,\theta),(\lambda,\alpha)) \lim_{h\to 0} \frac{\partial^j}{\partial h^j} \Psi_{\lambda+h\dot{\lambda},\gamma}(\alpha+h\dot{\alpha},\theta_2)d\alpha d\gamma \tag{A.61}$$

$$= \sum_{j=0}^{m-1} \int_\Theta \lim_{\mu\to\lambda^+} \frac{\partial}{\partial\mu} b_j((\mu,\theta),(\lambda,\alpha)) \lim_{h\to 0} \frac{\partial^j}{\partial h^j} \left[\int_0^\lambda \Psi_{\lambda+h\dot{\lambda},\gamma}(\alpha+h\dot{\alpha},\theta_2)d\gamma\right] d\alpha \tag{A.62}$$

$$= F_{\theta_1}\left[\int_0^\lambda \Psi_{\lambda,\gamma}(\theta_1,\theta_2)d\gamma\right]. \tag{A.63}$$

□

Lemma A.3.4. *Using the telescoping representation for $x_\lambda(\theta)$, a solution for $x_\lambda(\theta)$ is given as follows:*

$$x_\lambda(\theta) = \int_\Theta \Phi_{\lambda,\mu}(\theta,\alpha)x_\mu(\alpha)d\alpha + \int_\Theta \int_\mu^\lambda \Phi_{\lambda,\gamma}(\theta,\alpha)dw_\gamma(\alpha)d\alpha\,, \tag{A.64}$$

$$\frac{\partial}{\partial\lambda}\Phi_{\lambda,\mu}(\theta,\alpha) = F_\theta\left[\Phi_{\lambda,\mu}(\theta,\alpha)\right]\,, \Phi_{\lambda,\lambda} = \delta(\theta-\alpha)\,.$$

Proof. We show that (A.64) satisfies the differential equation in (2.47). Taking derivative of (A.64) with respect to λ, we have

$$dx_\lambda(\theta) = \int_\Theta \frac{\partial}{d\lambda}\Phi_{\lambda,\mu}(\theta,\alpha)x_\mu(\alpha)d\alpha d\lambda + \int_\Theta \Phi_{\lambda,\lambda}(\theta,\alpha)dw_\lambda(\alpha) + \int_\Theta\int_\mu^\lambda \frac{\partial}{d\lambda}\Phi_{\lambda,\gamma}(\theta,\alpha)dw_\gamma(\alpha)d\alpha \tag{A.65}$$

$$= \int_\Theta F_\theta\left[\Phi_{\lambda,\mu}(\theta,\alpha)\right]x_\mu(\alpha)d\alpha d\lambda + dw_\lambda(\theta) + \int_\Theta\int_\mu^\lambda F_\theta\left[\Phi_{\lambda,\gamma}(\theta,\alpha)\right]dw_\gamma(\alpha)d\alpha \tag{A.66}$$

$$= F_\theta\left[\int_\Theta \Phi_{\lambda,\mu}(\theta,\alpha)x_\mu(\alpha)d\alpha + \int_\Theta\int_\mu^\lambda \Phi_{\lambda,\gamma}(\theta,\alpha)db_\gamma(\alpha)d\alpha\right] + dw_\lambda(\theta) \tag{A.67}$$

$$= F_\theta[x_\lambda(\theta)] + dw_\lambda(\theta)\,. \tag{A.68}$$

To get (A.67), we use Theorem A.3.3 to take the integral transform F_θ outside the integral. Since the $x_\lambda(\theta)$ in (A.64) satisfies (2.47), it must be a solution. □

Step 3. **[Equation for $\widehat{x}_{\lambda|\lambda}(\theta)$]** Using (A.44) and (A.64), we can write $g_{\lambda,\mu}(\theta,\alpha)$ in (A.54) as

$$g_{\lambda,\mu}(\theta,\alpha) = \frac{\partial}{\partial\mu}E\left\{x_\lambda(\theta)\left[\int_0^\mu \frac{G_\gamma(\alpha)}{D_\gamma(\alpha)}\widetilde{x}_{\gamma|\gamma}(\alpha)d\gamma + n_\mu(\alpha)\right]\right\} \tag{A.69}$$

$$= \frac{\partial}{\partial\mu}\left[\int_0^u \frac{G_\gamma(\alpha)}{D_\gamma(\alpha)}E[x_\lambda(\theta)\widetilde{x}_{\gamma|\gamma}(\alpha)]d\gamma\right] \tag{A.70}$$

$$= \frac{\partial}{\partial\mu}\left\{\int_0^u \frac{G_\gamma(\alpha)}{D_\gamma(\alpha)}\int_\Theta \Phi_{\lambda,\gamma}(\theta,\beta)E[x_\gamma(\beta)\widetilde{x}_{\gamma|\gamma}(\alpha)]d\beta d\gamma\right\} \tag{A.71}$$

$$= \frac{G_\mu(\alpha)}{D_\mu(\alpha)} \int_\Theta \Phi_{\lambda,\mu}(\theta,\beta) E[x_\mu(\beta)\widetilde{x}_{\mu|\mu}(\alpha)] d\beta \tag{A.72}$$

$$= \frac{G_\mu(\alpha)}{D_\mu(\alpha)} \int_\Theta \Phi_{\lambda,\mu}(\theta,\beta) S_\mu(\beta,\alpha) d\beta \,. \tag{A.73}$$

To get (A.73), we use the fact that $\widehat{x}_{\mu|\mu}(\alpha) \perp \widetilde{x}_{\mu|\mu}(\beta)$, so that

$$E[x_\mu(\beta)\widetilde{x}_{\mu|\mu}(\alpha)] = E[\widetilde{x}_{\mu|\mu}(\beta)\widetilde{x}_{\mu|\mu}(\alpha)] = S_\mu(\beta,\alpha)\,.$$

Substituting (A.73) in the expression for $\widehat{x}_{\lambda|\lambda}(\theta)$ in (A.54) (Step 2), we get

$$\widehat{x}_{\lambda|\lambda}(\theta) = \int_0^\lambda \int_\Theta \frac{G_\mu(\alpha)}{D_\mu(\alpha)} \left[\int_\Theta \Phi_{\lambda,\mu}(\theta,\beta) S_\mu(\beta,\alpha) d\beta \right] de_\mu(\alpha) d\alpha \,. \tag{A.74}$$

Step 4. [Differential Equation for $\widehat{x}_{\lambda|\lambda}(\theta)$] Differentiating (A.74) with respect to λ, we get

$$d\widehat{x}_{\lambda|\lambda}(\theta) = \int_\Theta \frac{G_\lambda(\alpha)}{D_\lambda(\alpha)} S_\mu(\theta,\alpha) de_\lambda(\alpha) d\alpha \tag{A.75}$$

$$+ \int_0^\lambda \int_\Theta \frac{G_\mu(\alpha)}{D_\mu(\alpha)} \left[\int_\Theta F_\theta[\Phi_{\lambda,\mu}(\theta,\beta)] S_\mu(\beta,\alpha) d\beta \right] de_\mu(\alpha) d\alpha$$

$$= \int_\Theta \frac{G_\lambda(\alpha)}{D_\lambda(\alpha)} S_\lambda(\alpha,\theta) de_\lambda(\alpha) d\alpha + F_\theta[\widehat{x}_{\lambda|\lambda}(\theta)] d\lambda \tag{A.76}$$

$$= F_\theta[\widehat{x}_{\lambda|\lambda}(\theta)] d\lambda + K_\theta[de_\lambda(\theta)]\,, \tag{A.77}$$

where K_θ is the integral transform defined as in (2.60).

Step 5. [Differential Equation for $S_\lambda(\alpha,\theta)$] The error covariance $S_\lambda(\alpha,\theta)$ can be written as

$$S_\lambda(\alpha,\theta) = E[\widetilde{x}_{\lambda|\lambda}(\alpha)\widetilde{x}_{\lambda|\lambda}(\theta)] \tag{A.78}$$

$$= E[x_\lambda(\alpha)x_\lambda(\theta)] - E[\widehat{x}_{\lambda|\lambda}(\alpha)\widehat{x}_{\lambda|\lambda}(\theta)]\,. \tag{A.79}$$

Using expressions for $x_\lambda(\alpha)$ in (A.64), we can show that for $P_\lambda(\alpha,\beta) = E[x_\lambda(\alpha)x_\lambda(\theta)]$,

$$\frac{\partial P_\lambda(\alpha,\theta)}{d\lambda} = F_\alpha[P_\lambda(\alpha,\theta)] + F_\theta P_\lambda(\alpha,\theta) + C_\lambda(\alpha,\theta)\,. \tag{A.80}$$

Using the expression for $\widehat{x}_{\lambda|\lambda}(\alpha)$ in (A.53), it can be shown that

$$\begin{aligned}\frac{\partial E[\widehat{x}_{\lambda|\lambda}(\alpha)\widehat{x}_{\lambda|\lambda}(\theta)]}{d\lambda} &= F_\alpha[E[\widehat{x}_{\lambda|\lambda}(\alpha)\widehat{x}_{\lambda|\lambda}(\theta)]] + F_\theta[E[\widehat{x}_{\lambda|\lambda}(\alpha)\widehat{x}_{\lambda|\lambda}(\theta)]] \\ &\quad + \int_\Theta \frac{G_\lambda^2(\beta)}{D_\lambda^2(\beta)}\, S_\lambda(\alpha,\beta)S_\lambda(\theta,\beta)d\beta\,.\end{aligned} \tag{A.81}$$

Differentiating (A.79) and using (A.80) and (A.81), we get the desired equation:

$$\frac{\partial}{\partial\lambda}S_\lambda(\alpha,\theta) = F_\alpha[S_\lambda(\alpha,\theta)] + F_\theta[S_\lambda(\alpha,\theta)] + C_\lambda(\theta,\alpha) - \int_\Theta \frac{G_\lambda^2(\beta)}{D_\lambda^2(\beta)}S_\lambda(\alpha,\beta)S_\lambda(\theta,\beta)d\beta\,. \tag{A.82}$$

A.4 Proof of Theorem 2.6.2: Recursive Smoother

We now derive smoothing equations. Using similar steps as in Lemma A.3.2, we can show that

$$\widehat{x}_{\lambda|T}(\theta) = \int_0^1 \int_\Theta g_{\lambda,\mu}(\theta,\alpha)de_\mu(\alpha)d\alpha\,, \tag{A.83}$$

$$g_{\lambda,\mu}(\theta,\alpha) = \frac{\partial}{\partial\mu}E[x_\lambda(\theta)e_\mu(\alpha)]\,. \tag{A.84}$$

Define the error covariance $S_{\lambda,\mu}(\theta,\alpha)$ as

$$S_{\lambda,\mu}(\theta,\alpha) = E[\widetilde{x}_{\lambda|\lambda}(\theta)\widetilde{x}_{\mu|\mu}(\alpha)]\,. \tag{A.85}$$

We have the following result for the smoother:

Lemma A.4.1. *The smoothed estimator $\widehat{x}_{\lambda|T}(\theta)$ is given by*

$$\widehat{x}_{\lambda|T}(\theta) = \widehat{x}_{\lambda|\lambda}(\theta) + \int_\lambda^1 \int_\Theta g_{\lambda,\mu}(\theta,\alpha)de_\mu(\alpha)d\alpha\,, \tag{A.86}$$

where for $\mu \geq \lambda$,

$$g_{\lambda,\mu}(\theta,\alpha) = \frac{G_\mu(\alpha)}{D_\mu(\alpha)} S_{\lambda,\mu}(\theta,\alpha)\,. \tag{A.87}$$

Proof. Equation (A.86) immediately follows from (A.83) and Lemma A.3.2. Equation (A.87) follows by using (A.44) to compute $g_{\lambda,\mu}(\theta,\alpha)$ in (A.84). □

We now want to characterize the error covariance $S_{\lambda,\mu}(\theta,\alpha)$. Subtracting the telescoping representation in (2.47) and the filtering equation in (2.58), we get the following equation for the filtering error covariance:

$$d\widetilde{x}_{\mu|\mu}(\alpha) = \widetilde{F}_\theta[\widetilde{x}_{\mu|\mu}(\alpha)]d\mu + B_\mu(\alpha)dw_\mu(\alpha) - K_\alpha[dn_\mu(\alpha)]\,, \tag{A.88}$$

where $\widetilde{F}_\alpha$ is the integral transform

$$\widetilde{F}_\alpha[\widetilde{x}_{\mu|\mu}(\alpha)] = F_\alpha[\widetilde{x}_{\mu|\mu}(\alpha)] - K_\alpha\left[\frac{G_\mu(\alpha)}{D_\mu(\alpha)}\widetilde{x}_{\mu|\mu}(\alpha)\right]\,. \tag{A.89}$$

Just like we did in Lemma A.3.4, we can write a solution to (A.88) as

$$\widetilde{x}_{\mu|\mu}(\alpha) = \int_\Theta \widetilde{\Phi}_{\mu,\lambda}(\alpha,\theta)\widetilde{x}_{\lambda|\lambda}(\theta)d\theta + \int_\Theta\int_\lambda^\mu \widetilde{\Phi}_{\mu,\gamma}(\alpha,\theta)[B_\gamma(\theta)dw_\gamma(\theta) - K_\theta[dn_\gamma(\theta)]]d\theta \tag{A.90}$$

$$\frac{\partial}{\partial\mu}\widetilde{\Phi}_{\mu,\lambda}(\alpha,\theta) = \widetilde{F}_\alpha\widetilde{\Phi}_{\mu,\lambda}(\alpha,\theta) \text{ and } \widetilde{\Phi}_{\mu,\mu}(\alpha,\theta) = \delta(\alpha-\theta)\,. \tag{A.91}$$

Differentiating (A.90) with respect to λ, we can show that

$$\int_\Theta \frac{\partial}{\partial\lambda}\widetilde{\Phi}_{\mu,\lambda}(\alpha,\beta)\widetilde{x}_{\lambda|\lambda}(\beta)d\beta = -\int_\Theta \widetilde{\Phi}_{\mu,\lambda}(\alpha,\beta)\widetilde{F}_\beta\widetilde{x}_{\lambda|\lambda}(\beta)d\beta\,. \tag{A.92}$$

Substituting (A.90) in (A.88), we have the following relationship:

$$S_{\lambda,\mu}(\theta,\alpha) = \int_\Theta \widetilde{\Phi}_{\mu,\lambda}(\alpha,\beta)S_\lambda(\beta,\theta)d\beta\,. \tag{A.93}$$

Substituting (A.93) in (A.86) and (A.87), differentiating (A.86) and using (A.92) and (2.61), we get the following equation:

$$d\widehat{x}_{\lambda|T}(\theta) = F_\theta[\widehat{x}_{\lambda|T}(\theta)]d\lambda + \int_\lambda^1 \int_\Theta \frac{G_u(\alpha)}{D_u(\alpha)} \int_\Theta \widetilde{\Phi}_{\mu,\lambda}(\alpha,\beta) C_\lambda(\beta,\theta) d\beta de_\mu(\alpha) d\alpha \,. \tag{A.94}$$

Assuming $S_\lambda(\theta,\theta) > 0$, we get smoother equations using the following calculations:

$$d\widehat{x}_{\lambda|T}(\beta)\delta(\theta-\beta) = F_\beta[\widehat{x}_{\lambda|T}(\beta)]\delta(\theta-\beta)d\lambda + \int_\lambda^1 \int_\Theta \frac{G_u(\alpha)}{D_u(\alpha)} \widetilde{\Phi}_{\mu,\lambda}(\alpha,\beta) C_\lambda(\beta,\theta) de_\mu(\alpha) d\alpha \tag{A.95}$$

$$\begin{aligned} \frac{S_\lambda(\beta,\theta)}{C_\lambda(\beta,\theta)} d\widehat{x}_{\lambda|T}(\beta)\delta(\theta-\beta) &= \frac{S_\lambda(\beta,\theta)}{C_\lambda(\beta,\theta)} F_\beta[\widehat{x}_{\lambda|T}(\beta)]\delta(\theta-\beta)d\lambda \\ &\quad + \int_\lambda^1 \int_\Theta \frac{G_u(\alpha)}{D_u(\alpha)} \widetilde{\Phi}_{\mu,\lambda}(\alpha,\beta) S_\lambda(\beta,\theta) de_\mu(\alpha) d\alpha \end{aligned} \tag{A.96}$$

$$\begin{aligned} \frac{S_\lambda(\theta,\theta)}{C_\lambda(\theta,\theta)} d\widehat{x}_{\lambda|T}(\theta) &= \frac{S_\lambda(\theta,\theta)}{C_\lambda(\theta,\theta)} F_\theta[\widehat{x}_{\lambda|T}(\theta)]d\lambda \\ &\quad + \int_\lambda^1 \int_\Theta \frac{G_u(\alpha)}{D_u(\alpha)} \left(\int_\Theta \widetilde{\Phi}_{\mu,\lambda}(\alpha,\beta) S_\lambda(\beta,\theta) d\beta \right) de_\mu(\alpha) d\alpha \end{aligned} \tag{A.97}$$

$$d\widehat{x}_{\lambda|T}(\theta) = F_\theta[\widehat{x}_{\lambda|T}(\theta)]d\lambda + \frac{C_\lambda(\theta,\theta)}{S_\lambda(\theta,\theta)} \int_\lambda^1 \int_\Theta \frac{G_u(\alpha)}{D_u(\alpha)} S_{\lambda,\mu}(\theta,\alpha) de_\mu(\alpha) d\alpha \tag{A.98}$$

$$d\widehat{x}_{\lambda|T}(\theta) = F_\theta[\widehat{x}_{\lambda|T}(\theta)]d\lambda + \frac{C_\lambda(\theta,\theta)}{S_\lambda(\theta,\theta)} [\widehat{x}_{\lambda|T}(\theta) - \widehat{x}_{\lambda|\lambda}(\theta)] \,. \tag{A.99}$$

Equation (A.94) is equivalent to (A.95). We multiply (A.95) by $S_\lambda(\beta,\theta)/C_\lambda(\beta,\theta)$ to get (A.96). We integrate (A.96) for all β to get (A.97). To go from (A.97) to (A.98), we use (A.93). Equation (A.98) follows from (A.86).

To derive a differential equation for $S_{\lambda|T}(\alpha,\theta)$, we first note that

$$S_{\lambda|T}(\alpha,\theta) = E[\widetilde{x}_{\lambda|T}(\alpha)\widetilde{x}_{\lambda|T}(\theta)] \tag{A.100}$$

$$= E[x_\lambda(\alpha)x_\lambda(\theta)] - E[\widehat{x}_{\lambda|T}(\alpha)\widehat{x}_{\lambda|T}(\theta)] \,. \tag{A.101}$$

Using (A.86) to compute $E[\widehat{x}_{\lambda|T}(\alpha)\widehat{x}_{\lambda|T}(\theta)]$, we can find an expression for $S_{\lambda|T}(\alpha,\theta)$ as

$$S_{\lambda|T}(\alpha,\theta) = S_{\lambda}(\alpha,\theta) - \int_{\lambda}^{1}\int_{\Theta}\frac{G_{\mu}^{2}(\alpha)}{D_{\mu}^{2}(\alpha)}S_{\mu,\lambda}(\alpha_1,\alpha)S_{\mu,\lambda}(\alpha_1,\theta)d\mu d\alpha_1\,. \tag{A.102}$$

Taking derivative of (A.102), we get (2.68).

Bibliography

[1] M. B. Adams, A. S. Willsky, and B. C. Levy. Linear estimation of boundary value stochastic processes – Part I: The role and construction of complimentary models. *IEEE Trans. Autom. Control*, AC–29(9):803–811, September 1984.

[2] M. B. Adams, A. S. Willsky, and B. C. Levy. Linear estimation of boundary value stochastic processes – Part II: 1-D smoothing problems. *IEEE Trans. Autom. Control*, AC–29(9):811–821, September 1984.

[3] A. Anandkumar, V. Tan, and A. Willsky. High dimensional structure learning of Ising models on sparse random graphs. *arXiv:1011.0129v6 [math.ST]*, 2011.

[4] A. Anandkumar, J. Yukich, L. Tong, and A. Willsky. Detection Error Exponent for Spatially Dependent Samples in Random Networks. In *Proc. of IEEE ISIT*, Seoul, S. Korea, July 2009.

[5] S. Arnborg, D. G. Corneil, and A. Proskurowski. Complexity of finding embeddings in a k-tree. *SIAM J. Algebraic Discrete Methods*, 8(2):277–284, 1987.

[6] F. Badawi, A. Lindquist, and M. Pavon. A stochastic realization approach to the smoothing problem. *IEEE Trans. Autom. Control*, AC-24:878–888, 1979.

[7] A. Bagchi and H. Westdijk. Smoothing and likelihood ratio for Gaussian boundary value processes. *IEEE Trans. Autom. Control*, 34(9):954–962, September 1989.

[8] A. Becker and D. Geiger. A sufficiently fast algorithm for finding close to optimal junction trees. In *Proceedings of the 10th Annual Conference on Uncertainty in Artificial Intelligence (UAI-96)*, pages 81–89, 1996.

[9] S. Bernstein. Sur les liaisons entre les grandeurs aleatoires. *Proc. Int. Cong. of Math.*, pages 288–309, 1932.

[10] A. Berry, P. Heggernes, and G. Simonet. The minimum degree heuristic and the minimal triangulation process. In H. Bodlaender, editor, *Graph-Theoretic Concepts in Computer Science*, volume 2880 of *Lecture Notes in Computer Science*, pages 58–70. Springer Berlin / Heidelberg, 2003.

[11] J. Besag. Spatial interaction and the statistical analysis of lattice systems. *Journal of the Royal Statistical Society. Series B (Methodological)*, 36(2):192–236, 1974.

[12] H. L. Bodlaender and A. M. Koster. Treewidth computations I. upper bounds. *Information and Computation*, 208(3):259 – 275, 2010.

[13] W. S. Burdic. *Underwater Acoustic System Analysis*. Englewood Cliffs, NJ: Prentice Hall, 1984.

[14] Z. Chaczko and F. Ahmad. Wireless sensor network based system for fire endangered areas. In *Proceedings of the Third International Conference on Information Technology and Applications (ICITA'05) Volume 2 - Volume 02*, ICITA '05, pages 203–207, Washington, DC, USA, 2005. IEEE Computer Society.

[15] V. Chandrasekaran, N. Srebro, and P. Harsha. Complexity of inference in graphical models. In *Proceedings of the Proceedings of the Twenty-Fourth Conference Annual Conference on Uncertainty in Artificial Intelligence (UAI-08)*, pages 70–78, Corvallis, Oregon, 2008. AUAI Press.

[16] F. M. Coetzee and V. L. Stonick. On a natural homotopy between linear and nonlinear single layer networks. *IEEE Trans. Neural Networks*, 7:307–317, 1994.

[17] G. F. Cooper. *NESTOR: A computer-based medical diagnostic aid that integrates causal and probabilistic knowledge*. PhD thesis, Department of Computer Science, Stanford University, 1984.

[18] G. F. Cooper. The computational complexity of probabilistic inference using Bayesian belief networks (research note). *Artificial Intelligence*, 42(2-3):393–405, 1990.

[19] F. G. Cozman. Generalizing variable elimination in Bayesian networks. In *Workshop on Probabilistic Reasoning in Artificial Intelligence*, pages 27–32, 2000.

[20] U. S. J. M. F. M. D. Vats, Vishal Monga. Scalable robust hypothesis tests using graphical models. In *Proc. International Conference on Acoustics, Speech, and Signal Processing ICASSP*, Mar. 14–19, 2011.

[21] R. Dechter. Bucket elimination: A unifying framework for reasoning. *Artificial Intelligence*, 113(1-2):41–85, Sep 1999.

[22] P. Elias. List decoding for noisy channels. *Wescon Convention Record*, pages 94–107, 1957.

[23] P. Erdős and A. Rényi. On the evolution of random graphs. In *Publication of the Mathematical Institute of the Hungarian Academy of Sciences*, pages 17–61, 1960.

[24] P. Erdős and A. Rényi. On random graphs. I. *Publ. Math. Debrecen*, 6:290–297, 1959.

[25] E. Fabre and A. Guyader. Dealing with short cycles in graphical codes. In *IEEE International Symposium on Information Theory (ISIT), Sorrento*, June 2000.

[26] A. Ferrante and G. Picci. Minimal realization and dynamic properties of optimal smoothers. *IEEE Trans. Autom. Control*, 45:2028–2046, 2000.

[27] N. Friedman. Inferring Cellular Networks Using Probabilistic Graphical Models. *Science*, 303(5659):799–805, 2004.

[28] R. G. Gallagar. Low-density parity check codes. *IRE Trans. Inform. Theory.*, IT-8:21–28, 1962.

[29] E. N. Gilbert. Random graphs. *The Annals of Mathematics Statistics*, 30(4):1141–1144, 1959.

[30] A. Ihler, S. Kirshner, M. Ghil, A. Robertson, and P. Smyth. Graphical models for statistical inference and data assimilation. *Physica D: Nonlinear Phenomena*, 230:72–87, June 2007.

[31] M. O. Jackson. *Social and Economic Networks*. Princeton University Press, 2008.

[32] B. Jamison. Reciprocal processes: The stationary Gaussian case. *The Annals of Mathematical Statistics*, 41:1624–1630, 1970.

[33] F. Jensen and F. Jensen. Optimal junction trees. In *Proceedings of the 10th Annual Conference on Uncertainty in Artificial Intelligence (UAI-94)*, pages 360–36, San Francisco, CA, 1994. Morgan Kaufmann.

[34] F. V. Jenson, S. L. Lauritzen, and K. G. Oleson. Bayesian updating in causal probabilistic networks by local computation. *Computational Statistics Quarterly*, 4:269–282, 1990.

[35] M. Jordan, Z. Ghahramani, T. Jaakkola, and L. Saul. An introduction to variational methods for graphical models. *Machine Learning*, 37:183–233, 1999.

[36] P. R. Julian and A. Cline. The direct estimation of spatial wavenumber spectra of atmospheric variables. *J. Atmospheric Sci.*, 31:1526–1539, 1974.

[37] T. Kailath, A. H. Sayed, and B. Hassibi. *Linear Estimation*. Prentice Hall, 2000.

[38] Kallianpur and Mandrekar. The Markov property for generalized Gaussian random fields. *Ann. Inst. Fourier*, 24:143–167, 1974.

[39] R. E. Kalman. A new approach to linear filtering and prediction problems. *Transactions of the ASME–Journal of Basic Engineering*, 82(Series D):35–45, 1960.

[40] R. E. Kalman and R. Bucy. New results in linear filtering and prediction theory. *Transactions of the ASME–Journal of Basic Engineering*, 83(Series D):95–108, 1960.

[41] R. Kikuchi. A theory of cooperative phenomena. *Phys. Rev.*, 81(6):988– 988–1003, 1951.

[42] U. B. Kjaerulff. Triangulation of graphs - algorithms giving small total state space. Technical Report Research Report R-90-09, Department of Mathematics and Computer Science, Aalborg University, Denmark, 1990.

[43] A. J. Krener. Reciprocal processes and the stochastic realization problem for acausal systems. In C. I. Byrnes and A. Lindquist, editors, *Modelling, Identification, and Robust Control*, pages 197–209. Amsterdam: Elsevier, 1986.

[44] A. J. Krener. Realizations of reciprocal processes. *Stochastics and Stochastics Reports*, 34:29–56, 1988.

[45] A. J. Krener. Reciprocal diffusions and stochastic differential equations of second order. *Stochastics*, 24:393–422, 1988.

[46] A. J. Krener, R. Frezza, and B. C. Levy. Gaussian reciprocal processes and self-adjoint stochastic differential equations of second order. *Stochastics and Stochastics Reports*, 34:29–56, 1991.

[47] J. B. Kruskal. On the shortest spanning subtree of a graph and the traveling salesman problem. *Proceedings of the American Mathematical Society*, 7(1):48–50, February 1956.

[48] S. L. Lauritzen. *Graphical Models*. Oxford University Press, USA, 1996.

[49] S. L. Lauritzen and D. J. Spiegelhalter. Local computations with probabilities on graphical structures and their application to expert systems. *Journal of the Royal Statistical Society. Series B (Methodological)*, 50(2):157–224, 1988.

[50] C. Lee, J. Lee, and S. il Oum. Rank-width of random graphs. *arXiv:1001.0461v1*, 2010.

[51] B. C. Levy. Characterization of multivariate stationary Gaussian reciprocal diffusions. *Journal of Multivariate Analysis*, 62:74–79, July 1997.

[52] B. C. Levy. *Principles of Signal Detection and Parameter Estimation*. Springer Verlag, 2008.

[53] B. C. Levy, M. B. Adams, and A. S. Willsky. Solution and linear estimation of 2-D nearest-neighbor models. *Proc. IEEE*, 78(4):627–641, Apr. 1990.

[54] P. Lévy. A special problem of Brownian motion, and a general theory of Gaussian random functions. In *Proceedings of the Third Berkeley Symposium on Mathematical Statistics and Probability, 1954–1955, vol. II*, pages 133–175, Berkeley and Los Angeles, 1956. University of California Press.

[55] D. J. C. MacKay. *Learning in Graphical Models*, chapter Introduction to Monte Carlo methods. Kluwer Academic Publishers, 1997.

[56] H. M. Markowitz. The elimination form of the inverse and its application to linear programming. *Management Science*, 3(3):255–269, 1957.

[57] R. Mateescu, K. Kask, V. Gogate, and R. Dechter. Join-graph propagation algorithms. *Journal of Artificial Intelligence Research*, 37:279–328, 2010.

[58] H. P. McKean. Brownian motion with a several dimension time. *Theory of Probability and Applications*, 8:335–354, 1963.

[59] C. L. Mehta and E. Wolf. Coherence properties of black body radiation, parts I and II. *Phys. Rev.*, 134(4):1143–1153, 1964.

[60] M. Meila and M. I. Jordan. Learning with mixtures of trees. *Journal of Machine Learning Research*, pages 1–48, 2000.

[61] N. Meinshausen and P. Bühlmann. High-dimensional graphs and variable selection with the lasso. *Ann. Statist.*, 34(3):1436–1462, 2006.

[62] J. M. F. Moura and N. Balram. Recursive structure of noncausal Gauss-Markov random fields. *IEEE Trans. Inf. Theory*, IT-38(2):334–354, March 1992.

[63] J. M. F. Moura and S. Goswami. Gauss-Markov random fields (GMrf) with continuous indices. *IEEE Trans. Inf. Theory*, 43(5):1560–1573, September 1997.

[64] J. Munkres. *Topology*. Prentice Hall, 2000.

[65] J. R. Nevins, M. West, A. Dobra, A. Dobra, C. Hans, C. Hans, B. Jones, B. Jones, J. R. Nevins, and M. W. Abstract. Sparse graphical models for exploring gene expression data. *Journal of Multivariate Analysis*, 90:196–212, 2004.

[66] M. E. J. Newman, D. J. Watts, and S. H. Strogatz. Random graph models of social networks. *Proc. Natl. Acad. Sci. USA*, 99:2566–2572, 2002.

[67] R. Ogier and E. Wong. Recursive linear smoothing of two-dimensional random fields. *IEEE Trans. Inf. Theory*, 27(1):77–83, Jan. 1981.

[68] B. Oksendal. *Stochastic Differential Equations: An Introduction with Applications (Universitext)*. Springer, December 2005.

[69] J. Pearl. *Probabilistic Reasoning in Intelligent Systems: Networks of Plausible Inference*. Morgan Kaufmann, 1988.

[70] A. Pelizzola. Cluster variation method in statistical physics and probabilistic graphical models. *Journal of Physics A: Mathematical and General*, 38(33):R309–R339, 2005.

[71] Y. Peng and J. A. Reggia. Plausibility of diagnostic hypotheses. In *National Conference on Artificial Intelligence (AAAI'86)*, pages 140–145, 1986.

[72] G. Picci and F. Carli. Modelling and simulation of images by reciprocal processes. In *Tenth International Conference on Computer Modeling and Simulation*, pages 513–518, Washington, DC, USA, 2008. IEEE Computer Society.

[73] L. D. Pitt. A Markov property for Gaussian processes with a multidimensional parameter. *Arch. Ration. Mech. Anal.*, 43:367–391, 1971.

[74] R. C. Prim. Shortest connection networks and some generalizations. *Bell System Technical Journal*, 36:1389?1401, 1957.

[75] H. E. Rauch, F. Tung, and C. T. Stribel. Maximum likelihood estimates of linear dynamical systems. *AIAA J.*, 3(8):1445–1450, August 1965.

[76] P. Ravikumar, M. J. Wainwright, and J. Lafferty. High-dimensional Ising model selection using ℓ_1-regularized logistic regression. *Annals of Statistics*, 38(3):1287–1319, 2010.

[77] N. Robertson and P. D. Seymour. Graph minors. II. Algorithmic aspects of tree-width. *Journal of Algorithms*, 7(3):309 – 322, 1986.

[78] D. J. Rose, R. E. Tarjan, and G. S. Lueker. Algorithmic aspects of vertex elimination on graphs. *SIAM Journal on Computing*, 5(2):266–283, 1976.

[79] Y. A. Rozanov. *Markov Random Fields*. New York: Springer-Verlag, 1982.

[80] H. Rue and L. Held. *Gaussian Markov Random Fields: Theory and Applications (Monographs on Statistics and Applied Probability)*. Chapman & Hall/CRC, 1st edition, February 2005.

[81] E. Schrödinger. Über die Umkehrung der Naturgesetze. *Sitzungsber. Preuss. Akad. Wissen. Phys. Math. Kl.*, pages 144–153, 1931.

[82] G. Shafer and P. P. Shenoy. Probability propagation. *Annals of Mathematics and Artificial Intelligence*, (1-4):327–352, 1990.

[83] E. B. Sudderth, M. J. Wainwright, and A. S. Willsky. Embedded trees: estimation of Gaussian processes on graphs with cycles. *IEEE Trans. Signal Process.*, 52(11):3136–3150, Nov. 2004.

[84] A. H. Tewfik, B. C. Levy, and A. S. Willsky. Internal models and recursive estimation for 2-D isotropic random fields. *IEEE Trans. Inf. Theory*, 37(4):1055–1066, July 1991.

[85] J. Theiler, G. Cao, L. R. Bachega, and C. A. Bouman. Sparse matrix transform for hyperspectral image processing. *to appear in IEEE Selected Topics in Signal Process.*, 2011.

[86] E. Vanmarcke. *Random Fields: Analysis and Synthesis*. MIT Press, 1983.

[87] D. Vats and J. M. F. Moura. Recursive filtering and smoothing for discrete index Gaussian reciprocal processes. In *Proc. 43rd Annual Conference on Information Sciences and Systems CISS 2009*, pages 377–382, Mar. 18–20, 2009.

[88] D. Vats and J. M. F. Moura. Recursive filtering and smoothing for Gaussian reciprocal processes with continuous indices. In *IEEE International Symposium on Information Theory (ISIT)*, Seoul, Korea, 2009.

[89] D. Vats and J. M. F. Moura. Reciprocal fields: A model for random fields pinned to two boundaries. In *Proc. IEEE International Conference on Decision and Control*, Atlanta, Dec. 2010.

[90] D. Vats and J. M. F. Moura. A telescoping approach to recursive enhancement of noisy images. In *Proc. International Conference on Acoustics, Speech, and Signal Processing ICASSP*, Mar. 14–19, 2010.

[91] D. Vats and J. M. F. Moura. Necessary conditions for consistent graphical model selection. In *IEEE International Symposium on Information Theory (ISIT)*, Saint Petersburg, Russia, 2011.

[92] D. Vats and J. M. F. Moura. Telescoping recursive representations and estimation of Gauss-Markov random fields. *Trans. on Information Theory*, 57(3):1645 – 1663, 2011.

[93] M. J. Wainwright. *Stochastic Processes on Graphs: Geometric and Variational Approaches*. PhD thesis, Department of EECS, Massachusetts Institute of Technology, 2002.

[94] M. J. Wainwright, T. S. Jaakkola, and A. S. Willsky. Tree-based reparameterization framework for analysis of sum-product and related algorithms. *IEEE Trans. Inf. Theory*, 49:2003, 2003.

[95] M. J. Wainwright, T. S. Jaakkola, and A. S. Willsky. A new class of upper bounds on the log partition function. *IEEE Trans. on Information Theory*, 51:2313 – 2335, 2005.

[96] M. J. Wainwright and M. I. Jordan. *Graphical Models, Exponential Families, and Variational Inference*. Now Publishers Inc., Hanover, MA, USA, 2008.

[97] G. N. Watson. *A Treatise on the Theory of Bessel Functions*. Cambridge University Press, second edition edition, 1995.

[98] Y. Weiss and W. T. Freeman. On the optimality of solutions of the max-product belief propagation algorithm in arbitrary graphs. *IEEE Transactions on Information Theory*, 47:723–735, 2001.

[99] M. Welling. On the choice of regions for generalized belief propagation. In *Proceedings of the 20th conference on Uncertainty in artificial intelligence*, UAI '04, pages 585–592, Arlington, Virginia, United States, 2004. AUAI Press.

[100] M. Welling, T. Minka, and Y. W. Teh. Structured region graphs: Morphing EP into GBP. In *Proceedings of the International Conference on Uncertainty in Artificial Intelligence*, volume 21, 2005.

[101] D. B. West. *Introduction to Graph Theory*. Prentice Hall, 2nd edition, 2000.

[102] P. Whittle. On stationary processes in the plane. *Biometrika*, 41(3/4):434–449, 1954.

[103] E. Wong. Two-dimensional random fields and representation of images. *SIAM Journal on Applied Mathematics*, 16(4):756–770, 1968.

[104] E. Wong. A likelihood ratio formula for two-dimensional random fields. *IEEE Trans. Inf. Theory*, 20(4):418–422, July 1974.

[105] E. Wong. Recursive filtering for two-dimensional random fields (corresp.). *IEEE Trans. Inf. Theory*, 21(1):84–86, Jan. 1975.

[106] E. Wong. Recursive causal linear filtering for two-dimensional random fields. *IEEE Trans. Inf. Theory*, 24(1):50–59, Jan. 1978.

[107] E. Wong and B. Hajek. *Stochastic Processes in Engineering Systems*. Springer-Verlag New York Inc, 1985.

[108] E. Wong and E. Tsui. One-sided recursive filters for two-dimensional random fields (corresp.). *IEEE Trans. Inf. Theory*, 23(5):633–637, Sept. 1977.

[109] E. Wong and M. Zakai. Markov processes on the plane. *Stochastics*, 15:311–333, 1985.

[110] J. W. Woods and C. Radewan. Kalman filtering in two dimensions. *IEEE Trans. Inf. Theory*, 23(4):473–482, Jul 1977.

[111] E. P. Xing, M. I. Jordan, and S. Russell. A generalized mean field algorithm for variational inference in exponential families. In *Proceedings of the 20th conference on*

Uncertainty in artificial intelligence, UAI '04, pages 602–610, Arlington, Virginia, United States, 2003. AUAI Press.

[112] E. P. Xing, M. I. Jordan, and S. Russell. Graph partition strategies for generalized mean field inference. In *Proceedings of the 20th conference on Uncertainty in artificial intelligence*, UAI '04, pages 602–610, Arlington, Virginia, United States, 2004. AUAI Press.

[113] C. Yanover and Y. Weiss. Approximate inference and protein folding. In *Advances in Neural Information Processing Systems*, pages 84–86. MIT Press, 2002.

[114] J. Yedidia, W. Freeman, and Y. Weiss. Bethe free energy, Kikuchi approximations, and belief propagation algorithms. Technical Report TR2001-16, Mitsubishi Electric Research Laboratories, 2001.

[115] J. S. Yedidia, W. T. Freeman, and Y. Weiss. Generalized belief propagation. In *NIPS*, 2001.

[116] J. S. Yedidia, W. T. Freeman, and Y. Weiss. Constructing free energy approximations and generalized belief propagation algorithms. *IEEE Transactions on Information Theory*, 51:2282–2312, 2005.

[117] N. Zhang and D. Poole. A simple approach to Bayesian network computations. In *Proceedings of the Tenth Canadian Conference on Artificial Intelligence*, pages 171–178, 1994.

[118] F. Zhao, J. Peng, J. Debartolo, K. F. Freed, T. R. Sosnick, and J. Xu. A probabilistic graphical model for ab initio folding. In *Proceedings of the 13th Annual International Conference on Research in Computational Molecular Biology*, RECOMB 2'09, pages 59–73, Berlin, Heidelberg, 2009. Springer-Verlag.